7-10-2013

Metal-silicate Partitioning Behavior of Molybdenum, Tungsten, and Nickel: Implications for Core Formation

Laura Burkemper

Laura K. Burkemper
Candidate

Earth and Planetary Sciences
Department

This dissertation is approved, and it is acceptable in quality and form for publication:

Approved by the Dissertation Committee:

Carl Agee , Chairperson

Adrian Brearley

Charles Shearer

Francis McCubbin

Jie Li

METAL-SILICATE PARTITIONING BEHAVIOR OF MOLYBDENUM, TUNGSTEN, AND NICKEL: IMPLICATIONS FOR CORE FORMATION

by

LAURA K. BURKEMPER

B.S., Chemistry, Saint Louis University, 2006
M.S., Chemistry, Saint Louis University, 2007

DISSERTATION

Submitted in Partial Fulfillment of the
Requirements For the Degree of

Doctor of Philosophy
Earth and Planetary Sciences

The University of New Mexico
Albuquerque, NM

May, 2013

ACKOWLEDGEMENTS

There are many people that will always have my sincere gratitude for supporting me in a number of ways throughout my time at the University of New Mexico. First, I would like to thank Dave Draper for his encouragement and training in the high pressure lab, and Mike Spilde for his extreme patience and assistance with the electron microprobe. I thank Kurt Leinenweber and the Multi-Anvil Cell Assembly Initiative at Arizona State University for fabricating my sample capsules. Yingwei Fei is thanked for his help and guidance on the multi-anvil press at the Carnegie Institute of Washington. Additionally, I greatly appreciate the generous funding this work has received over the years from the NASA Cosmochemistry program, the New Mexico Space Grant Consortium, and the Department of Earth and Planetary Sciences Scholarship fund.

My deepest thanks goes out to my family and friends who believed in me when I did not even believe in myself, and for supporting me no matter what crazy decisions I made. I could not have made it this far without the love of my parents and sister, and their reminders that there is life beyond graduate school. I would like to thank my friends from St. Louis: Rachel and Kyle (and Emily) Jameson, Jessi Mueller, Kelly Ravenscraft, Chrissy Stehr, Jennifer Fraser, and David Bromm, whose support was not lessoned by the fact that they live 1000 miles away. I thank my friends in the department: Euan Mitchell, Kathleen Vander Kaaden, Nina Lanza, Ann Ollila, Alison Santos, and Steve Elardo, who made coming to school everyday fun, and for their constant reminders that we are all in this together. I also thank Garvaghy, whose constant tail wagging made even the hardest day a bit brighter.

I would also like to thank Cindy Jaramillo, Lee Ann Lloyd, and Shannon Clark for their much needed guidance in navigating the graduate program requirements. Chip Shearer, Adrian Brearely, and Jie (Jackie) Li are thanked for their support and especially their advice. I thank Francis McCubbin for his incredibly helpful discussions and suggestions on lab problems, writing papers, and science and life in general. Finally, my sincerest thanks goes to Carl Agee, my advisor and mentor, whose unfailing confidence and support made this all possible.

METAL-SILICATE PARTITIONING BEHAVIOR OF MOLYBDENUM, TUNGSTEN, AND NICKEL: IMPLICATIONS FOR CORE FORMATION

by

Laura K. Burkemper

B.S., Chemistry, Saint Louis University, 2006
M.S., Chemistry, Saint Louis University, 2007
Ph.D., Earth and Planetary Sciences, 2013

ABSTRACT

The interior structure of Earth, particularly the metal core, is responsible for the core dynamo and thus our magnetic field and supplying the mantle with heat to encourage solid state convection and thus decompression melting and hot spot volcanism. Therefore determining how Earth's core formed and if that process was unique to our planet in the solar system is of great scientific interest. Core formation can be studied experimentally by examining the metal-silicate partitioning behavior of siderophile elements and using the results to explain their observed upper mantle depletions relative to bulk Earth abundances. This study investigated the partitioning behavior of the moderately siderophile elements molybdenum and tungsten by conducting experiments using multi-anvil presses and obtaining compositional analyses of the run products using electron probe microanalysis. Molybdenum was found to dissolve as Mo^{4+} in silicate melts, whereas tungsten dissolved as W^{6+}. The partition coefficients [D_i = c_i(metal)/c_i(silicate)] for both molybdenum and tungsten decrease with increasing pressure; however, D_W increases slightly with increasing temperature whereas D_{Mo} decreases. Both elements become less siderophile as silicate melt polymerization

decreases. The addition of carbon to the metal phase causes D_{Mo} and D_W to increase, while addition of sulfur causes D_{Mo} and D_W to decrease. Parameterization of the data from this study and literature data allowed for core formation modeling to determine what conditions could explain Earth's mantle abundances of molybdenum, tungsten, and nickel (the most extensively studied element). The modeling suggests that the abundances of these elements were set by a global magma ocean near the end of accretion with conditions of 35-37 GPa (~1100 km depth) and 2950-3000 K with $X_C = 0.07$, $X_S = 0.05$, and $X_{Si} = 0.06$. Thus implying that large impacts in the late stages of Earth's accretion were energetic enough to re-equilibrate the already differentiated metal and silicate, leaving the distinct chemical signature of a single equilibration event in the mantle. Applying the parameterizations to other differentiated bodies for which we have compositional data indicates that magma oceans were common occurrences in the early solar system, but each body underwent a unique differentiation history.

TABLE OF CONTENTS

1.0 Introduction to Terrestrial Core Formation: Current Theories and Experimental Background

1.1 How do planetary cores form and why do we care?

Core formation is a two step process that involves first, separating metal from the silicate portion of a planet and second, the metal sinking to the center of the planet to form a core. From moment of inertia estimates and studies on iron meteorites, it is thought that all of the terrestrial planets (including the Moon and certain asteroids) have cores, and thus underwent core formation (e.g. Yoder 1995, Sohl et al. 2005, Haack and McCoy 2005, Smith et al. 2012). Therefore, understanding how core formation occurs is essential for understanding terrestrial planet evolution. Core formation represents an incredible example of mass transfer; the outcome of which determines mantle, and therefore crustal, compositions. Additionally, the structure of Earth's core is important because convection in the liquid outer core gives rise to the magnetic field which protects us from the Sun's rays, without which there would probably be no life on Earth; and provides heat to the mantle, both primordial and latent (through inner core crystalization), helping drive processes like hot-spot volcanism. Although theories on how Earth's core formed have been around since the 1960's (e.g. Ringwood 1966), no one theory is yet agreed upon.

The upper mantle is depleted in the refractory siderophile (iron-loving) elements relative to their bulk (chondritic) abundances, and since the refractory lithophile (rock-loving) elements are not depleted, Figure 1-1, the depletion of the siderophile elements is confidently attributed to core formation due to their preference for the metal phase during core separation (e.g. Ringwood 1966). Therefore, any successful core formation theory

must be able to explain these observed elemental depletions, so having a thorough understanding of the metal-silicate partitioning behavior of the siderophile elements is imperative. Decades of experimental work on partitioning behavior has determined that metal-silicate partitioning is affected by pressure, temperature, oxygen fugacity, and metal and silicate composition (see Section 1.2 for more details). In 1981, Wänke suggested that the mantle depletions of the siderophile elements could be explained by simply varying the oxygen fugacity of the material accreting to form Earth. This inhomogeneous accretion hypothesis states that the accreting material started off relatively reduced, and became more oxidized as accretion progressed. Jones and Drake (1986) alternatively suggested the inefficient core formation hypothesis, where some metal is left behind in the mantle and later oxidized and homogenized. This hypothesis was suggested in explanation of data from equilibrium metal-silicate partitioning studies at 1 bar that determined partition coefficients [$D_i = c_i$(metal)/c_i(silicate)] too large to explain the mantle depletions of the siderophile elements, suggesting an excess of siderophile elements in the mantle relative to what is expected from equilibrium core formation (e.g. Jones and Drake 1986). However, further studies at pressures >1 bar showed that the D values for certain siderophile elements decrease with increasing pressure and reach the D values required to explain the observed mantle depletions at pressures >25 GPa, Figure 1-2. This finding led to the promotion of the magma ocean hypothesis, in which metal-silicate equilibrium occurred at high pressure at the base of a layer of liquid silicate (magma ocean, e.g. Li and Agee 1996).

The magma ocean scenario also gained popularity due to geophysical evidence for large-scale melting early in Earth's history. Numerical simulations showed that large

impacts were likely during the late stages of planetary accretion (Wetherill 1985, Canup and Agnor 2000). The energy released from these impacts would produce enough heat to partially, or completely, melt a growing planet, thus causing one or more magma oceans (Melosh 1990, Tonks and Melosh 1993). Furthermore, Hf-W isotopes provide evidence that Earth accreted within 30 My of solar system formation (Kleine et al. 2002, Yin et al. 2002); such rapid accretion and subsequent release of gravitational energy would also have promoted large-scale melting. Additional heat sources inside the growing Earth include the decay of the short-lived ^{26}Al and ^{60}Fe isotopes and latent heat from metal-silicate separation. This all provides evidence for high temperature conditions on early Earth and is in contrast to the cold accretion, protracted core formation theories that dominated previously (e.g Anderson et al. 1971). Figure 1-3 shows a schematic of the magma ocean scenario as outlined by Stevenson (1990). Metal droplets would separate out of a layer of liquid silicate and equilibrate with the surrounding silicate as they sink to the silicate liquidus. The metal would pond at the liquidus where equilibration would stop (Rubie et al. 2003), thus the last point of metal-silicate equilibration would be at the base of the magma ocean. The metal would then sink through the solid silicate to the core in the form of large diapirs (Karato and Murthy 1997).

The three theories for core formation that were briefly described above each imply something different and significant about the early solar system. Inhomogeneous (or heterogeneous) accretion suggests that the oxygen fugacity of accreting material changed over time, which has implications for protoplanetary disc evolution. Recently, it has been suggested that planetary feeding zones increased as accretion progressed, therefore providing more oxidized, volatile rich material from further away from the Sun

(O'Brien et al. 2006). Inefficient core formation calls upon oxidation of the metal left behind in the mantle, thus requiring a mechanism for doing so. The most effective way of oxidizing that much metal would be through interaction with water, and therefore has implications for the availability of water on early Earth (Wood et al. 2006). The magma ocean hypothesis suggests large-scale melting, most likely as a result of large impacts in the inner solar system during accretion. Therefore, determining how planetary cores form has very widespread implications. Each theory has its merits and over the past 25 years, the magma ocean hypothesis has gained a lot of support due to its ability to explain the mantle abundance of many siderophile elements. However, the partitioning behavior of all the siderophile elements has not been fully explored and more work is needed. A brief review of previous work is given below.

1.2 Previous metal-silicate partitioning work

The first major geochemical support of the magma ocean hypothesis came from high pressure partitioning experiments on the moderately siderophile elements Ni and Co. At low pressures, D_{Ni} and D_{Co} are too large to explain the mantle abundances of Ni and Co (Jones and Drake, 1986; Schmitt et al. 1989). Additionally, Ni and Co are found in chondritic relative abundance in the mantle, Figure 1-1, and at low pressure Ni is more siderophile than Co, indicating that equilibrium core formation at shallow conditions would not result in their having similar depletions. At the advent of high pressure partitioning research, multiple groups determined that increasing pressure causes both Ni and Co to become more lithophile (Walker et al. 1993, Hillgren et al. 1994, Righter and Drake 1995, Thibault and Walter 1995). Li and Agee (1996) determined that not only do

D_{Ni} and D_{Co} decrease with increasing pressure, but at ~28 GPa and 2000 °C, the D values converge to give the values required to explain their depletions, Figure 1-2. They suggested that these conditions correspond to the last point of metal-silicate equilibration during core formation and imply a magma ocean of 750-1100 km depth. Further studies have supported this finding and provided a large database of Ni and Co partitioning experiments. Since Ni and Co are both 2+ cations in silicate melts, oxygen fugacity has only a moderate effect on their partitioning behavior, as a result of only one oxygen being required to form a stable oxide species (e.g. Holzheid et al. 1994). Changing silicate composition has a slight effect on D_{Ni} and D_{Co}; as does temperature, with both elements becoming less siderophile with increasing temperature (Jana and Walker 1997a, Chabot et al. 2005). A recent study that investigated the effect of pressure up to 52 GPa determined that above 30 GPa, the D_{Ni} and D_{Co} values remain similar thus providing evidence for a magma ocean up to 1600 km deep (Bouhifd and Jephcoat 2011).

V, Cr, and Mn are also moderately siderophile elements and offer further constraints on the conditions of core formation. In contrast to Ni and Co, partitioning experiments at 1 bar and 1260 °C produced partition coefficients too low to explain the observed mantle abundances, which led Drake et al. (1989) to conclude that the V, Cr, and Mn depletions were better explained by loss due to volatility, not core formation. Also in contrast to Ni and Co, pressure does not affect the partitioning behavior of V, Cr, and Mn (Chabot et al. 2003, Gessmann and Rubie 2000). However, their partitioning behavior is strongly affected by temperature, with increasing temperature causing a moderate increase in D_{Cr} and strong increases in D_V and D_{Mn} (Chabot et al. 2003, Gessmann and Rubie 2000). Yet, at a temperature of 4500 K and an oxygen fugacity 0.4

log units below the iron-wüstite buffer (-0.4ΔIW), the D values are still too low to explain the depletions (Chabot et al. 2003). The valences of Cr and Mn in silicate melts are both 2+, whereas V usually exists as a 3+ cation at oxygen fugacities relative to core formation, around -2ΔIW (Drake et al. 1989). Changing the oxygen fugacity from -0.4ΔIW to -2.3 ΔIW increases the siderophile behavior of all three elements and brings the D values into the required range (Chabot et al. 2003), thus making V, Cr, and Mn compatible with the magma ocean hypothesis as long as the conditions are hot and reducing enough. However, Righter (2011) suggested that these elements may also be housed in lower mantle minerals (i.e. garnet, magnesiowüstite, perovskite), due to D(crystal/silicate) being larger than the D(metal/silicate), thus negating the need to find compatible magma ocean conditions (see also Righter et al. 2011).

Although the lithophile elements tend not to be depleted in the mantle, they can still offer insight into core formation; for example, any set of conditions that would cause these elements to become siderophile can be ruled out. Mann et al. (2009) investigated the partitioning behavior of lithophile and weakly siderophile elements, some of which are also volatile. Volatile elements are more complicated to address than refractory elements because their depletion due to volatility must be accounted for, and separated from that due to core formation. Ga and Mn have similar depletions in the upper mantle even though Ga has a lower condensation temperature, Figure 1-1. Any magma ocean conditions that would fractionate these elements that could not be reversed by their different volatilities can therefore be excluded. At moderate pressures (~20 GPa), D_{Ga} is much larger than D_{Mn}, such that if core formation took place at pressures of ~20 GPa, Ga would be much more depleted in the mantle than Mn because of its greater siderophile

tendency and volatility, but this is not observed (Figure 1-1, Mann et al. 2009). D_{Ga} decreases with increasing pressure, therefore at higher pressures (>30 GPa), $D_{Ga}/D_{Mn} \leq 1$, which is compatible with their observed depletions (Mann et al. 2009). The same situation occurs for In and Zn. At low pressures D_{In} is larger than D_{Zn}, yet they have the similar mantle depletions and In is more volatile than Zn (Mann et al. 2009). However, due to the stronger pressure dependence of D_{In}, their similar depletions can be explained by magma ocean conditions >30 GPa (Mann et al. 2009). A final piece of evidence for high pressure core formation comes from the refractory, lithophile element Nb. The D range required to explain the Nb depletion is 0-0.9, which can be obtained at pressures >30 GPa, but at lower pressures D_{Nb} is greater than one (Mann et al. 2009).

High pressure core formation can explain many of the elemental depletions shown in Figure 1-1. However, the highly siderophile elements (HSE) are problematic. They are an order of magnitude more depleted than the moderately siderophile elements and all have similar depletions. Their strong affinity for the metal phase leads to analytical difficulties with measuring their concentrations in the silicate phase. Additionally, experiments on the HSEs are plagued by the formation of nanonuggets. Nanonuggets are nanometer sized metal blebs that form in the silicate phase either during the experiment or upon quench and produce extreme heterogeneity in the measured concentrations (e.g. Ertel et al. 2008), therefore making it difficult to obtain an accurate partition coefficient. They are most prominent at low oxygen fugacities and some studies have been able to circumvent this issue by doing experiments at higher oxygen fugacities or by using analytical subtraction methods (e.g. Ertel et al. 2006). Studies that have determined HSE D values almost exclusively conclude that the measured D values are much too large to

explain the mantle depletions (Re: Ertel et al. 2001; Os: Fortenfant 2006, Brenan and McDonough 2009; Ir: Brenan and McDonough 2009; Rh: Ertel et al. 1999, Pt: Holzheid et al. 2000, Ertel et al. 2006; Pd: Holzheid et al. 2000). Based on their own experimental determinations, O'Neill et al. (1995) suggested that the abundances of the HSEs in the mantle are from a 'late veneer' of chondritic material added to Earth after the completion of core formation (see also Holzheid et al. 2000). However, recent work on Pd, Pt, and Au suggests that high P-T conditions can lower the D values, even to the required range (Danielson et al. 2005, Cottrell and Walker 2006, Righter et al. 2008). Thus allowing for the idea that there may be a set of magma ocean conditions that can explain the HSE depletions that more high P-T experimental work would reveal. However, Brenan and McDonough (2009) determined that equilibrium core formation can explain the Au mantle abundance, but not Os or Ir, suggesting that multiple processes may have been involved in establishing the mantle abundances of the HSEs.

To summarize thus far, previous work has determined that explaining the mantle abundances of Ni and Co requires magma ocean pressure conditions of 30-52 GPa, which are compatible with the high pressures suggested for Nb, Ga, Zn, In, Au, Pt, and Pd. The elements V, Cr, and Mn, additionally require high temperatures and reducing oxygen fugacity conditions, and most of the HSEs require a late veneer. However, a successful core formation hypothesis has to be able to explain all the elemental depletions, so what about the moderately siderophile elements Mo and W? Mo is the most depleted moderately siderophile element; therefore, magma ocean conditions that can explain its depletion may provide insight into conditions that could explain the highly siderophile elements. Also, Mo and W are found in the same group of the periodic table and are thus

considered ‘geochemical twins’ and expected to have similar chemical properties. Yet, they exhibit vastly different depletions in the mantle, Figure 1-1. Any successful core formation theory must be able to explain this difference in partitioning behavior.

Literature data on W partitioning is quite extensive, but the results are contradictory. Walter and Thibault (1995) determined that at constant silicate composition and oxygen fugacity, increasing pressure and temperature together has no effect on D_W. However, Siebert et al. (2011) determined that increasing pressure causes a slight decrease in D_W. A third suggestion by Cottrell et al. (2009) is that below 5 GPa, increasing pressure causes D_W to increase strongly, but above 5 GPa a moderate decrease is observed. This bimodal trend was refuted by Righter (2011), in favor of a single decreasing trend, similar to that suggested by Siebert et al. (2011). Additionally, Cottrell et al. (2009) and Siebert et al. (2011) determined that temperature has an insignificant effect on D_W, whereas Righter et al. (2010) showed a prominent increasing trend. A further complication with examining W is that it has been shown to be in multiple valence states in silicate melts, both 4+ and 6+ (O’Neill et al. 2008). Exactly where the change from dominantly 4+ valence to dominantly 6+ occurs at the high P-T conditions found in a magma ocean is uncertain and has lead previous investigators to assume one valence over the other (e.g. Siebert et al. 2011). Previous work does agree that D_W is highly dependent on silicate composition (Walter and Thibault 1995, Hillgren et al. 1996, Jana and Walker 1997a, O’Neill et al. 2008, Cottrell et al. 2009, Siebert et al. 2011). Finally, Cottrell et al. (2010) and Siebert et al. (2011) suggest similar magma ocean conditions, 10-40 and 32-42 GPa, respectively, which are compatible with the other elements discussed above; however, the discrepancies in the literature data need to be

resolved before tungsten's compatibility with the magma ocean hypothesis can be fully assessed.

The literature data for Mo is not contradictory, but it is also not abundant. There are well over 300 experiments in the literature for both Ni and Co, but less than 200 for Mo. Additionally, the majority of those experiments were performed at pressures below 2 GPa, thus introducing large errors when results are extrapolated to magma ocean pressure conditions of >30 GPa. Molybdenum is a multi-valence cation but by performing solubility experiments, O'Neill and Eggins (2002) determined that at the oxygen fugacity conditions suggested for core formation, Mo^{4+} is the dominant valence state, in agreement with that determined previously by Holzheid et al. (1994). Similar to D_W, D_{Mo} is strongly dependent on silicate melt composition (Walter and Thibault 1995, Hillgren et al. 1996, Jana and Walker 1997a). Furthermore, D_{Mo} was found to decrease with increasing pressure and temperature (Walter and Thibault 1995, Righter et al. 2010, Siebert et al. 2011). Based on the limited datasets, magma ocean conditions of 23-42 GPa have been suggested (Righter et al. 2010, Siebert et al. 2011); however, these conditions are not robust and would greatly benefit from additional experiments.

As mentioned above, Mo is much more depleted in Earth's mantle than W. Possible reasons for the different depletions could be due to the opposing temperature effects, if D_W does indeed increase with increasing temperature, while D_{Mo} decreases. Also, if the dominant tungsten valence is W^{6+}, in contrast to Mo^{4+}, this could cause dissimilar partitioning behavior due to the different effect oxygen fugacity would have on each element. Finally, it could be that D_W and D_{Mo} are affected differently by the presence of light elements in the metal phase. We have known since the 1950's that the

outer core contains ~10 wt.% of a light element due to the density difference between the outer core and liquid iron (Birch 1952). The most probable light element candidates include H, O, C, Si, and S because they are lighter than iron, alloy readily with iron, and cosmochemically abundant enough for a significant amount to be present in the core (Hillgren et al. 2000). The effect of O in the metal phase is difficult to examine experimentally and its effect on element partitioning has only just started to be explored (e.g. Corgne et al. 2009). However, the effects of C, Si, and S have been quite extensively explored for most of the siderophile elements. For example, Ni and Co are not significantly affected by the addition of C and have only a modest dependence on S and Si (Jana and Walker 1997b, Chabot et al. 2005, Tuff et al. 2011). In contrast, Mo and W are strongly affected by the presence of light elements (Lodders and Palme 1991, Jana and Walker 1997b, Tuff et al. 2011), which may provide an explanation for their different mantle depletions. In conclusion, Mo and W display complex partitioning behaviors that are not yet thoroughly understood.

The present study employed two different types of experiments, solubility (pure Mo metal phase) and partitioning (Fe-rich metal phase), in order to obtain a comprehensive understanding of molybdenum's behavior in silicate melts. We investigated the effect of pressure, temperature, and composition on Mo partitioning and performed W partitioning experiments in order to resolve the conflicting literature data and to compare the partitioning behavior of Mo with W. This study seeks to answer the questions: Can the Mo and W mantle depletions be explained by equilibrium core formation out of a magma ocean? If not, what other core formation hypothesis could explain them? If a magma ocean can explain the depletions, what constraints do our

results place on the conditions within that magma ocean? And what, if anything, does this tell us about terrestrial planet evolution and early solar system processes? The following chapters address these questions in detail; Chapter 2 discusses the Mo solubility results, Chapter 3 discusses the Mo and Ni partitioning results, Chapter 4 discusses the W partitioning results, and Chapter 5 brings everything together with a discussion of terrestrial planet evolution.

1.3 Useful equations

The following chapters employ a few, rather important equations which are discussed here in order to acquaint the unfamiliar reader. Partition coefficients are calculated for all partitioning experiments and are used to assess an element's preference for one phase over another, they are calculated according to,

$$D_i = \frac{C_i^{metal}}{C_i^{silicate}} \tag{1-1}$$

where C is the concentration of element i in the metal and silicate phases, by weight. This ratio is affected by pressure, temperature, oxygen fugacity, and phase compositions in accordance with the thermodynamic properties of the reaction

$$M + \frac{n}{4}O_2 \leftrightarrow MO_{\frac{n}{2}} \tag{1-2}$$

where M is the partitioning element and n is the valence of M. Equation 1-1 assumes that the system is not in violation of Henry's Law, meaning D is not dependent on the amount of i present in the system. Thermodynamically speaking, γMO and γM remain constant. Henry's law has been shown to hold true up to very large concentrations of siderophile elements in the silicate melt, for example, up to 12 wt.% W (Ertel et al. 1996).

Partition coefficients are calculated for systems in equilibrium, and the equilibrium constant for Equation 1-2 is

$$K = \frac{a_{MO}}{(a_M)(a_{O_2})^{\frac{n}{4}}} \tag{1-3}$$

where *a* is activity. Equation 1-3 shows that partitioning is dependant on the activity of oxygen in the system. Since O_2 is a gas under ambient conditions, the activity of oxygen is typically termed oxygen fugacity – the effective pressure of the free oxygen not associated with the MO component. Equation 1-3 can be rearranged to yield the equation for calculating oxygen fugacity relative to some buffer species (M-MO),

$$\log fO_2 = \frac{4}{n} \log \frac{a_{MO}}{(a_M)} \tag{1-4}$$

where fO_2 is oxygen fugacity. The common buffer species for core formation studies is iron-wüstite, due to the predominance of Fe in the core. Measuring oxygen fugacity relative to a buffer species is ideal because absolute oxygen fugacity changes with pressure and temperature whereas, relative oxygen fugacity, by following the slope of a buffer curve, takes those changes into account. Furthermore, based on the amount of FeO in the mantle (8 wt.%) and Fe in the core (85 wt.%), we can assume that final core equilibration took place at roughly -2.2ΔIW.

Experimental capabilities limit the pressures and temperatures that partitioning studies can reliably attain. Therefore, the results are frequently extrapolated to the high P-T conditions of core formation. This is done by parameterizing the data following thermodynamic principles (as done by Righter et al. 1997). The equilibrium constant is related to Gibbs free energy (*G*) according to

$$\ln K = \frac{-\Delta G^o}{RT} \tag{1-5}$$

Substituting in Equations 1-3 and 1-4 and expanding the ln term gives

$$\frac{-\Delta G^o}{RT} = \ln a_{MO} - \ln a_M - \frac{n}{4}\ln fO_2 \tag{1-6}$$

Rearranging yields

$$\ln a_M - \ln a_{MO} = -\frac{n}{4}\ln fO_2 + \frac{\Delta G^o}{RT} \tag{1-7}$$

and combining the left side ln terms and substituting D for the activities gives

$$\ln D = -\frac{n}{4}\ln fO_2 + \frac{\Delta G^o}{RT} \tag{1-8}$$

Expanding the $\Delta G°$ term yields

$$\ln D = -\frac{n}{4}\ln fO_2 + \frac{\Delta H^o}{RT} - \frac{T\Delta S^o}{RT} + \frac{P\Delta V^o}{RT} \tag{1-9}$$

where H is enthalpy, S is entropy, and V is volume and then replacing these terms with generic coefficients yields

$$\ln D = -a\ln fO_2 + \frac{b}{T} + \frac{cP}{T} - d \tag{1-10}$$

This is the general form of the equation used to parameterize metal-silicate partitioning data, where *a-d* are determined by multiple linear regression coefficients and as shown in Equation 1-9, *a-d* are related to n/4, ΔH°/R, ΔV°/R, and ΔS°/R, respectively. Equation 1-10 takes into account the effects of oxygen fugacity, pressure, and temperature on partitioning but not metal and silicate phase compositions. Silicate composition can be taken into account by adding terms such as NBO/T (non-bridging oxygens over tetrahedrally coordinated oxygens – Mysen 1983, Righter et al. 1997), oxide mole

fractions (Righter et al. 1999), or using a regular solution model (O'Neill and Eggins 2002). Light elements in the metal phase can also be accounted for by adding empirical terms (Righter et al. 1997) or by estimating metal activity coefficients and correcting the D values (Wade and Wood 2005). Therefore, there are multiple parameterization equations used in the literature, but they are all modified forms of Equation 1-10.

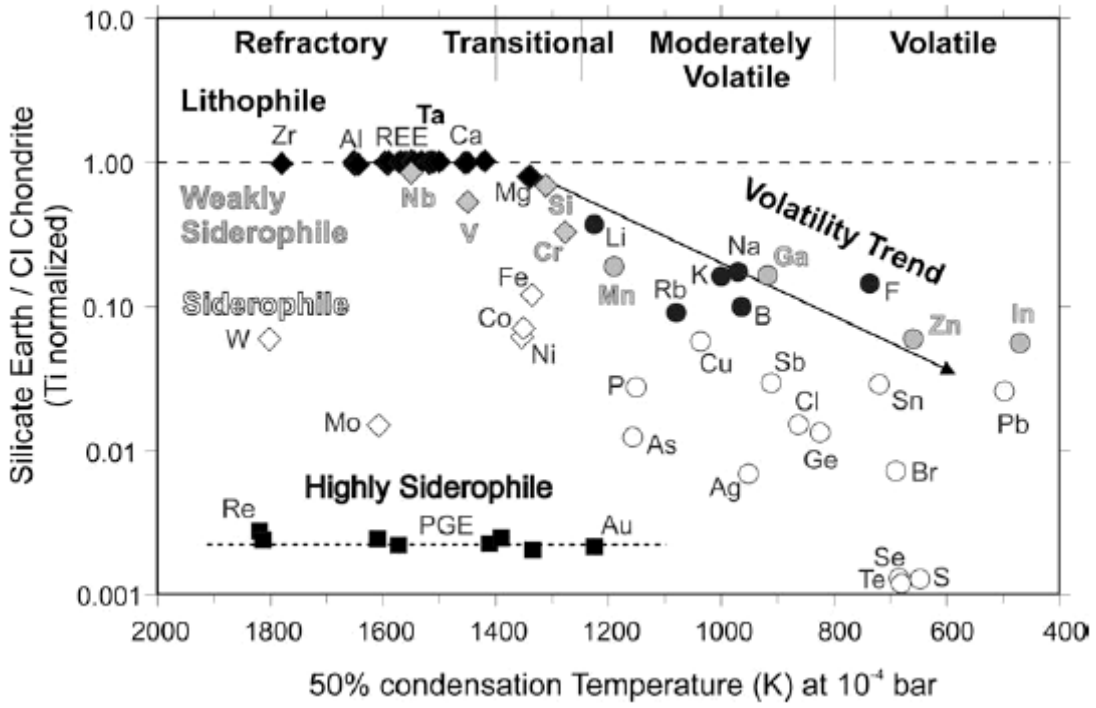

Figure 1-1. Upper mantle elemental depletions relative to CI chondrites and normalized to the refractory element Ti. The plot shows the elemental ratios of the silicate Earth to CI chondrites versus 50% condensation temperature, a measure of volatility. The most volatile elements are on the far right and the least volatile (refractory) are on the far left. Image from Mann et al. (2009).

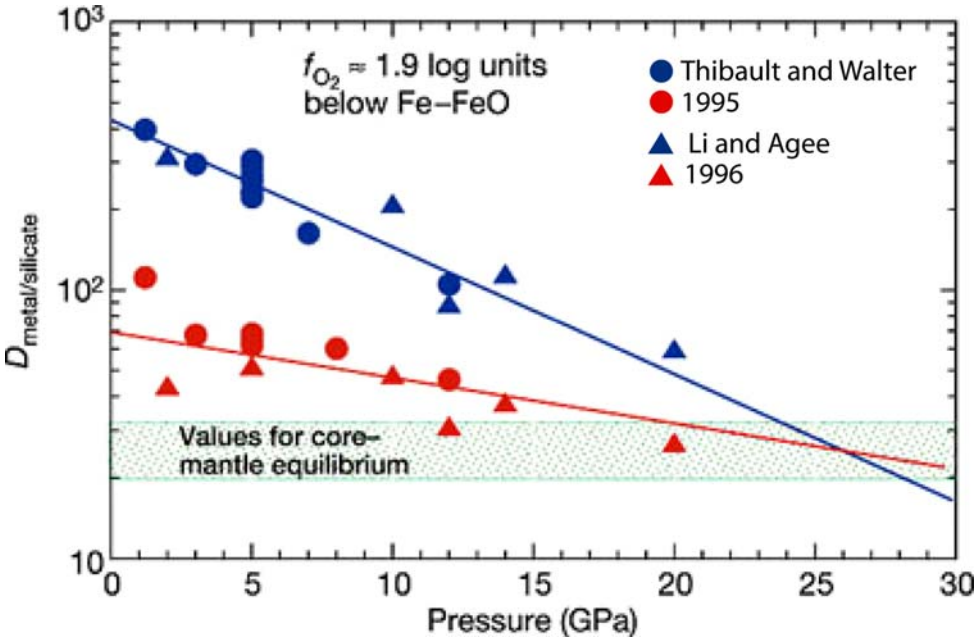

Figure 1-2. Plot of Ni and Co partition coefficients versus pressure. Both D_{Ni} and D_{Co} decrease with increasing pressure and reach the required D values for equilibrium core formation (shaded green) at pressures ~26 GPa. Image modified from Wood et al. (2006).

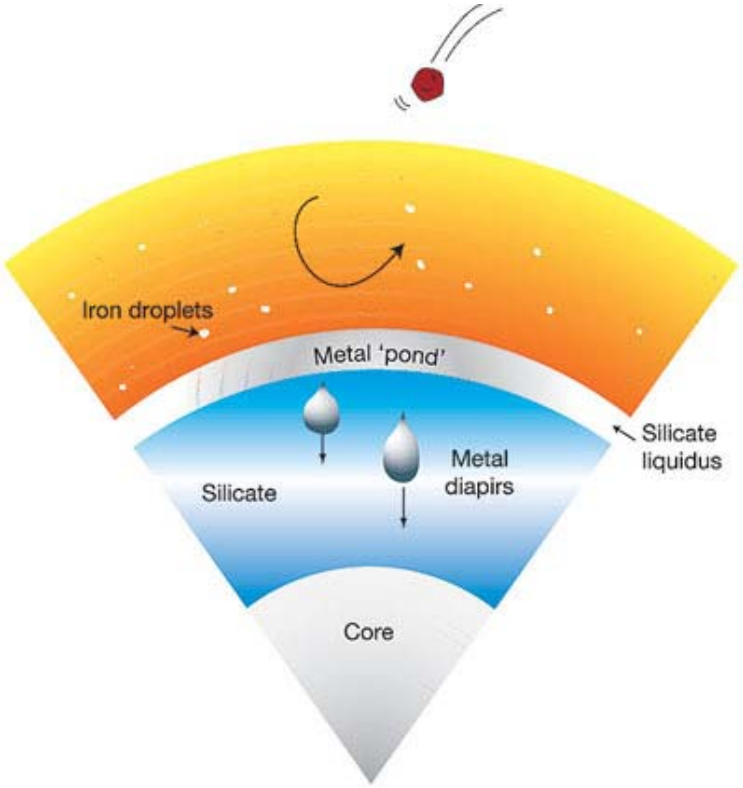

Figure 1-3. Magma ocean schematic illustrating liquid silicate in orange, solid silicate in blue, and metal in gray. The schematic shows the liquid metal droplets sinking to the peridotite liquidus at some depth where the metal ponds before sinking to the core in large diapirs. Image from Wood et al. (2006).

1.4 References

Anderson, D.L., Sammis, C., Jordan, T. (1971) Composition and evolution of the mantle and core. Science 171, 1103-1112

Birch, F. (1952) Elasticity and constitution of Earth's interior. Journal of Geophysical Research 57, 227-286

Bouhifd, M.A., Jephcoat, A.P. (2011) Convergence of Ni and Co metal-silicate partition coefficients in the deep magma-ocean and coupled silicon-oxygen solubility in iron melts at high pressures. Earth and Planetary Science Letters 307, 341-348

Brenan, J.M., McDonough, W.F. (2009) Core formation and metal-silicate fractionation of osmium and iridium from gold. Nature Geoscience 2, 798-801

Canup, R.M., Agnor, C.B. (2000) Accretion of the terrestrial planets and the Earth-Moon system. In: Canup, R. M. and Righter, K. eds. *Origin of the Earth and Moon*. The University of Arizona Press, Tucson AZ, 113-129

Chabot, N.L., Agee, C.B. (2003) Core formation in the Earth and Moon: new experimental constraints from V, Cr, and Mn. Geochimica et Cosmochimica Acta 67, 2077-2091

Chabot, N.L., Draper, D.S., Agee, C.B. (2005) Conditions of core formation in the Earth: constraints from nickel and cobalt partitioning. Geochimica et Cosmochimica Acta 69, 2141-2151

Cottrell, E., Walker, D. (2006) Constraints on core formation from Pt partitioning in mafic silicate liquids at high temperatures. Geochimica et Cosmochimica Acta 70, 1565-1580

Cottrell, E., Walter, M.J., Walker, D. (2009) Metal-silicate partitioning of tungsten at high pressure and temperature: Implications for equilibrium core formation in Earth. Earth and Planetary Science Letters 281, 275-287

Cottrell, E., Walter, M.J., Walker, D. (2010) Erratum to "Metal-silicate partitioning of tungsten at high pressure and temperature: Implications for equilibrium core formation in Earth" [Earth and Planetary Science Letters 281 (2009) 275-287]. Earth and Planetary Science Letters 289, 631-634

Danielson, L.R., Sharp, T.G., Hervig, R.L. (2005) Implications for core formation of the Earth from high pressure-temperature Au partitioning experiments. LPSC XXXVI, abstract #1955

Drake, M.J., Newsom, H.E., Capobianco, C.J. (1989) V, Cr, and Mn in the Earth, Moon, EPB, and SPB and the origin of the Moon: Experimental studies. Geochimica et Cosmochimica Acta 53, 2101-2111

Ertel, W., O'Neill, H.S.C., Dingwell, D.B., Spettel, B. (1996) Solubility of tungsten in a haplobasaltic melt as a function of temperature and oxygen fugacity. Geochimica et Cosmochimica Acta 60, 1171-1180

Ertel, W., O'Neill, H.S.C., Sylvester, P.J., Dingwell, D.B. (1999) Solubilities of Pt and Rh in a haplobasaltic silicate melt at 1300 °C. Geochimica et Cosmochimica Acta 63, 2439-2449

Ertel, W., O'Neill, H.S.C., Sylvester, P.J., Dingwell, D.B., Spettel, B. (2001) The solubility of rhenium in silicate melts: Implications for the geochemical properties of rhenium at high temperatures. Geochimica et Cosmochimica Acta 65, 2161-2170

Ertel, W., Walter, M.J., Drake, M.J., Sylvester, P.J. (2006) Experimental study of platinum solubility in silicate melt to 14 GPa and 2273 K: Implications for accretion and core formation in Earth. Geochimica et Cosmochimica Acta 70, 2591-2602

Ertel, W., Dingwell, D.B., Sylvester, P.J. (2008) Siderophile element in silicate melts - A review of the mechanically assisted equilibration technique and the nanonugget issue. Chemical Geology 248, 119-139

Flasar, F.M., Birch, F. (1973) Energetics of core formation: A correction. Journal of Geophysical Research 78, 6101-6103

Fortenfant, S.S., Dingwell, D.B., Ertel-Ingrisch, W., Capmas, F., Birck, J.L., Dalpe, C. (2006) Oxygen fugacity dependence of Os solubility in haplobasaltic melt. Geochimica et Cosmochimica Acta 70, 742-756

Gessmann, C.K., Rubie, D.C. (2000) The origin of the depletions of V, Cr, and Mn in the mantles of the Earth and Moon. Earth and Planetary Science Letters 184, 95-107

Haack, H., McCoy, T.J. (2005) Iron and stony-iron meteorites. In: Davis, A.M. ed., *Treatise on Geochemistry, Vol. 1, Meteorites, Comets, and Planets.* Elsevier Ltd, 325-345

Hillgren, V.J., Drake, M.J., Rubie, D.C. (1994) High-pressure and high-temperature experiments on core-mantle segregation in the accreting Earth. Science 264, 1442-1445

Hillgren, V.J., Drake, M.J., Rubie, D.C. (1996) High pressure and high temperature metal-silicate partitioning of siderophile elements: The importance of silicate liquid composition. Geochimica et Cosmochimica Acta 60, 2257-2263

Hillgren, V.J., Gessmann, C.K., Li, J. (2000) An experimental perspective on the light element in Earth's core. In: Canup, R. M. and Righter, K. eds. *Origin of the Earth and Moon*. The University of Arizona Press, Tucson AZ, 245-263

Holzheid, A., Borisov, A., Palme, H. (1994) The effect of oxygen fugacity and temperature on solubilities of nickel, cobalt, and molybdenum in silicate melts. Geochimica et Cosmochimica Acta 58, 1975-1981

Holzheid, A., Sylvester, P.J., O'Neill, H., Rubie, D.C., Palme, H. (2000) Evidence for a late chondritic veneer in the Earth's mantle from high-pressure partitioning of palladium and platinum. Nature 406, 396-399

Jana, D., Walker, D. (1997a) The influence of silicate melt composition on distribution of siderophile elements among metal and silicate liquids. Earth and Planetary Science Letters 150, 463-472

Jana, D., Walker, D. (1997b) The impact of carbon on element distribution during core formation. Geochimica et Cosmochimica Acta 61, 2759-2763

Jones, J.H., Drake, M.J. (1986) Geochemical constraints on core formation in the Earth. Nature 322, 221-228

Karato, S., Murthy, V.R. (1997) Core formation and chemical equilibrium in the earth - I. Physical considerations. Physics of the Earth and Planetary Interiors 100, 61-79

Kleine, T., Mezger, K., Munker, C., Palme, H., Bischoff, A. (2004) ^{182}Hf-^{182}W isotope systematics of chondrites, eucrites, and martian meteorites: Chronology of core formation and early mantle differentiation in Vesta and Mars. Geochimica et Cosmochimica Acta 68, 2935-2946

Li, J., Agee, C.B. (1996) Geochemistry of mantle-core differentiation at high pressure. Nature 381, 686-689

Lodders, K., Palme, H. (1991) On the chalcophile character of molybdenum: Determination of sulfide/silicate partition coefficients of Mo and W. Earth and Planetary Science Letters 103, 311-324

Mann, U., Frost, D.J., Rubie, D.C. (2009) Evidence for high-pressure core-mantle differentiation from the metal-silicate partitioning of lithophile and weakly-siderophile elements. Geochimica et Cosmochimica Acta 73, 7360-7386

Melosh, H.J. (1990) Giant impacts and the thermal state of the early Earth. In: Newsom, H.E. and Jones, J.H. eds. *Origin of the Earth*. Oxford University Press, 69-83

Mysen, B.O. (1983) The structure of silicate melts. Annual Review of Earth and Planetary Science 11, 75-97

O'Neill, H.S.C., Dingwell, D.B., Borisov, A., Spettel, B., Palme, H. (1995) Experimental petrochemistry of some highly siderophile elements at high temperatures, and some implications for core formation and the mantle's early history. Chemical Geology 120, 255-273

O'Neill, H.S.C., Eggins, S.M. (2002) The effect of melt composition on trace element partitioning: An experimental investigation of the activity coefficient of FeO, NiO, CoO, MoO2, MoO3 in silicate melts. Chemical Geology 186, 151-181

O'Neill, H.S.C., Berry, A.J., Eggins, S.M. (2008) The solubility and oxidation state of tungsten in silicate melts: Implications for the comparative chemistry of W and Mo in planetary differentiation processes. Chemical Geology 255, 346-359

O'Brien, D.P., Morbidelli, A., Levison, H.F. (2006) Terrestrial planet formation with strong dynamical fiction. Icarus 184, 39-58

Righter, K., Drake, M.J. (1995) The effect of pressure on siderophile-element (nickel, cobalt, molybdenum, tungsten, and phosphorus) metal-silicate partition coefficients. Meteoritics 30, 565-566

Righter, K., Drake, M.J., Yaxley, G. (1997) Prediction of siderophile element metal-silicate partition coefficients to 20 GPa and 2800 °C: The effects of pressure, temperature, oxygen fugacity, and silicate and metallic melt compositions. Physics of the Earth and Planetary Interiors 100, 115-134

Righter, K., Drake, M.J. (1999) Effect of water on metal-silicate partitioning of siderophile elements: A high pressure and temperature terrestrial magma ocean and core formation. Earth and Planetary Science Letters 171, 383-399

Righter, K., Humayun, M., Danielson, L. (2008) Partitioning of palladium at high pressures and temperatures during core formation. Nature 1, 321-323

Righter, K., Pando, K.M., Danielson, L., Lee, C.T. (2010) Partitioning of Mo, P and other siderophile elements (Cu, Ga, Sn, Ni, Co, Cr, Mn, V, and W) between metal and silicate melt as a function of temperature and silicate composition. Earth and Planetary Science Letters 291, 1-9

Righter, K. (2011) Prediction of metal-silicate partition coefficients for siderophile elements: An update and assessment of PT conditions for metal-silicate equilibrium during accretion of the Earth. Earth and Planetary Science Letters 304, 158-167

Righter, K., Sutton, S., Danielson, L., Pando, K., Schmidt, G., Yang, H., Berthet, S., Newville, M., Choi, Y., Downs, R. T., Malavergne, V. (2011) The effect of fO_2 on the partitioning and valence of V and Cr in garnet/melt pairs and the relation to terrestrial mantle V and Cr content. American Mineralogist 96, 1278-1290

Ringwood, A.E. (1966) Chemical evolution of the terrestrial planets. Geochimica et Cosmochimica Acta 30, 41-104

Rubie, D.C., Melosh, H.J., Reid, J.E., Liebske, C., Righter, K. (2003) Mechanisms of metal-silicate equilibration in the terrestrial magma ocean. Earth and Planetary Science Letters 205, 239-255

Schmitt, W., Palme, H., Wänke, H. (1989) Experimental determination of metal/silicate partition coefficients for P, Co, Ni, Cu, Ga, Ge, Mo, and W and some implications for the early evolution of the Earth. Geochimica et Cosmochimica Acta 53, 173-185

Siebert, J., Corgne, A., Ryerson, F.J. (2011) Systematics of metal-silicate partitioning for many siderophile elements applied to Earth's core formation. Geochimica et Cosmochimica Acta 75, 1451-1489

Smith, D.E., Zuber, M.T., Phillips, R.J., Solomon, S.C., Hauck II, S.A., Lemoine, F.G., Mazarico, E., Neumann, G.A., Peale, S.J., Margot, J.-L., Johnson, C.L., Torrence, M.H., Perry, M.E., Rowlands, D.D., Goossens, S., Head, J.W., Taylor, A.H. (2012) Gravity field and internal structure of Mercury from MESSENGER. Science 336, 214-214

Sohl, F., Schubert, G., and Spohn, T., 2005. Geophysical constraints on the composition and structure of the Martian interior. Journal of Geophysical Research 110, E12008, doi: 10.1029/2005JE002520

Stevenson, D.J. (1990) Fluid dynamics of core formation. In: Newsom, H.E. and Jones, J.H. Eds., *Origin of the Earth*. Oxford University Press, New York, 231-249

Thibault, Y., Walter, M.J. (1995) The influence of pressure and temperature on the metal-silicate partition coefficients of nickel and cobalt in a model C1 chondrite and implications for metal segregation in a deep magma ocean. Geochimica et Cosmochimica Acta 59, 991-1002

Tonks, W.B., Melosh, H.J. (1993) Magma ocean formation due to giant impacts. Journal of Geophysical Research 98, 5319-5333

Tuff, J., Wood, B.J., Wade, J. (2011) The effect of Si on metal-silicate partitioning of siderophile elements and implications for the conditions of core formation. Geochimica et Cosmochimica Acta 75, 673-690

Wade, J., Wood, B.J. (2005) Core formation and the oxidation state of the Earth. Earth and Planetary Science Letters 236, 78-95

Walker, D., Norby, L., Jones, J.H. (1993) Superheating effects on metal-silicate partitioning of siderophile elements. Science 262, 1858-1861

Walter, M.J., Thibault, Y. (1995) Partitioning of tungsten and molybdenum between metallic liquid and silicate melt. Science 270, 1186-1189

Wänke, H. (1981) Constitution of terrestrial planets. Philosophical Transactions of the Royal Society of London A 303, 287-302

Wetherill, G.W. (1985) Occurrence of giant impacts during the growth of the terrestrial planets. Science 228, 877-879

Wood, B.J., Walter, M.J., Wade, J. (2006) Accretion of the Earth and segregation of its core. Nature 441, 825-833

Yin, Q., Jacobsen, S.B., Yamashita, K., Blichert-Toft, J., Telouk, P., Albarede, F. (2002) A short timescale for terrestrial planet formation from Hf-W chronometry of meteorites. Nature 418, 949-959

Yoder, C.F. (1995) Astrometric and geodetic properties of Earth and the Solar System. In: Ahrens, T.J. ed. *Global Earth Physics: A Handbook of Physical Constants*. AGU Reference Shelf, 1-31

2.0 Constraints on Core Formation from Molybdenum Solubility in Silicate Melts at High Pressure

Abstract

We report results from 43 new molybdenum solubility experiments performed in order to test molybdenum's compatibility with the magma ocean hypothesis for core formation. A Walker-type multi-anvil press was used for all experiments and we investigated the pressure range of 2.5-12 GPa and temperature range of 1585-2200 °C. Eight different silicate compositions were also employed. Our data show that increasing temperature causes solubility to increase, whereas pressure has a negligible effect over the range investigated here. In general, increasing silicate melt polymerization causes solubility to decrease; however, the effect of silicate composition is best addressed by looking at the effects of individual oxides versus a universal melt parameter such as NBO/T (ratio of non-bridging oxygens to tetrahedrally coordinated cations). From our solubility data, we calculated metal-silicate partition coefficients at infinite iron dilution. Parameterization of our data plus data from the literature shows that there is no discrepancy between partition coefficients determined directly from experiments and those calculated from solubility data, so long as all variables are taken into account, i.e. changes in metal phase composition. Additionally, most of the experiments in the literature were conducted at pressures below 2 GPa, therefore the addition of our high pressure data set makes extrapolations to deep magma ocean conditions more accurate. We determined that the observed mantle abundance of Mo can be explained by both single-stage and multi-stage magma ocean models. Previous siderophile element studies have suggested a wide range of possible single-stage core formation conditions, from 10

to 60 GPa along the peridotite liquidus. Our results narrowed this range by constraining the P-T conditions to 40-54 GPa and 3050-3400 K. Our results also further constrained the multi-stage core formation models by limiting the depth of metal-silicate equilibration during the final impacts of accretion to 31-42% of the core-mantle boundary.

2.1 Introduction

Earth's mantle depletion of the siderophile elements, relative to chondritic abundances, was first noticed in the 1960's and confidently attributed to the separation of the core from the mantle (Ringwood 1966). Since that time, scientists have been formulating core formation hypotheses that attempt to explain these observed mantle depletions, and even after four decades, no one theory is agreed upon. In order to explain the various depletions, Wänke (1981) suggested a heterogeneous accretion hypothesis in which early accreting materials were more reduced than later accreting materials, therefore changing an element's tendency to enter the metallic phase. Revised versions of this hypothesis are still strongly supported, most recently by Rubie et al. (2011). Equilibrium metal-silicate partitioning experiments at 1 bar produced partition coefficients [$D_i = c_i$(metal)/c_i(silicate)] that were too large to explain the observed mantle depletions, leading to the inefficient core formation hypothesis (Jones and Drake 1986), which states that some metal was left behind in the mantle and later oxidized and homogenized. However, over the last 15 years, partitioning experiments conducted at pressures above 1 bar suggest that the required D values of certain siderophile elements may be attainable at higher pressures, leading to the promotion of the magma ocean hypothesis (e.g. Li and Agee 1996, Righter et al. 1997, Gessmann and Rubie 2000,

Chabot and Agee 2003, Chabot et al. 2005, Righter et al. 2008, Cottrell et al. 2009, Righter 2011).

The magma ocean hypothesis gained popularity in the 1980's due to strong geophysical evidence. Numerical simulations of planetary accretion showed that large impacts were common during the later stages of accretion (Wetherill 1985, Canup and Agnor 2000). The energy released from these impacts would have produced enough heat to partially or even completely melt Earth, causing localized or global magma ocean(s) (Melosh 1990, Tonks and Melosh 1993). The magma ocean scenario outlined by Stevenson (1990) states that liquid metal droplets would separate out of the liquid silicate and sink to the peridotite liquidus/solidus region, where final equilibration would occur. The metal would eventually sink through the solid silicate as large diapirs. In this scenario, the last point of metal-silicate equilibration would be at the bottom of the magma ocean. In order to understand this equilibration process, high pressure partitioning experiments are needed. The first and most substantial geochemical support for this hypothesis came from experiments on Ni and Co. Li and Agee (1996) determined that D_{Ni} and D_{Co} become less siderophile with increasing pressure and converge to give the required D values at temperatures above 2000 °C and a pressure of ~28 GPa, suggesting a magma ocean of depth 750-1100 km. Other studies have corroborated this result and with the expanded experimental database, concluded that the Ni and Co abundance in the mantle can be explained by equilibrium core formation out of a magma ocean of sufficient depth (e.g. Righter et al. 1997, Li and Agee 2001, Chabot et al. 2005, Bouhifd and Jephcoat 2011).

Molybdenum is an ideal element for studying core formation. It is refractory, so there is no need for a volatility correction to determine its abundance in the bulk Earth (assumed to be chondritic). Molybdenum is also moderately siderophile, as opposed to highly siderophile, thus it is present in the mantle in great enough abundance to measure with some accuracy. Yet, compared to Ni and Co, experimental data on Mo are sparse, and parameterizations of the existing data may bias the effects of certain parameters (i.e. pressure, P, and temperature, T) because of the wide range of experimental conditions from various studies in which multiple variables are changed simultaneously. Experiments which employ the typical alumina, magnesia, or graphite capsules are at a disadvantage in this respect because these materials drastically change the silicate (alumina and magnesia) and metal (graphite) compositions during the experiment. Furthermore, MgO contamination from a magnesia capsule has been shown to increase as temperature increases (Righter et al. 2010), making it difficult to distinguish between the two effects; and C addition to the metal phase has been shown to have a large effect on element partitioning (Jana and Walker 1997b). In this study, we avoided unwanted silicate and metal phase contamination by performing Mo solubility experiments (solubility experiments = pure metal phase), in which the desired metal phase, in this case Mo, was the capsule material. This makes it easy to hold composition constant as changes in P and T are made, in order to elucidate the effects of each variable. In addition, O'Neill et al. (2008) noted that partition coefficients determined directly from partitioning experiments, when extrapolated to the same conditions, do not agree with those calculated from solubility experiments. Our solubility experiments will allow us to address this discrepancy.

In the current study, we present results from the first Mo solubility experiments conducted at high pressure. Previous solubility studies, investigating the effect of oxygen fugacity, determined that the valence state of Mo changes from 4+ to 6+ at approximately 1 log unit below the iron-wüstite buffer (-1ΔIW) using an anorthite-diopside eutectic composition at 1 bar (Holzheid et al. 1994, O'Neill and Eggins 2002). Additionally, O'Neill and Eggins (2002) looked at the effect of silicate melt composition in FeO-free systems, and Holzheid et al. (1994) looked at the effect of temperature over the range of 1349-1438 °C. The present study has filled in gaps in the data set by examining the effect of silicate melt composition in systems that contain FeO, and expanding the P-T space covered to 12 GPa and 2200 °C. This was done in order to identify pressure, temperature, and compositional trends, to further constrain the conditions of core formation, and to determine if the observed mantle Mo depletion is compatible with the magma ocean hypothesis. This work is the first part of a comprehensive study that involves both solubility and partitioning experiments in order to fully understand the behavior of Mo in silicate melts.

2.2 Methods

2.2.1 Strategy

We conducted a systematic study of Mo solubility in which 43 new experiments were performed. Pressure, temperature, and silicate composition were examined by holding all parameters constant, except the one in question, in order to elucidate the specific effects of each. This was done over a wide range of pressure, temperature, and compositional space: 2.5-12 GPa 1585-2200 °C, and with silicate compositions that

varied in degree of polymerization from peridotite to andesite. The Mo source for all of our experiments was the Mo capsule, and we ran all of our experiments using a multi-anvil press, in contrast to the traditional metal loop technique used in most solubility experiments. This is similar to the approach of Ertel et al. (2006), who used a piston cylinder and multi-anvil to investigate Pt solubility. One advantage of this method is the ability to do experiments at pressure, but the tradeoff with using the multi-anvil is that oxygen fugacity cannot be independently controlled (see Section 2.3.3 for full discussion).

2.2.2 Starting materials

Eight different starting silicate compositions were employed in this study, including both natural and synthetic materials (Table 2-1). The natural compositions included a powdered basalt, NB219, from southeastern Oregon (Draper 1991) and the USGS andesite standard, AGV-2, that was fired at 1000 °C for 1 hour to remove water. Synthetic compositions included two peridotitic compositions that differed in Mg# (89 and 81); two high FeO, high TiO_2 ultramafic compositions (Apollo 14 black glass); and two low FeO, high TiO_2 ultramafic compositions. The peridotitic compositions best represent the primordial mantle composition; however, the other compositions were examined to obtain a thorough understanding of the effects of silicate melt composition on Mo solubility. The synthetic compositions were prepared from reagent grade oxide/silicate powders at the Institute of Meteoritics. The powders were mixed under ethanol, which was then evaporated off in a 100 °C oven. Iron was added as Fe_2SiO_4 and Ca as $CaSiO_3$ and "CaO" (see Appendix for details). The Mo capsules and lids were machined at Arizona State University from high purity Mo rods.

2.2.3 Experimental

The starting silicate compositions were loaded into molybdenum capsules that were sealed with a friction fit lid. All experiments were performed on Walker-type multi-anvil presses at the Institute of Meteoritics (IOM) using the same cell assembly, procedures, and pressure calibrations found in Agee et al. (1995). Briefly, octahedra cast from Aremco Ceramacast® 584 ceramic were used as the compression medium. They were fitted with rhenium heaters and temperature was measured with W/Re thermocouple wires inserted perpendicular to the rhenium heater and temperature was monitored with a Eurotherm 3504 controller. The octahedron assembly was surrounded by eight tungsten-carbide cubes with 8 mm truncated edges. Run times for the experiments were 2-120 minutes depending on the P-T conditions of the run. The run times were limited by Re heater instability. The heater tended to fail after ~2 minutes for high temperature (>2000 °C) runs. The heater was more stable for lower temperature (<1800 °C) runs, but still tended to fail after ~1 hour. However, these run times are comparable to previous work (Righter et al. 1997, Ertel et al. 2006) and a full discussion of the approach to equilibrium is found in Section 2.3.2. A run was quenched by cutting the power to the system, after which the temperature fell below 200 °C in <30 s.

2.2.4 Analytical

All experimental run products were analyzed on a JEOL 8200 Electron Probe Microanalyzer (IOM). An accelerating voltage of 15 keV, 20 nA beam current, and a 20 μm spot size were employed. A list of the standards utilized can be found in the Appendix. Molybdenum was assumed to be in the form of MoO_2 in the silicate melt due to the experiment saturation in Mo metal. All compositional data can be seen in the Table

2-2. The detection limit for Mo on this instrument is ~120 ppm and the lowest concentration of Mo in the melt is 1.05 wt.% so we were well above the detection limit. The large concentration of Mo dissolved in the silicate brings the question of whether the experiments are in the range of Henry's Law behavior. Molybdenum and tungsten are in the same group of the periodic table, and therefore should have similar geochemical behavior. Ertel et al. (1996) showed that WO_2 is Henrian in silicate melts up to 14 wt.%, which is twice the highest MoO_2 composition in our experiments. Additionally, we have performed Mo partitioning experiments in MgO capsules where the bulk Mo concentration was varied, and Henry's Law behavior holds through our highest Mo concentration of 12 wt.% (see Chapter 3).

Some of the silicate melts contained evenly dispersed Mo metal quench features (Figure 2-1a) that were most prominent at low pressure in the black glass compositions. However, there were also larger, heterogeneously dispersed Mo metal blebs found in some samples. When these blebs and the surrounding silicate were analyzed as oxides with the microprobe broad beam, the totals were well above 100%, due to the incorrect assignment of oxygen to the Mo in the metal bleb. These blebs were easily avoided when analyzing the silicate.

2.3 Results

2.3.1 Textures and phase relations

In the typical run products, the solid Mo capsule formed a distinct boundary around the quenched silicate. In the peridotitic melts, the liquid silicate did not quench to a glass, but formed elongated crystals and melt pockets upon quench (Figure 2-1a). At

high temperatures (>2000 °C) and pressures (>4 GPa) in the black glass composition, a separate solid MoFe metal phase would form, presumably due to the large amounts of iron found in this composition. This phase was usually accompanied by a liquid metal phase (Figure 2-1b), similar to that found in Cottrell et al. (2009) for their W capsule experiments. The solid metal composition was ~97.5 wt.% Mo and 2.5 wt.% Fe. The liquid metal phase showed a dendritic quench texture with the bright phase having a similar composition to the solid metal phase. The darker phase surrounding the quench texture was found to contain a small amount of dissolved oxygen, identified by EDS. Broad beam analysis over the quenched area yields a composition of ~80 wt.% Mo, 12 wt.% Fe, and < 2 wt.% other components (SiMgAlCaMnZrTi), suggesting ~2-6 wt.% oxygen in the liquid metal. This result is in line with studies done on the solubility of oxygen in liquid iron-nickel, iron-tungsten, and iron-molybdenum alloys (Tankins et al. 1965, Rubie et al. 2004). Tankins et al. (1965) and Floridis and Chipman (1958) also showed that in an Fe-rich liquid, the activity coefficient of oxygen increases more upon addition of W to the metal phase than upon Mo addition. This explains why no dissolved oxygen was reported in the liquid metal phase of Cottrell et al. (2009), for their W capsule experiments. In the case of experiment #7, the presence of the Fe-containing metal phase significantly depleted the silicate melt in FeO and is therefore not shown in the constant composition plots for black glass 1.

2.3.2 Approach to equilibrium

Great care was taken to ensure that the experiments reached a steady state in terms of Mo concentration in the melt, and multiple assessment techniques were used to prove as such. Traverses across run products showed no diffusion gradients in Mo

concentration, as would be expected if the experiments were not at a steady state. Two experiments (#42-43) using the peridotite 1 starting composition were below the liquidus and crystallized olivine, allowing for the calculation of Fe-Mg Kd values. At 1950 °C and 3.5 GPa, the Kd value was 0.34 ± 0.03 and at 2100 °C and 6.5 GPa, the Kd value was 0.37 ± 0.02. Both of these values are in agreement with the Toplis (2005) predicted equilibrium values of 0.31 and 0.37, respectively. This demonstrates the increase in equilibrium Kd values with pressure noted by Ulmer (1989), although the increase is not as extreme as that paper showed. Additionally, a suite of time-series experiments were conducted and the results can be seen in Figure 2-2. The results indicate that a steady state was reached in 90 minutes at 1585 °C, 60 minutes at 1650 °C, and in 2 minutes at 2000 °C.

2.3.3 Oxygen fugacity

In high pressure partitioning experiments, oxygen fugacity is usually determined relative to the iron-wüstite (IW) buffer using the amount of Fe in the metal and the amount of FeO in the silicate. In our experiments, there was no iron in the metal so we employed a different approach. The oxygen fugacity of our experiments was controlled by the Mo capsule, keeping it relatively constant below the Mo-MoO_2 (MMO) buffer. The amount of Mo that goes into the melt obeys the relationship,

$$Mo + O_2 \leftrightarrow MoO_2 \tag{2-1}$$

therefore, the oxygen fugacity of each experiment can be approximated relative to the MMO buffer according to

$$\Delta MMO = \log\left(\frac{a_{MoO_2}^{silicate}}{a_{Mo}^{metal}}\right) \tag{2-2}$$

where a is the activity of MoO_2 in the silicate and Mo in the metal. In pure Mo, a_{Mo}^{metal} is equal to 1, so $a_{Mo}^{metal} = X_{Mo} = 1$. By assuming ideal behavior, $a_{MoO_2}^{silicate}$ can also be replaced with X_{MoO_2}, in order to calculate ΔMMO. The oxygen fugacity relative to the MMO buffer was calculated in this way for each experiment (Table 2-2). A source of error in this approximation of oxygen fugacity is that pressure and temperature also affect how much Mo dissolves into the silicate. This was taken into account by averaging the ΔMMO for all the experiments done on a particular composition, and using the averaged value as the ΔMMO for every experiment done on that composition (Table 2-3). This approach is justified by the following: since the Mo capsule is ubiquitous in the experiments, the only way to change the relative oxygen fugacity is to change the oxygen content of the silicate composition. Therefore, all experiments done on the same silicate composition should have the same ΔMMO. However, in our two lowest T experiments (#1-2), a stable MoO_2 phase formed, indicating the oxygen fugacity of these two experiments is near the MMO buffer, see Table 2-3.

In order to compare our results to previous work that report oxygen fugacity relative to the IW buffer, and to better relate them to Earth's core formation, the ΔIW for each experiment must be known. Campbell et al. (2009) showed that pressure has a large effect on the IW buffer curve, causing it to shift upward to increasing oxygen fugacity values as pressure is increased. The effect of pressure on the MMO buffer curve has not yet been determined experimentally; therefore, we calculated the MMO buffer curve at pressure to see how it relates to IW. This was done using Equation 6 of Campbell et al. (2009),

$$\log fO_2 = \log fO_2(1bar) + \frac{0.4343}{RT}\int \Delta V dP \qquad (2\text{-}3)$$

where T is temperature in Kelvin, P is pressure in GPa, and ΔV is the volume change between the oxide and the metal of the buffer species in question. The constant is half of that in their equation because of the 4+ valence of Mo compared to the 2+ of Fe. We calculated the volume of the buffer species at pressure using the Murnaghan equation of state (EOS),

$$V(P) = V_o\left(1 + B'_o \frac{P}{B_o}\right)^{-\frac{1}{B'_o}} \qquad (2\text{-}4)$$

where V_o is the volume at standard state, B_o is the isothermal bulk modulus, and B'_o is the pressure derivative of the isothermal bulk modulus. These parameters were obtained for Mo from the database of Fried et al. (2002) and the 1 bar MMO buffer of O'Neill (1986) was used. For consistency, we also used the parameters of Fried et al. (2002) and the 1 bar buffer of O'Neill and Pownceby (1993) to calculate the IW buffer in order to determine the difference between the MMO and IW buffer curves at the pressure of our experiments. Using the EOS or experimental data (as in Campbell et al. 2009) to determine ΔV gives very similar results for the IW buffer, as can be seen in Figure 2-3. The MMO buffer curve relative to the IW buffer can be seen in Figure 2-4. At higher temperatures, the MMO buffer is more oxidizing than the IW buffer, but the difference between MMO and IW decreases slightly as pressure increases. Once these two buffers were known, we were then able to calculate the oxygen fugacity of our experiments relative to IW (Table 2-3). It should be emphasized that this is just an estimation of oxygen fugacity, and the data plots discussed below have not been corrected to constant ΔIW to avoid introducing error. The approach outlined above is the same as that used by

Cottrell et al. (2009) for their W capsule experiments except they used the difference between the IW and W-WO_2 buffers at 1 bar to determine ΔIW. An error assessment of this method is found in the Appendix.

2.3.4 Effect of temperature, pressure, and silicate composition

Compared to the previous solubility studies, our experiments contained much more Mo dissolved in the silicate for experiments at similar oxygen fugacities (-1ΔIW). Holzheid et al. (1994) and O'Neill and Eggins (2002) reported Mo concentrations at the ppm-level, whereas all of the solubilities reported here are at the weight percent-level. This difference is not surprising considering the vastly different silicate compositions employed. Previous work resided solely in the CMAS system, and silicate composition can have large effects on an element's behavior in silicate melts (e.g. Jana and Walker 1997a). Additionally, the P-T conditions used in the present study are much higher, suggesting that increasing P and T will cause an increase in solubility. Our data set lends itself nicely to examining the effects of individual parameters because of the systematic approach.

The effect of temperature can be seen in Figure 2-5a. The plot shows the temperature data for the black glass 1 experiments because it is our largest isobaric, constant composition data set. As temperature was increased, solubility increased at constant relative oxygen fugacity. This is the same relationship determined by Holzheid et al. (1994) at lower temperatures, indicating a consistent increasing trend over a T range of 1622-2273 K. The effect of pressure on molybdenum solubility can be seen in Figure 2-5b. The plot shows three different isothermal data sets for three different silicate compositions. All three data sets show that at constant relative oxygen fugacity, over the

pressure range investigated here, pressure has a negligible effect on Mo solubility. A direct comparison with previous lower pressure work is difficult because of the different temperatures and silicate compositions. As mentioned above, the higher concentration of Mo found in our high P-T experiments compared to previous low P-T experiments, suggests that increasing pressure would cause solubility to increase; however, the concentration difference could be solely due to temperature and compositional effects.

The silicate compositions used in the current study covered the NBO/T (ratio of non-bridging oxygens to tetrahedrally coordinated cations, Mysen 1983) range of 0.2-3.25. Overall, solubility increases as melt polymerization decreases (NBO/T increases, Figure 2-6), but there is significant scatter in the data. Similarly, O'Neill and Eggins (2002) determined that the compositional trend was better represented by looking at the effect of individual oxides, i.e. CaO. Due to the scatter on Figure 2-6, we will also employ that method here and examine our constant P-T data more closely. The difference between exp #20 and #30 is an increase in TiO_2 and MgO and a decrease in SiO_2 (Table 2-2), which caused solubility to increase. This is expected because Mg^{2+} is a network modifier, which decreases polymerization and would cause an increase in solubility, and Si^{4+} is a network former, which increases polymerization and would cause solubility to decrease. Our calculation of NBO/T placed Ti^{4+} as a network former (similar to Si^{4+}, Mysen 1983), causing a decrease in NBO/T, which would be expected to cause a decrease in Mo solubility. This is the opposite of what we see here and could account for some of the scatter in Figure 2-6. O'Neill and Eggins (2002) also investigated the effect of TiO_2 and suggested that Ti opens sites in the melt structure that are favorable to Mo because of their similar charge (4+) and size (0.68 Å ionic radius). The difference

between exp #19 and #6 is a ~3wt.% increase in ZrO_2, this increase caused solubility to increase. The effect of ZrO_2 can be explained similarly to that of TiO_2. ZrO_2 also has a 4+ valence and a slightly larger ionic radius of 0.79 Å and therefore may open up melt structural sites that are favorable to Mo. The most surprising compositional effect is the difference between exp #32 and #40 where there is an increase in SiO_2 and a decrease in MgO and CaO. This would be expected to cause a decrease in solubility based on melt polymerization; however, the opposite occurs, possibly because of the presence of the K^+ ion in the andesite composition (exp# 40), which may open melt structure sites simply due to its large size (1.33 Å). In summary, because the individual oxides appear to be having more of an effect on Mo solubility than that simply due to changes in melt polymerization, in the following parameterization we will use oxide mole fractions to account for silicate composition (as in Righter and Drake 1999) instead of a universal melt parameter, such as NBO/T.

2.4 Discussion

2.4.1 Calculating partition coefficients from solubility data

In order to apply our solubility data to core formation, they must be converted to metal-silicate partition coefficients in which the metal phase is Fe-rich. To do this, we used the method outlined by O'Neill et al. (2008) which employs the activity coefficient of molybdenum at infinite dilution in iron ($\gamma^{Feliq,\infty}$). The calculated $\gamma^{Feliq,\infty}$ values for our experiments were between 1.026 and 1.524, depending on the temperature of the experiment, with the higher temperature runs being closer to ideal. The amount of molybdenum dissolved in the silicate is inversely related to partition coefficient, and our

calculated partition coefficients can be seen in Table 2-3. For consistency, we also used the O'Neill et al. (2008) method to calculate D values for all the previous solubility experiments of Holzheid et al. (1994), O'Neill and Eggins (2002), and Holzheid and Palme (2007). See Appendix for more details.

2.4.2 Parameterization and comparison to partitioning data

The 43 new experiments presented here greatly expand the Mo data set found in the literature, and the following parameterization includes both solubility and partitioning data. The solubility data include those from the present work (exps #41-43 were kept out to serve as an independent check), 18 from Holzheid et al. (1994), 2 from Holzheid and Palme (2007), and 17 from O'Neill and Eggins (2002). The partitioning data included 9 from Hillgren (1993), 17 from Walter and Thibault (1995), 4 from Righter et al. (1997), 2 from Jana and Walker (1997a), 2 from Jana and Walker (1997b), 2 from Hillgren et al. (1996), 2 from Ohtani et al. (1997), 3 from Wade and Wood (2001), 9 from Righter et al. (2010), and 11 from Siebert et al. (2011). Righter (2011) compared two different parameterization approaches for accounting for trace siderophile elements in the metal phase, one using ε interaction parameters (as in Wade and Wood 2005), the other using empirical terms that resemble the Margules parameter (as in Righter et al. 1997). It was found that both approaches produce the same extrapolated result, so we adopted an approach similar to that of Righter et al. (1997) and parameterized all the data according to

$$\log D_{Mo} = a\Delta IW + b\frac{1}{T} + c\frac{P}{T} + \sum d_i X_i + e\left[\log\left(1 - X_C\right)\right] + f\left[\log\left(1 - X_S\right)\right] + g\left[\log\left(1 - X_{Si}\right)\right] + h \quad (2\text{-}5)$$

where D_{Mo} is the metal-silicate partition coefficient, ΔIW is the oxygen fugacity relative to the iron-wüstite buffer, T is temperature in Kelvin, P is pressure in GPa, X_i is the mole fraction of oxide i in the silicate phase, X_C, X_S, and X_{Si} are the mole fraction of carbon, sulfur, and silicon in the metal phase, respectively, and a-h are linear regression coefficients. It is important to note that Equation 2-5 is an empirical fit to the data and has been criticized for violating the Gibbs-Duhem equation (see Righter 2011). O'Neill and Eggins (2002) applied a regular solution model to define the silicate composition for their experiments because it obeys the Gibbs-Duhem equation. This model does not predict the data as well as the empirical approach and was therefore not used; however, the Appendix contains a detailed comparison of the two parameterization approaches for accounting for silicate composition. The coefficients we determined are listed in Table 2-4. Our parameterization is different from the most recent previous comprehensive parameterization for Mo (Righter et al. 2010), in that it includes a TiO_2 term, because many of the silicate compositions have large amounts of Ti, and an X_{Si} term, because two of the experiments in Wade and Wood (2001) have large amounts of Si in the metal phase.

How well the expression fits the data can be seen in Figure 2-7. The three experiments kept out of the regression were the two below the peridotite liquidus and our highest pressure (12 GPa) experiment, and the parameterization does an excellent job at predicting their D values. Furthermore, the parameterization does just as well predicting D values from partitioning experiments as it does from solubility experiments. For example, if only the solubility experiments are plotted in Figure 2-7, the R^2 value is 0.97, and 0.92 if only the partitioning data are plotted, indicating good fits to both types of

data. The discrepancy noted by O'Neill et al. (2008), as they suggested, was probably due to a wide range of metal phase compositions, and once those are taken into account, as in the present parameterization, the data are in agreement. A critique of previous parameterizations is that the included experiments were conducted over a wide range of conditions without focusing on the individual effects of each parameter, which may lead to errors in the predicted trends. The addition of our data set, which was obtained systematically, will minimize this problem in the present parameterization.

The *a* coefficient of -1.12 yields an apparent Mo valence of 4.5+; however, this more likely suggests a mixed valence, with 4+ being the dominant valence and minor contribution from 6+. This is similar to what previous studies have determined (e.g. Righter et al. 2010, Siebert et al. 2011). Plots of the effect of temperature and pressure predicted by the parameterization can be seen in Figure 2-8. The parameterization predicts D_{Mo} to decrease with increasing temperature, which is in agreement with our solubility data. It is also in agreement with the partitioning data of Walter and Thibault (1995), Siebert et al. (2011), and Righter et al. (2010) for their graphite capsule experiments. The parameterization predicts a moderate decrease in D with pressure, a 0.2 drop in logD over the pressure range of our black glass 1 experiments (2.5-9.7 GPa). This trend is in agreement with the MgO capsule data of Siebert et al. (2011) and the predicted pressure effect of Righter et al. (2010), both showing D_{Mo} decreasing with increasing pressure. It is in contrast to our solubility data that showed no clear pressure trend. However, the 0.2 decrease predicted is within the scatter of our isothermal, constant composition datasets, so it could be that the change is too small to notice or is within the error caused by the scatter. Another possibility is that the pressure trend is being

erroneously influenced by previous partitioning work that increased T while also increasing P (e.g. Walter and Thibault 1995). However, if only the solubility data are parameterized, the pressure trend is the same, so we do not believe this is the case. A final possibility is that the pressure trend is not linear over the entire pressure range, as assumed by the parameterization. Increasing pressure could cause D_{Mo} to decrease at low pressures, but level out at higher pressures. 46 of the 136 experiments parameterized were at 1 bar, which could be dominating the pressure trend. This could also explain the large error (almost 33% relative error) on the P/T regression term. However, more experiments at higher pressures will need to be performed before there is enough data to say for certain.

The use of individual oxides in the parameterization does well at predicting D values from experiments performed on a wide range of silicate compositions. According to our solubility data, D_{Mo} decreases with increasing NBO/T, as also shown by Walter and Thibault (1995) and Jana and Walker (1997a), but the opposite of the effect Righter et al. (2010) determined. This contradiction is probably due to the varying effects of the different oxides, as noted by Righter et al. (2010) and as discussed in Section 2.3.4, and demonstrates the importance of taking this into account. The large coefficients on the light element terms in the parameterization indicate that the metal phase composition has a large effect on Mo partitioning. Addition of carbon causes an increase in D_{Mo}, whereas addition of sulfur and silicon cause a decrease in D_{Mo}. This effect appears to be especially important for Si; however, this result is based on only two experiments (Wade and Wood 2001). The parameterization included 25 experiments that contained carbon and 9 that contained sulfur, demonstrating the need for more data on the effect of light elements.

2.4.3 Implications for core formation

The parameterization equation and regression coefficients determined above can be used to find core formation conditions that would produce the observed mantle abundance of Mo. By using this abundance and assuming a CI chondrite bulk Earth, the amount of Mo in the core can be calculated by mass balance. From this, the required D needed to explain the observed mantle abundance is 40-100, this range takes into account the different bulk silicate Earth and CI Mo abundances measured by Newsom (1995), McDonough and Sun (1995), Palme and O'Neill (2003), and McDonough (2003). To determine a P-T solution set, we kept silicate composition constant, using KLB-1 peridotite (Davis et al. 2009), which has an NBO/T of 2.73. Oxygen fugacity was also kept constant at -2.2ΔIW, calculated from the present day FeO and Fe contents in the mantle and core, respectively (McDonough 2003). By assuming the magma ocean scenario described in the introduction, in which no entrainment of the metal phase occurs, a further constraint that can be placed on the P-T conditions is that they must lie on the peridotite liquidus. By applying these constraints to our parameterization, we determined that D_{Mo} will reach the required values between 40 and 54 GPa and 3050-3400 K if no light elements are considered. As can be seen in Figure 2-9, these conditions lie on the peridotite liquidus. They are also comparable with those suggested by Chabot et al. (2005) of 30-60 GPa and >2000 K based on Ni and Co partitioning and just overlap with the high end of those suggested by Cottrell et al. (2010) of 10-40 GPa and 2300-3100 K based on W partitioning. The particular set of P-T conditions determined here could be indicative of single-stage core formation. A large impact near the end of Earth's accretion may have produced enough melting to cause large-scale re-equilibration; therefore, the

mantle abundances reflect only the deep magma ocean conditions of final equilibration, as suggested by Righter (2011). Taking the effect of the light elements into account greatly expands the possible P-T range. Since C has the opposite effect of S and Si on D_{Mo}, there are many combinations of light elements that would still be compatible with single-stage core formation. Addition of Si and/or S to the core would lower the P-T conditions, whereas adding C would increase the P-T conditions. If we assume the core contains 6 wt.% Si, 2 wt.% S, and 0.2 wt.% C (based on cosmochemical abundance, McDonough 2003), the required near-liquidus P-T range changes to 19-27 GPa and 2500-2750 K, Figure 2-9.

These sets of workable conditions could also reflect the average conditions from multiple impact events over the time period of accretion. Earth accreted from a series of impacts and it has been shown that heat from these impacts will begin to melt Earth when it has reached 10% of its present mass (Canup and Agnor 2000, Melosh 1990). Therefore, core formation was a continuous process with the P-T conditions increasing as the size of Earth increased. When Earth was small, the P-T trends determined here show that early D_{Mo} values would be very high, causing a very low Mo mantle abundance. As accretion progressed and the size of Earth and the impactors increased, the depth of the magma ocean would increase, causing equilibration to be at higher P-T and D_{Mo} to be much smaller, increasing the Mo mantle abundance. Unlike the single-stage model, the multi-stage model implies that these final impacts did not completely erase the chemical signature from previous equilibration events. The mantle signature we see today would be the combined result of these events. Recent multi-stage core formation models also call upon progressive oxidation in order to explain the mantle abundance of certain

siderophile elements, mainly V and Cr (Wade and Wood 2005, Wood et al. 2009, Rubie et al. 2011). Figure 2-10 shows the average D_{Mo} values for three different multi-stage models, one with constant oxygen fugacity and two with progressive oxidation, both using the parameterization determined here. Both Wood et al. (2009) models produce final average D values that can explain the observed mantle abundance of Mo. It is interesting to note that changing the oxidation state from -4.25 to -2.26ΔIW results in the same final D_{Mo} value as keeping the oxygen fugacity at a constant -2.26ΔIW throughout accretion. However, adjusting the depth of the magma ocean (35 to 46% of the depth to the core-mantle boundary, CMB) does significantly change the final D value. The Wade and Wood (2005) model assumes metal-silicate equilibration at the base of a magma ocean that is 46% of the depth to the CMB throughout accretion, which produces a final D_{Mo} value too low to explain the observed depletion. This is because, even though the chemical signature from previous low P impacts is not being completely erased, Mo is so siderophile in the early stages of accretion that these impacts do not contribute much Mo to the mantle. As the impacts become larger and the P-T conditions of equilibration increase, Mo becomes much less siderophile and it is these final impacts that impart the majority of Mo to the mantle. Due to the magma ocean depth being fixed at 46% of the CMB, the final impacts in the Wade and Wood (2005) model are at P-T conditions too high (up to 60 GPa) to result in the required D_{Mo}. The final impacts in the Wood et al. (2009) model are at lower P-T conditions and produce D values in the required range. This indicates that both single-stage and multi-stage models work for Mo as long as the base of the magma ocean for the multi-stage model is between 31 and 42% of the depth to the CMB.

2.5 Conclusions

A downfall of partitioning experiments employing magnesia or alumina capsules is the inability to change the P and T of an experiment without simultaneously changing the silicate composition. The solubility experiments performed here with Mo capsules enabled us to avoid this problem and elucidate the specific effects of P, T, and silicate composition. Additionally, this work greatly increased the number of Mo experiments in the literature (especially at high pressure) and a total of 136 experiments were parameterized, yet this is still a far cry from the >300 that have been performed on both Ni and Co. In particular, more data are needed at higher pressures and that specifically address the effect light elements have on partitioning.

Parameterization of our data and literature data allowed us to determine a predictive expression for D_{Mo}. This expression was able to accurately predict partition coefficients calculated from solubility data and those determined directly from partitioning experiments, indicating there is no discrepancy between D values determined by the two different methods. Furthermore, we determined that Mo is compatible with both single-stage and multi-stage magma ocean models for core formation. We narrowed the suggested P-T conditions found in the literature for the single-stage model by constraining them to 40-54 GPa along the peridotite liquidus. Lastly, we further constrained the multi-stage core formation models by placing limits on the depth of metal-silicate equilibration during the final impacts of accretion.

Table 2-1. Compositions of the eight different starting materials in wt.% and their calculated NBO/T values. Compositions were determined from averaging the probe measurements of each experiment done on the same composition after correcting for the Mo content.

	peridotite 1	peridotite 2	black glass 1	black glass 2	Ti-rich 1	Ti-rich 2	basalt	andesite
SiO_2	45.7	47.2	35.0	35.3	30.8	35.1	48.9	58.5
TiO_2	-	-	13.4	15.5	10.4	14.0	0.6	1.0
Al_2O_3	6.1	7.9	5.2	4.8	4.2	17.1	17.9	19.2
FeO	8.3	12.1	23.4	23.5	9.6	8.7	8.5	5.7
MgO	36.9	28.9	13.9	13.5	41.9	14.2	10.5	2.6
CaO	2.8	4.5	5.1	6.7	2.5	5.3	11.4	5.0
K_2O	-	-	-	-	-	-	-	2.9
MnO	-	-	0.4	0.3	-	0.3	-	0.1
Na_2O	-	-	-	0.2	-	-	2.2	4.0
SrO	-	-	0.2	-	-	0.3	-	-
ZrO_2	-	-	3.0	-	-	3.3	-	-
P_2O_5	-	-	-	-	-	-	-	0.4
Cr_2O_3	-	-	-	0.9	-	-	-	-
TOTAL	99.8	100.7	99.7	100.7	99.3	98.3	99.9	99.4
NBO/T	2.3	1.9	1.7	1.7	3.2	0.7	0.8	0.2

Table 2-2. Microprobe data for all experiments in wt.% and the ΔMMO values calculated for each experiment as described in Section 3.3. The numbers in parentheses are standard deviations of the probe measurements, np = not probed.

Exp #	SiO_2	TiO_2	Al_2O_3	FeO	MgO	CaO	K_2O	MnO	Na_2O	SrO	ZrO_2	P_2O_5	Cr_2O_3	MoO_2	**TOTAL**	# of analyses	ΔMo-MoO_2
1	34.04 (0.33)	12.89 (0.18)	4.93 (0.08)	23.71 (0.23)	13.56 (0.36)	4.77 (0.24)	np	0.29 (0.02)	np	0.11 (0.04)	2.98 (0.14)	np	np	2.58 (0.37)	99.85 (0.42)	23	-0.18
2	33.59 (0.37)	12.64 (0.49)	4.86 (0.19)	24.21 (0.48)	13.19 (0.47)	4.68 (0.46)	np	0.38 (0.02)	np	0.15 (0.09)	2.91 (0.19)	np	np	3.27 (0.44)	99.89 (0.76)	24	-0.17
3	31.38 (0.72)	12.40 (0.24)	5.05 (0.11)	23.56 (0.39)	12.80 (0.43)	4.55 (0.29)	np	0.36 (0.01)	np	0.22 (0.05)	2.76 (0.10)	np	np	5.80 (1.43)	98.87 (0.68)	27	-1.53
4	32.04 (0.74)	12.49 (0.37)	4.68 (0.11)	23.77 (0.49)	12.66 (0.49)	4.59 (0.25)	np	0.35 (0.02)	np	0.22 (0.06)	2.84 (0.15)	np	np	6.31 (1.71)	99.97 (0.59)	24	-1.49
5	31.39 (0.51)	12.16 (0.53)	4.57 (0.29)	23.85 (0.49)	11.97 (0.78)	4.95 (0.57)	np	0.44 (0.02)	np	0.25 (0.10)	2.83 (0.21)	np	np	5.93 (0.70)	98.33 (0.66)	27	-1.51
6	31.66 (0.73)	12.21 (0.27)	5.30 (0.22)	21.98 (0.42)	12.72 (0.41)	4.50 (0.16)	np	0.37 (0.02)	np	0.24 (0.04)	2.72 (0.11)	np	np	7.12 (1.44)	98.80 (0.45)	28	-1.44
7	33.79 (0.38)	13.29 (0.26)	5.19 (0.15)	19.72 (0.36)	13.43 (0.19)	5.02 (0.09)	np	0.37 (0.01)	np	0.23 (0.05)	2.96 (0.07)	np	np	4.45 (0.61)	98.44 (0.45)	20	-1.65
8	31.95 (1.43)	12.22 (0.66)	4.67 (0.21)	24.24 (0.56)	12.80 (0.86)	4.82 (0.50)	np	0.46 (0.03)	np	0.25 (0.13)	2.92 (0.49)	np	np	4.70 (1.73)	99.03 (0.77)	41	-1.62
9	33.11 (0.66)	12.88 (0.23)	4.80 (0.13)	21.84 (0.37)	13.14 (0.56)	4.77 (0.18)	np	0.41 (0.02)	np	0.27 (0.04)	2.87 (0.21)	np	np	5.67 (1.27)	99.75 (0.37)	21	-1.54
10	32.09 (1.44)	12.60 (0.50)	4.89 (0.32)	23.54 (0.56)	13.16 (0.60)	4.71 (0.37)	np	0.43 (0.02)	np	0.21 (0.12)	2.83 (0.64)	np	np	5.75 (1.22)	100.22 (0.73)	40	-1.54
11	33.01 (0.66)	12.30 (0.19)	4.82 (0.09)	23.46 (0.37)	13.27 (0.32)	4.53 (0.21)	np	0.37 (0.02)	np	0.18 (0.07)	2.65 (0.20)	np	np	4.83 (1.05)	99.44 (0.40)	19	-1.61
12	33.13 (0.60)	12.93 (0.40)	4.95 (0.18)	21.89 (0.43)	12.85 (0.33)	4.88 (0.42)	np	0.37 (0.02)	np	0.24 (0.13)	2.91 (0.20)	np	np	5.32 (1.04)	99.47 (0.57)	24	-1.57
13	34.01 (0.70)	13.52 (0.16)	5.11 (0.11)	21.51 (0.54)	13.82 (0.38)	5.00 (0.28)	np	0.46 (0.02)	np	0.24 (0.10)	2.97 (0.22)	np	np	3.87 (0.57)	100.50 (0.76)	25	-1.72
14	33.40 (0.34)	12.62 (0.13)	4.96 (0.05)	22.95 (0.39)	13.17 (0.18)	4.67 (0.06)	np	0.42 (0.02)	np	0.22 (0.06)	2.85 (0.16)	np	np	5.06 (0.74)	100.31 (0.37)	12	-1.60
15	34.68 (1.28)	13.23 (0.69)	5.32 (0.11)	20.47 (0.65)	14.10 (0.56)	5.06 (0.15)	np	0.39 (0.02)	np	0.22 (0.10)	3.12 (0.76)	np	np	4.09 (0.43)	100.68 (0.47)	35	-1.70

Table 2-2 (con't). Microprobe data for all experiments in wt.% and the ΔMMO values calculated for each experiment as described in Section 3.3. The numbers in parentheses are standard deviations of the probe measurements, np = not probed.

Exp #	SiO_2	TiO_2	Al_2O_3	FeO	MgO	CaO	K_2O	MnO	Na_2O	SrO	ZrO_2	P_2O_5	Cr_2O_3	MoO_2	**TOTAL**	# of analyses	ΔMo-MoO_2
16	35.25 (1.05)	12.67 (0.45)	5.25 (0.09)	20.40 (1.02)	14.04 (0.45)	4.95 (0.15)	np	0.46 (0.02)	np	0.19 (0.04)	2.83 (0.42)	np	np	4.47 (0.30)	100.51 (0.37)	16	-1.66
17	34.90 (0.82)	13.46 (0.66)	5.21 (0.43)	19.23 (0.57)	14.13 (0.36)	5.14 (0.12)	np	0.40 (0.02)	np	0.26 (0.04)	2.94 (0.16)	np	np	4.06 (0.37)	99.71 (0.35)	24	-1.70
18	35.19 (0.52)	12.99 (0.45)	5.23 (0.07)	20.00 (0.41)	13.56 (0.23)	4.87 (0.06)	np	0.41 (0.01)	np	0.22 (0.03)	3.03 (0.23)	np	np	4.53 (0.16)	100.01 (0.33)	15	-1.65
19	34.35 (0.86)	15.08 (0.22)	4.63 (0.08)	22.85 (0.68)	13.08 (0.34)	6.50 (0.19)	np	0.30 (0.01)	0.15 (0.02)	np	np	np	0.83 (0.21)	2.79 (0.69)	100.58 (0.33)	30	-1.87
20	44.65 (0.43)	np	7.86 (0.63)	6.86 (0.14)	34.00 (1.62)	2.41 (0.20)	np	np	np	np	np	np	np	3.45 (0.50)	99.23 (0.46)	26	-1.83
21	43.00 (0.31)	np	7.06 (0.78)	8.74 (0.12)	33.72 (0.64)	2.74 (0.09)	np	np	np	np	np	np	np	3.85 (0.14)	99.11 (0.34)	20	-1.78
22	42.63 (0.81)	np	5.44 (0.27)	9.28 (0.10)	35.28 (0.55)	2.86 (0.17)	np	np	np	np	np	np	np	4.66 (0.48)	100.14 (0.79)	26	-1.71
23	44.69 (0.80)	np	6.11 (0.68)	7.22 (0.27)	35.16 (1.51)	2.39 (0.35)	np	np	np	np	np	np	np	4.12 (0.63)	99.70 (0.41)	28	-1.76
24	43.42 (0.65)	np	5.20 (0.40)	8.72 (0.25)	34.84 (1.16)	2.85 (0.30)	np	np	np	np	np	np	np	4.50 (0.42)	99.53 (0.57)	25	-1.72
25	42.80 (0.53)	np	5.32 (0.27)	8.70 (0.18)	35.04 (0.85)	2.83 (0.14)	np	np	np	np	np	np	np	3.99 (0.30)	98.67 (0.83)	26	-1.77
26	45.33 (0.54)	np	5.46 (0.53)	7.13 (0.32)	36.52 (1.62)	2.92 (0.34)	np	np	np	np	np	np	np	3.48 (0.47)	100.84 (0.29)	40	-1.84
27	44.86 (0.52)	np	5.46 (0.37)	7.99 (0.30)	36.13 (0.90)	2.82 (0.22)	np	np	np	np	np	np	np	3.50 (0.35)	100.76 (0.35)	50	-1.84
28	44.93 (0.75)	np	5.49 (0.58)	7.04 (0.40)	36.58 (1.74)	2.84 (0.32)	np	np	np	np	np	np	np	3.51 (0.67)	100.38 (0.35)	32	-1.84
29	45.36 (0.43)	np	7.59 (0.28)	11.65 (0.58)	27.80 (0.53)	4.36 (0.15)	np	np	np	np	np	np	np	3.96 (0.61)	100.72 (0.43)	33	-1.76

Table 2-2 (con't). Microprobe data for all experiments in wt.% and the ΔMMO values calculated for each experiment as described in Section 3.3. The numbers in parentheses are standard deviations of the probe measurements, np = not probed.

Exp #	SiO_2	TiO_2	Al_2O_3	FeO	MgO	CaO	K_2O	MnO	Na_2O	SrO	ZrO_2	P_2O_5	Cr_2O_3	MoO_2	**TOTAL**	# of analyses	ΔMo-MoO_2
30	29.44 (1.54)	9.92 (1.36)	4.00 (1.98)	9.16 (0.66)	40.05 (2.18)	2.39 (0.52)	np	np	np	np	np	np	np	4.30 (0.94)	99.26 (0.94)	24	-1.74
31	48.04 (0.30)	0.65 (0.03)	17.93 (0.13)	8.42 (0.06)	9.68 (0.09)	11.54 (0.07)	0.17 (0.01)	0.16 (0.01)	2.25 (0.05)	np	np	0.11 (0.02)	np	1.44 (0.05)	100.38 (0.41)	25	-2.15
32	48.40 (0.27)	0.70 (0.03)	16.73 (0.39)	8.31 (0.08)	10.12 (0.07)	11.44 (0.10)	np	np	2.13 (0.04)	np	np	np	np	1.35 (0.09)	99.18 (0.36)	20	-2.18
33	47.83 (0.47)	0.67 (0.03)	17.50 (0.13)	8.61 (0.06)	10.28 (0.09)	11.36 (0.13)	np	np	2.13 (0.03)	np	np	np	np	1.51 (0.08)	99.89 (0.52)	23	-2.13
34	48.73 (0.28)	0.65 (0.03)	17.61 (0.11)	8.49 (0.07)	9.99 (0.07)	11.56 (0.11)	np	np	2.21 (0.04)	np	np	np	np	1.53 (0.08)	100.77 (0.41)	23	-2.13
35	48.74 (0.37)	0.68 (0.02)	17.65 (0.13)	8.48 (0.10)	9.98 (0.14)	11.52 (0.10)	np	np	2.19 (0.06)	np	np	np	np	1.42 (0.11)	100.65 (0.45)	20	-2.16
36	47.76 (0.46)	0.63 (0.03)	17.24 (0.26)	8.47 (0.15)	10.13 (0.21)	11.19 (0.09)	np	np	2.18 (0.06)	np	np	np	np	1.99 (0.14)	99.56 (0.68)	15	-2.01
37	48.71 (0.27)	0.63 (0.04)	17.23 (0.11)	8.47 (0.21)	10.19 (0.17)	11.49 (0.08)	np	np	2.20 (0.06)	np	np	np	np	1.70 (0.24)	100.61 (0.48)	20	-2.08
38	48.81 (0.25)	0.64 (0.04)	17.16 (0.10)	8.42 (0.11)	10.15 (0.09)	11.28 (0.09)	np	np	2.17 (0.03)	np	np	np	np	2.08 (0.20)	100.71 (0.33)	31	-2.00
39	46.99 (0.47)	0.62 (0.05)	17.64 (0.14)	8.47 (0.25)	9.67 (0.14)	11.70 (0.11)	np	np	2.27 (0.06)	np	np	np	np	1.61 (0.30)	98.97 (0.51)	15	-2.10
40	57.70 (1.79)	0.97 (0.05)	18.95 (1.52)	5.65 (0.16)	2.55 (0.52)	4.93 (0.14)	2.84 (0.18)	0.09 (0.01)	3.90 (0.09)	np	np	0.43 (0.04)	np	1.40 (0.10)	99.41 (0.51)	30	-2.14
41	34.28 (0.55)	13.71 (0.91)	16.68 (1.91)	8.51 (0.33)	13.88 (0.88)	5.13 (0.60)	np	0.27 (0.11)	np	0.26 (0.08)	3.23 (0.32)	np	np	2.29 (0.48)	98.24 (0.87)	9	-1.93
42	42.23 (1.03)	np	5.56 (0.57)	8.99 (0.45)	34.51 (1.88)	2.81 (0.47)	np	np	np	np	np	np	np	5.80 (0.58)	99.89 (0.47)	8	-1.61
43	45.98 (0.96)	np	6.60 (0.28)	7.01 (0.34)	33.26 (1.42)	3.27 (0.24)	np	np	np	np	np	np	np	2.94 (0.39)	99.44 (0.11)	9	-1.90

Table 2-3. Experimental conditions, calculated oxygen fugacities, silicate MoO_2 concentration, and calculated log D_{Mo} values

Exp #	Silicate Comp	P (GPa)	T (°C)	t (min)	avg. ΔMMO*	est. ΔIW†	MoO_2 wt.%	log D
1	black glass 1	2.5	1585	120	-0.18§	0.41	2.58 (0.37)	1.71
2	black glass 1	2.5	1650	90	-0.17§	0.47	3.27 (0.44)	1.62
3	black glass 1	2.5	1750	25	-1.62	-0.92	5.80 (1.43)	1.40
4	black glass 1	2.5	1800	20	-1.62	-0.89	6.31 (1.71)	1.38
5	black glass 1	2.5	1900	3	-1.62	-0.84	5.93 (0.70)	1.43
6	black glass 1	2.5	2000	2	-1.62	-0.79	7.12 (1.44)	1.38
7	black glass 1	2.5	2100	2	-1.62	-0.75	4.45 (0.61)	1.61
8	black glass 1	3.5	2000	30	-1.62	-0.80	4.70 (1.73)	1.58
9	black glass 1	4.0	2000	2	-1.62	-0.81	5.67 (1.27)	1.49
10	black glass 1	4.5	1800	12	-1.62	-0.92	5.75 (1.22)	1.43
11	black glass 1	4.5	1900	5	-1.62	-0.86	4.83 (1.05)	1.53
12	black glass 1	4.5	2000	5	-1.62	-0.81	5.32 (1.04)	1.52
13	black glass 1	4.5	2100	2	-1.62	-0.77	3.87 (0.57)	1.68
14	black glass 1	5.0	2000	2	-1.62	-0.82	5.06 (0.74)	1.54
15	black glass 1	6.0	2000	2	-1.62	-0.83	4.09 (0.43)	1.64
16	black glass 1	7.0	2000	2	-1.62	-0.85	4.47 (0.30)	1.60
17	black glass 1	9.0	2000	2	-1.62	-0.87	4.06 (0.37)	1.63
18	black glass 1	9.7	2000	3	-1.62	-0.88	4.53 (0.16)	1.59
19	black glass 2	2.5	2000	2	-1.87	-1.04	2.79 (0.69)	1.81
20	peridotite 1	2.5	2100	5	-1.79	-0.92	3.45 (0.50)	1.80
21	peridotite 1	2.5	2100	2	-1.79	-0.92	3.85 (0.14)	1.75

* averaged oxygen fugacity for each silicate composition relative to the molybdenum-molybdenum oxide buffer, see section 3.3

† estimated oxygen fugacity relative to the iron-wüstite buffer, see section 3.3

§ run product contained a stable MoO2 phase indicating MoO2 saturation and an oxygen fugacity near the MMO buffer, the MoO2 content (~83 wt.%) of this phase and the Mo content of the capsule were used in Equation 2-2 to calculate ΔMMO for these experiments

Table 2-3 (con't). Experimental conditions, calculated oxygen fugacities, silicate MoO_2 concentration, and calculated log D_{Mo} values

Exp #	Silicate Comp	P (GPa)	T (°C)	t (min)	avg. ΔMMO*	est. ΔIW†	MoO_2 wt.%	log D
22	peridotite 1	3.5	1975	11	-1.79	-0.98	4.66 (0.48)	1.64
23	peridotite 1	3.5	2100	7	-1.79	-0.93	4.12 (0.63)	1.72
24	peridotite 1	3.5	2100	8	-1.79	-0.93	4.50 (0.42)	1.69
25	peridotite 1	3.5	2200	2	-1.79	-0.89	3.99 (0.30)	1.76
26	peridotite 1	4.5	2100	13	-1.79	-0.94	3.48 (0.47)	1.81
27	peridotite 1	5.3	2100	14	-1.79	-0.95	3.50 (0.35)	1.81
28	peridotite 1	6.0	2100	16	-1.79	-0.96	3.51 (0.67)	1.81
29	peridotite 2	3.5	2100	5	-1.76	-0.90	3.96 (0.61)	1.73
30	Ti-rich 1	2.5	2100	3	-1.74	-0.87	4.30 (0.94)	1.71
31	basalt	2.5	1800	40	-2.10	-1.37	1.44 (0.05)	2.04
32	basalt	2.5	2100	7	-2.10	-1.23	1.35 (0.09)	2.15
33	basalt	3.0	2000	35	-2.10	-1.28	1.51 (0.08)	2.08
34	basalt	3.5	2000	34	-2.10	-1.28	1.53 (0.08)	2.07
35	basalt	4.0	2000	30	-2.10	-1.29	1.42 (0.11)	2.11
36	basalt	4.5	2000	28	-2.10	-1.29	1.99 (0.14)	1.95
37	basalt	5.0	2000	20	-2.10	-1.30	1.70 (0.24)	2.03
38	basalt	5.5	2000	23	-2.10	-1.31	2.08 (0.20)	1.94
39	basalt	6.0	2000	25	-2.10	-1.31	1.61 (0.30)	2.04
40	andesite	2.5	2100	8	-2.14	-1.27	1.40 (0.10)	2.10
41	Ti-rich 2	12.0	2200	2	-1.93	-1.13	2.29 (0.48)	1.91
42	peridotite 1	3.5	1950	15	-1.61	-0.82	5.80 (0.58)	1.53
43	peridotite 1	6.5	2100	20	-1.90	-1.07	2.94 (0.39)	1.87

* averaged oxygen fugacity for each silicate composition relative to the molybdenum-molybdenum oxide buffer, see section 3.3

† estimated oxygen fugacity relative to the iron-wüstite buffer, see section 3.3

§ run product contained a stable MoO2 phase indicating MoO2 saturation and an oxygen fugacity near the MMO buffer, the MoO2 content (~83 wt.%) of this phase and the Mo content of the capsule were used in Equation 2 to calculate ΔMMO for these experiments

Table 2-4. Multiple linear regression coefficients for the parameterization

Parameter	Value	St. Error
ΔIW	-1.12	0.03
1/T	7382	559
P/T	-56.29	18.36
SiO_2	13.30	1.92
Al_2O_3	9.78	2.42
FeO	10.51	2.02
MgO	10.78	1.95
CaO	9.72	1.98
TiO_2	12.24	2.56
log(1-Xc)	-5.87	0.70
log(1-Xs)	4.67	1.25
log(1-Xsi)	15.92	2.12
Intercept	-13.82	1.85

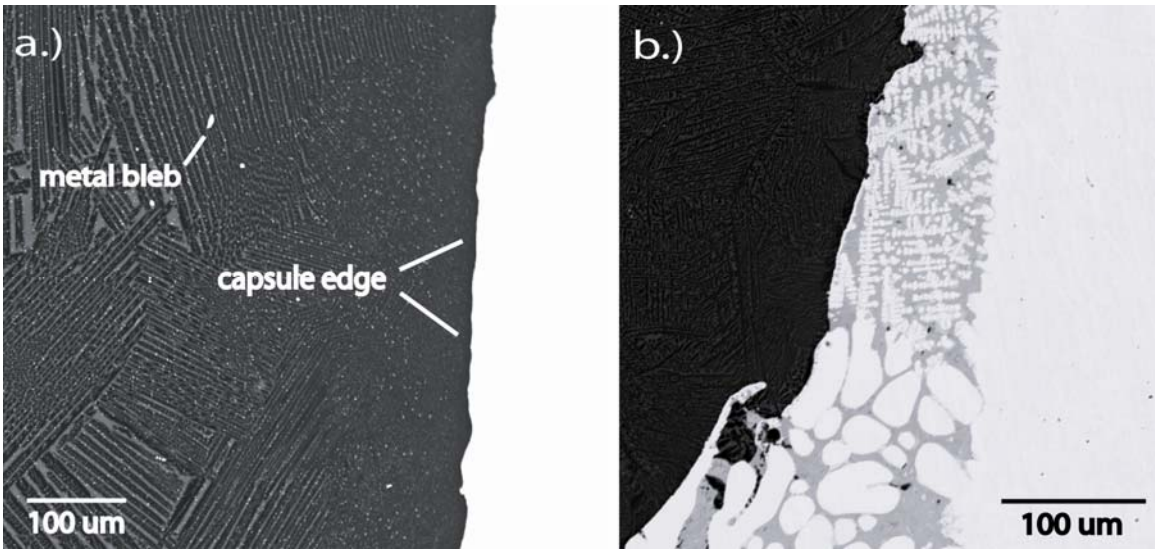

Figure 2-1. Backscattered electron images of run products. a.) close up of experiment #20 showing silicate quench texture and the distinct border between the silicate and capsule typical of most experiments. This image also shows the homogeneously distributed quench micronuggets along with larger heterogeneously distributed metal blebs. b.) close up of experiment #15, dark area on the left is quenched silicate, bright area on the right is the Mo capsule, in between is the solid MoFe metal phase – large round bright areas, and the liquid MoFe phase showing dendritic quench texture.

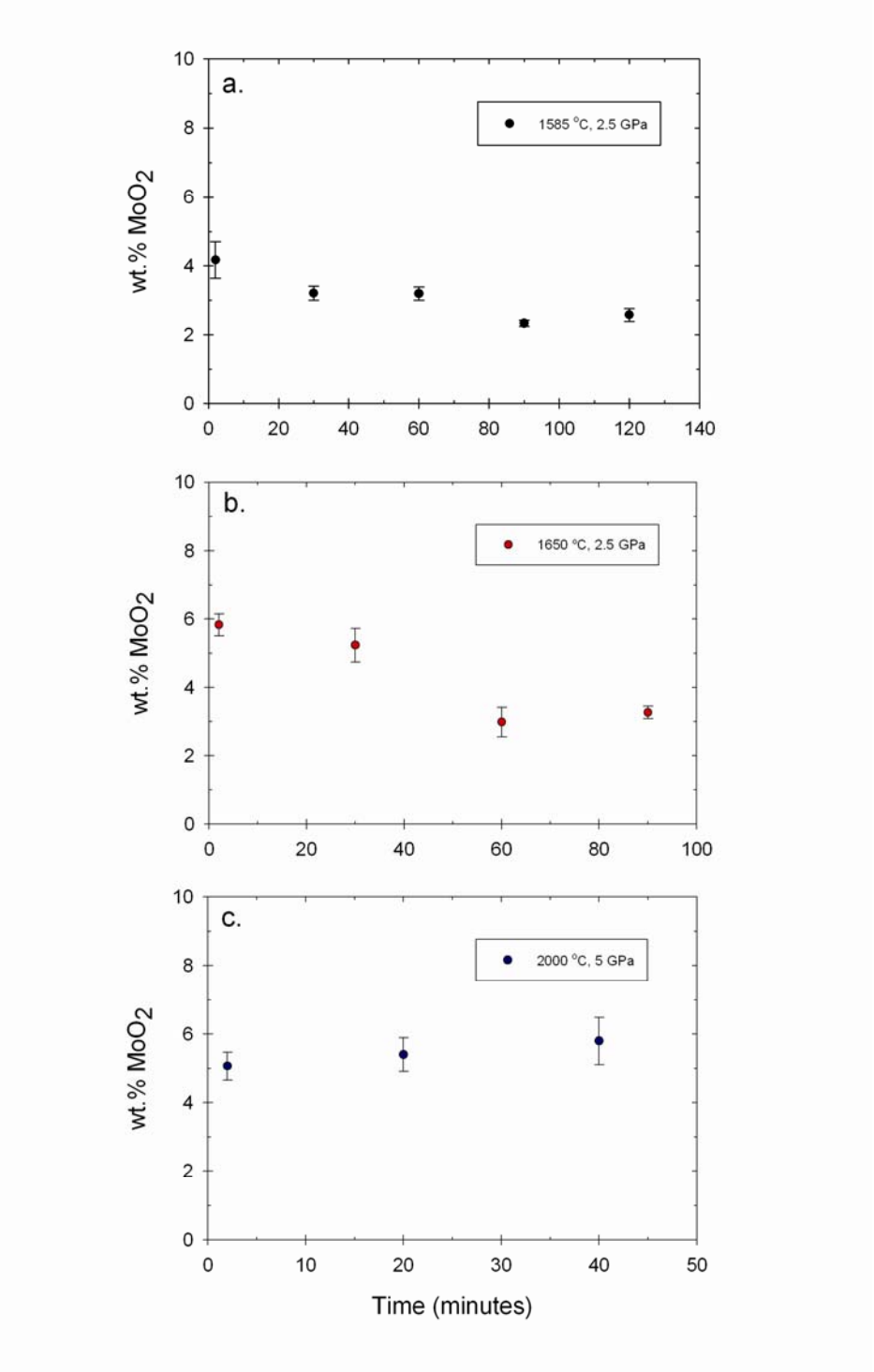

Figure 2-2. Plots of wt.% MoO_2 in the silicate melt vs. time for the suite of time series experiments. All plots are for the black glass 1 silicate composition. The general trend of an initial high solubility and then lowering to a steady state was also seen in the time series data of Ertel et al. (2006). a.) Time series experiments at 1585 °C and 2.5 GPa. b.) Time series experiments at 1650 °C and 2.5 GPa. c.) Time series experiments at 2000 °C and 5 GPa.

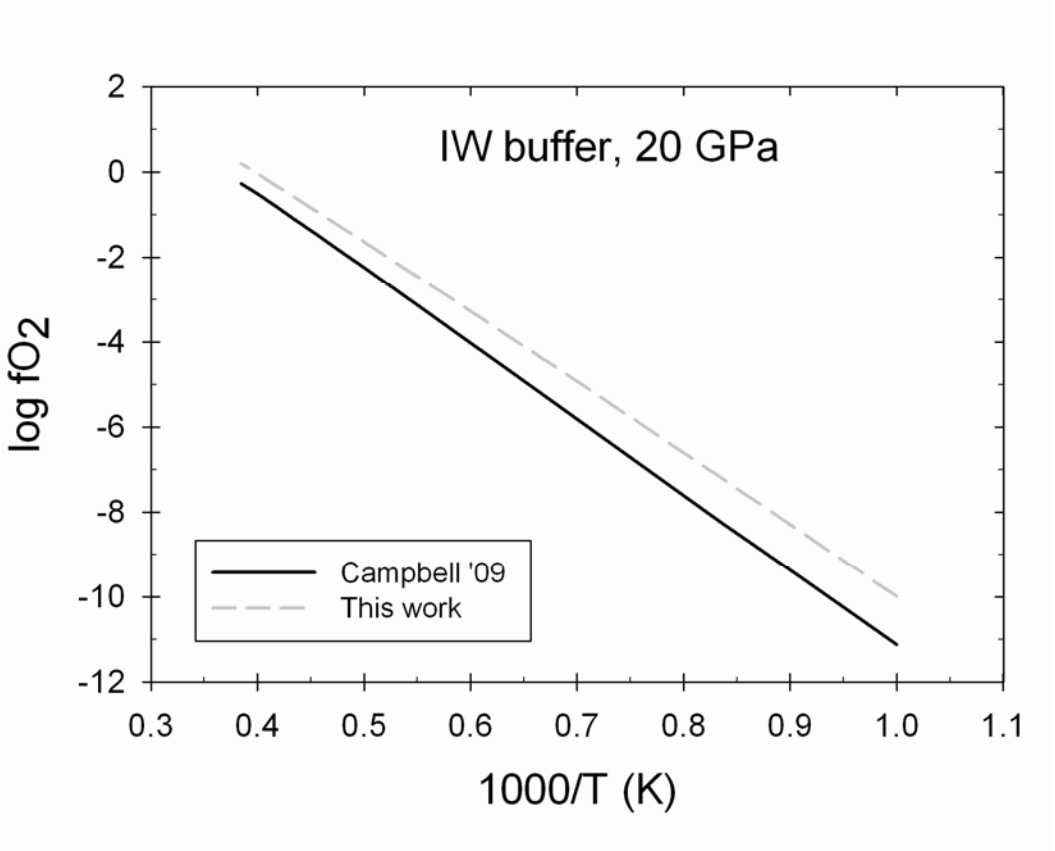

Figure 2-3. Plot of log(fO_2) vs. 1000/temperature showing the IW buffer at 20 GPa from Campbell et al. (2009) and that calculated using the method described in Section 2.3.3. The largest difference between the two methods is about 1 log unit at the lowest temperatures. Most of this difference is due to the fact that Campbell et al. (2009) calculated the 1 bar buffer from data in Chase (1998) and we used the 1 bar buffer from O'Neill and Pownceby (1993).

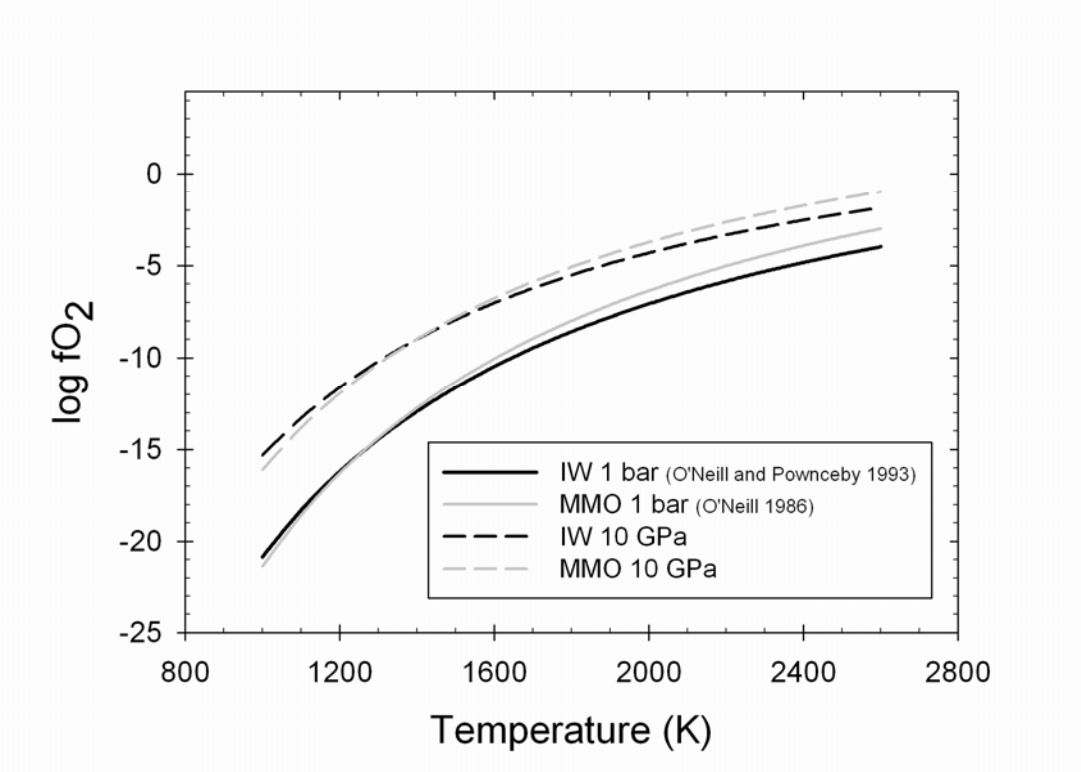

Figure 2-4. Plot of log fO_2 vs. temperature showing the IW and MMO buffers at 1 bar (references above) and 10 GPa. The high pressure buffers were calculated as described in Section 2.3.3. The EOS parameters used were from Fried et al. (2002): $V_o(Fe)$ = 7.11 mL/mol, $V_o(FeO)$ = 12.6 $V_o(Mo)$ = 9.41, $V_o(MoO_2)$ = 19.77; $B_o(Fe)$ = 139 GPa, $B_o(FeO)$ = 143, $B_o(Mo)$ = 270, $B_o(MoO_2)$ = 162; $B_o'(Fe)$ = 4.7, $B_o'(FeO)$ = 5.0, $B_o'(Mo)$ = 3.9, $B_o'(MoO_2)$ = 5.0. Over the pressure and temperature range of our experiments the MMO buffer curve is always more oxidizing than IW.

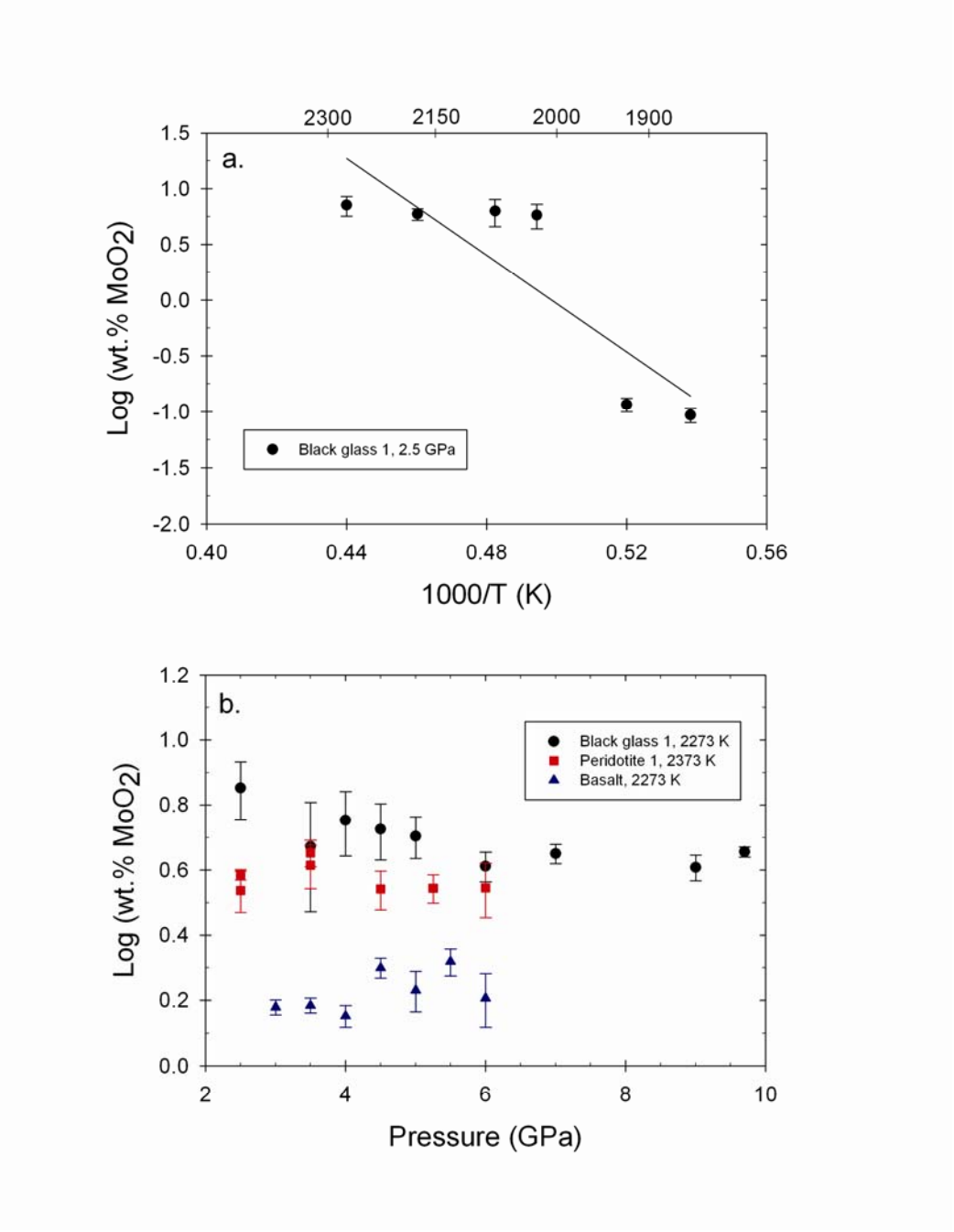

Figure 2-5. The effect of temperature and pressure on Mo solubility. a.) Plot of log(wt.%MoO_2) vs. 1000/temperature. The data are all the black glass 1 silicate composition at a constant pressure of 2.5 GPa. Data are at constant relative oxygen fugacity, the 1858 K and 1923 K have been adjusted to -1.62ΔMMO according to $\log(c_2) = (\Delta MMO)_2 - (\Delta MMO)_1 + \log(c_1)$, where c is wt.% MoO_2 (see Table 2-3). b.) Plot of log(wt.%MoO_2) vs. pressure. The plot shows data for three constant composition data sets at constant temperature. Error bars are standard deviations on the probe measurements.

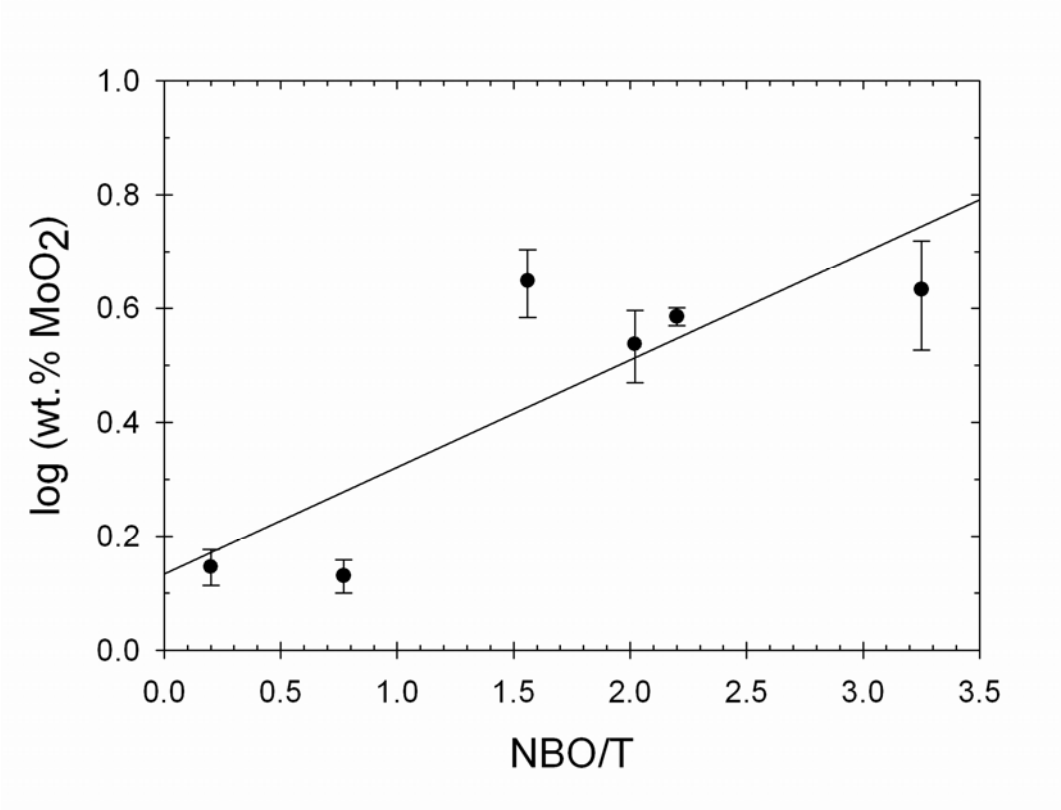

Figure 2-6. Plot of log(wt.%MoO_2) vs. NBO/T. All data points are from experiments at 2.5 GPa and 2373 K. The line is showing the least squares linear regression of the data, with a slope of 0.19.

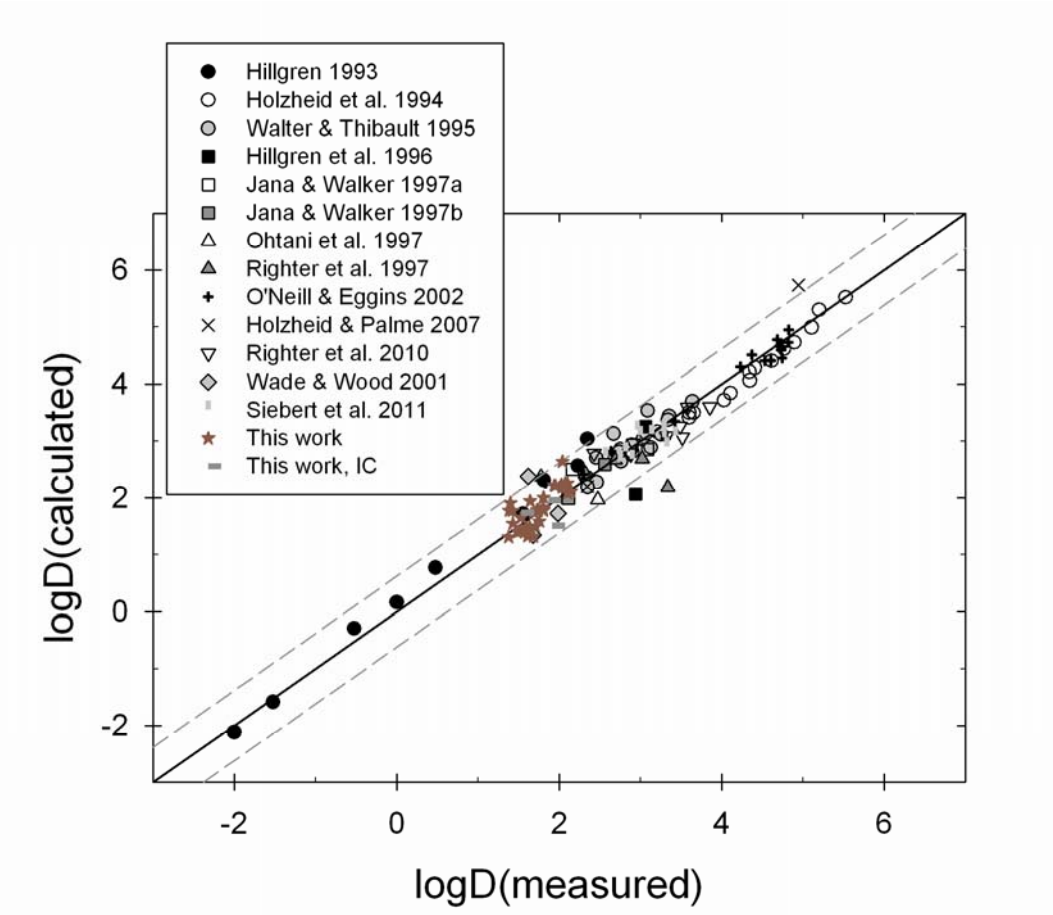

Figure 2-7. Plot of logD(calculated) vs. logD(measured). The calculated values were determined from the parameterization. The previous work included in the parameterization is comprehensive with the exception of the graphite capsule experiments of Siebert et al. (2011), due to the uncertain amount of carbon in the metal phase, and the data of Tuff et al. (2011). The data of Tuff et al. (2011) contain large amounts of Si in the metal phase and were not used because the regression breaks down when they are included. It is unclear why this occurs since the data of Wade and Wood (2001) are predicted well and contain up to 16.4 wt.% Si in the metal, but it is presumably due to the strong interactions between Mo and Si in the metal phase. Data from 1 bar experiments were included in the data set in order to better constrain the effect of oxygen fugacity since that parameter cannot be independently controlled in high pressure experiments. However, in order not to bias the data set with low pressure data, only a fraction of the O'Neill and Eggins (2002) data set was used; those at -11.63 log fO_2 for their AD and A-F melts, and those at -10.20 log fO_2 for their MAS and CAS melts. The regression gives an $R^2 = 0.95$. The solid black line is a 1:1 line. The standard error on the calculated log D values is 0.29 and the two dashed lines show two times this standard error. Only a few points lie outside the dashed lines, IC = independent check.

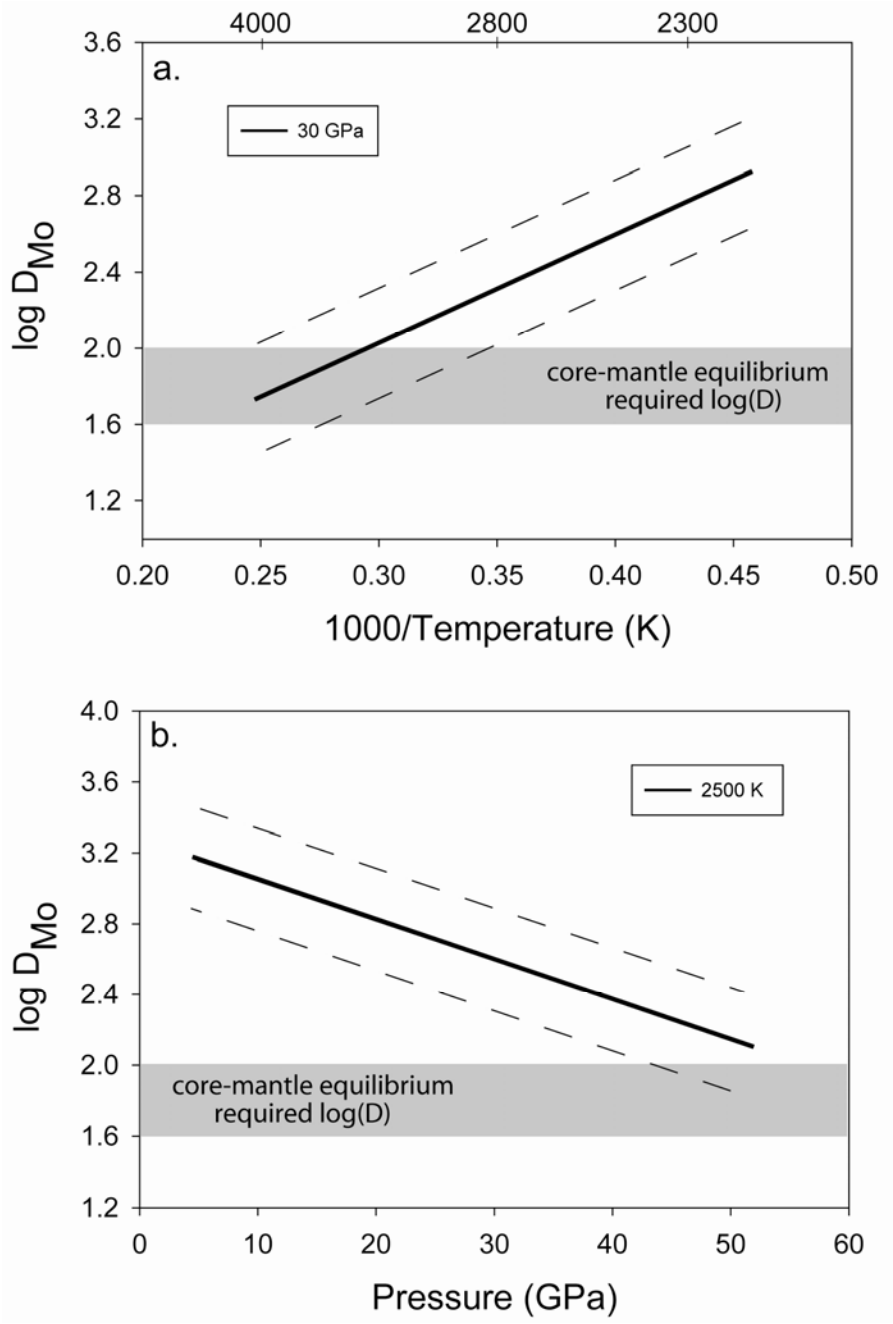

Figure 2-8. The effect of temperature and pressure on D_{Mo} determined from parameterization of the data from the present work and literature data. Oxygen fugacity was kept constant at -2.2ΔIW and silicate composition was also kept constant using KLB-1 peridotite composition from Davis et al. (2009). No light elements were considered for these plots. Dashed lines indicate the standard error on the parameterization and the shaded region is the required D_{Mo} values to explain the observed mantle abundance of Mo. a.) Plot of calculated log D_{Mo} vs. 1000/temperature at a constant pressure of 30 GPa. b.) Plot of calculated log D_{Mo} vs. pressure at a constant temperature of 2500 K.

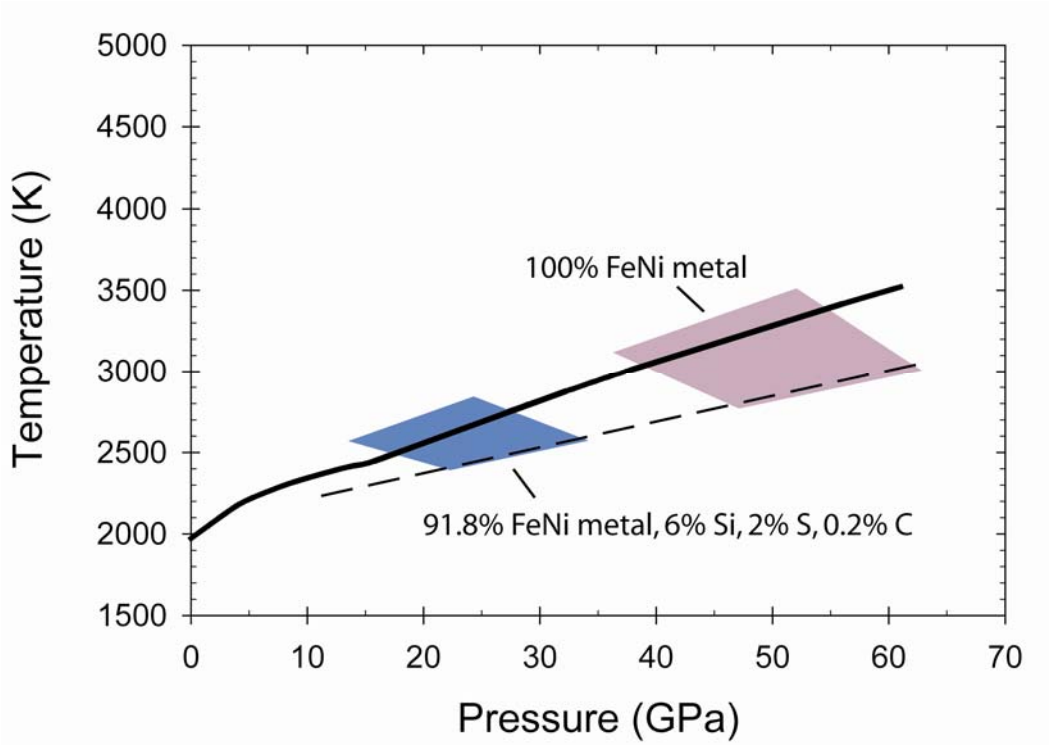

Figure 2-9. Pressure-temperature solution sets for single-stage core formation determined from the parameterization. Oxygen fugacity was kept constant at -2.2ΔIW and silicate composition was also kept constant using KLB-1 peridotite composition from Davis et al. (2009). A set of conditions was considered a solution if it gave D_{Mo} = 40-100. The solid line is the peridotite liquidus from Zhang and Herzberg (1994) for pressures of 0-23 GPa and from Andrault et al. (2011) for >23 GPa, and the dashed line is the mantle solidus from Andrault et al. (2011). Two solution sets are shown; one that does not consider light elements in the core, and one that bases the light element content on cosmochemical abundances.

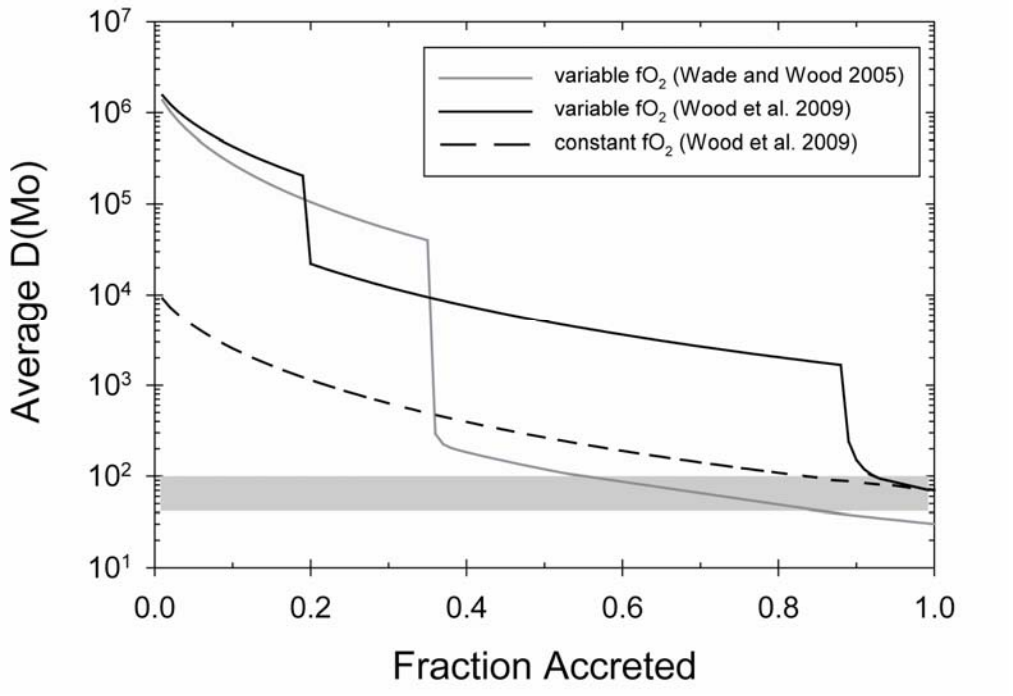

Figure 2-10. Average D_{Mo} from multi-stage core formation vs. fraction of Earth accreted. The models used are from Wade and Wood (2005) and Wood et al. (2009) in which the metal from each impactor equilibrates with the entire silicate mantle before being segregated to the core where no further equilibration takes place. In Wade and Wood (2005), Earth is accreted in 1% steps with the base of the magma ocean assumed to be 46% of the depth to the core-mantle boundary for each step. Temperature increases with pressure along the peridotite liquidus and there is an oxygen fugacity jump corresponding to an increase in Fe content of the mantle from 0.63 to 6.36 wt.% (-4.25 to -2.25ΔIW) after 35% accretion. Wade and Wood (2005) point out that increasing the oxygen fugacity gradually instead of step-wise does not significantly alter the final average D values. In Wood et al. (2009), Earth is again accreted in 1% steps and temperature is fixed to the peridotite liquidus, but the base of the magma ocean is assumed to be 35% of the depth of the core-mantle boundary. In the variable fO_2 model, oxygen fugacity is increased in two steps, corresponding to 0.6 to 1.6 wt.% Fe in the mantle (-4.25 to -3.41ΔIW) at 20% accretion and from 1.6 to 6.26 wt.% Fe (-3.41 to -2.26ΔIW) at 89% accretion. The constant fO_2 model assumes 6.26 wt.% Fe in the mantle throughout accretion. The gray shaded region shows the final D required to explain the observed mantle abundance of Mo.

2.6 References

Agee, C.B., Li, J., Shannon, M.C. (1995) Pressure-temperature phase diagram for the Allende meteorite. Journal of Geophysical Research 100, 17725-17740

Andrault, D., Bolfan-Casanova, N., Lo Nigro, G., Bouhifd, M.A., Garbarino, G., Mezouar, M. (2011) Solidus and liquidus profiles of chondritic mantle: Implication for melting of Earth across its history. Earth and Planetary Science Letters 304, 251-259

Bouhifd, M.A., Jephcoat, A.P. (2011) Convergence of Ni and Co metal-silicate partition coefficients in the deep magma-ocean and coupled silicon-oxygen solubility in iron melts at high pressures. Earth and Planetary Science Letters 307, 341-348

Campbell, A.J., Danielson, L., Righter, K., Seagle, C.T., Wang, Y., Prakapenka, V.B. (2009) High pressure effects on the iron-iron oxide nickel-nickel oxide oxygen fugacity buffers. Earth and Planetary Science Letters 286, 556-564

Canup, R.M., Agnor, C.B. (2000) Accretion of the terrestrial planets and the Earth-Moon system. In: Canup, R. M. and Righter, K. eds. *Origin of the Earth and Moon*. The University of Arizona Press, Tucson AZ, 113-129

Chabot, N.L., Agee, C.B. (2003) Core formation in the Earth and Moon: New experimental constraints from V, Cr, and Mn. Geochimica et Cosmochimica Acta 67, 2077-2091

Chabot, N.L., Draper, D.S., Agee, C.B. (2005) Conditions of core formation in the Earth: Constraints from nickel and cobalt partitioning. Geochimica et Cosmochimica Acta 69, 2141-2151

Chase Jr., M.W. (1998) NIST-JANAF Thermochemical Tables, 4th ed. Journal of Physical and Chemical Reference Data Monograph No. 9 American Institute of Physics

Cottrell, E., Walter, M.J., Walker, D. (2009) Metal-silicate partitioning of tungsten at high pressure and temperature: Implications for equilibrium core formation in Earth. Earth and Planetary Science Letters 281, 275-287

Cottrell, E., Walter, M.J., Walker, D. (2010) Erratum to "Metal-silicate partitioning of tungsten at high pressure and temperature: Implications for equilibrium core formation in Earth" [Earth and Planetary Science Letters 281 (2009) 275-287]. Earth and Planetary Science Letters 289, 631-634

Davis, F.A., Tangeman, J.A., Tenner, T.J., Hirschmann, M.M. (2009) The composition of KLB-1 peridotite. American Mineralogist 94, 176-180

Draper, D.S. (1991) Late Cenozoic bimodal magmatism in the northern Basin and Range Province of southeastern Oregon. Journal of Volcanology and Geothermal Research 47, 299-328

Ertel, W., O'Neill, H.S.C., Dingwell, D.B., Spettel, B. (1996) Solubility of tungsten in a haplobasaltic melt as a function of temperature and oxygen fugacity. Geochimica et Cosmochimica Acta 60, 1171-1180

Ertel, W., Walter, M.J., Drake, M.J., Sylvester, P.J. (2006) Experimental study of platinum solubility in silicate melt to 14 GPa and 2273 K: Implications for accretion and core formation in Earth. Geochimica et Cosmochimica Acta 70, 2591-2602

Floridis, T.P., Chipman, J. (1958) Activity of oxygen in liquid iron alloys. Transactions of the metallurgical society of AIME 212, 549-553

Fried, L.E., Howard, W.M., Souers, P.C. (2002) EXP6: A new equation of state library for high pressure thermochemistry. 12th International Detonation Symposium, San Diego, CA

Gessmann, C.K., Rubie, D.C. (2000) The origin of the depletions of V, Cr, and Mn in the mantles of the Earth and Moon. Earth and Planetary Science Letters 184, 95-107

Hillgren, V.J. (1993) Partitioning behavior of moderately siderophile elements in Ni-rich systems: Implications for the Earth and Moon. PhD thesis. University of Arizona, 423 pp

Hillgren, V.J., Drake, M.J., Rubie, D.C. (1996) High pressure and high temperature metal-silicate partitioning of siderophile elements: The importance of silicate liquid composition. Geochimica et Cosmochimica Acta 60, 2257-2263

Holzheid, A., Borisov, A., Palme, H. (1994) The effect of oxygen fugacity and temperature on solubilities of nickel, cobalt, and molybdenum in silicate melts. Geochimica et Cosmochimica Acta 58, 1975-1981

Holzheid, A., Palme, H. (2007) The formation of eucrites: Constraints from metal-silicate partition coefficients. Meteoritics and Planetary Science 42, 1817-1829

Jana, D., Walker, D. (1997a) The influence of silicate melt composition on distribution of siderophile elements among metal and silicate liquids. Earth and Planetary Science Letters 150, 463-472

Jana, D., Walker, D. (1997b) The impact of carbon on element distribution during core formation. Geochimica et Cosmochimica Acta 61, 2759-2763

Jones, J.H. and Drake, M.J. (1986) Geochemical constraints on core formation in the Earth. Nature 322, 221-228

Li, J., Agee, C.B. (1996) Geochemistry of mantle-core differentiation at high pressure. Nature 381, 686-689

Li, J., Agee, C.B. (2001) The effect of pressure, temperature, oxygen fugacity, and composition on partitioning of nickel and cobalt between liquid Fe-Ni-S alloy and liquid silicate: Implications for the Earth's core formation. Geochimica et Cosmochimica Acta 65, 1821-1832

McDonough, W.F., Sun, S.-s. (1995) The composition of the Earth. Chemical Geology 120, 223-253

McDonough, W.F., (2003) Compositional model for the Earth's core. In: Carlson, R.W. ed. *Treatise on Geochemistry, Vol. 2, The Mantle and Core.* Elsevier Ltd, 547-568

Melosh, H.J. (1990) Giant impacts and the thermal state of the early Earth. In: Newsom, H.E. and Jones, J.H. eds. *Origin of the Earth*. Oxford University Press, 69-83

Mysen, B.O. (1983) The structure of silicate melts. Annual Review of Earth and Planetary Science 11, 75-97

Newsom, H. E. (1995) Composition of the solar system, planets, meteorites, and major terrestrial reservoirs. In: Ahrens, T.J. ed. *Global Earth Physics: A Handbook of Physical Constants*. AGU Reference Shelf, 159-189

Ohtani, E., Yurimoto, H., Seto, S. (1997) Element partitioning between metallic liquid, silicate liquid, and lower-mantle minerals: Implications for core formation of the Earth. Physics of the Earth and Planetary Interiors 100, 97-114

O'Neill, H.S.C. (1986) Mo-MoO_2 (MOM) oxygen buffer and the free energy of formation of MoO_2. American Mineralogist 71, 1007-1010

O'Neill, H.S.C., Pownceby, M.I. (1993) Thermodynamic data from redox reactions at high temperatures. I. An experimental and theoretical assessment of the electrochemical method using stabilized zirconia electrolytes, with revised values for the Fe-"FeO", Co-CoO, Ni-NiO and Cu-Cu_2O oxygen buffers, and new data for the W-WO_2 buffer. Contributions to Mineralogy and Petrology 114, 296-314

O'Neill, H.S.C., Eggins, S.M. (2002) The effect of melt composition on trace element partitioning: An experimental investigation of the activity coefficient of FeO, NiO, CoO, MoO_2, MoO_3 in silicate melts. Chemical Geology 186, 151-181

O'Neill, H.S.C., Berry, A.J., Eggins, S.M. (2008) The solubility and oxidation state of tungsten in silicate melts: Implications for the comparative chemistry of W and Mo in planetary differentiation processes. Chemical Geology 255, 346-359

Palme, H., O'Neill, H.S.C. (2003) Cosmochemical estimates of mantle composition. In: Carlson, R.W. ed. *Treatise on Geochemistry, Vol. 2, The Mantle and Core.* Elsevier Ltd, 1-38

Righter, K., Drake, M.J., Yaxley, G. (1997) Prediction of siderophile element metal-silicate partition coefficients to 20 GPa and 2800 ^{o}C: The effects of pressure, temperature, oxygen fugacity, and silicate and metallic melt compositions. Physics of the Earth and Planetary Interiors 100, 115-134

Righter, K., Drake, M.J. (1999) Effect of water on metal-silicate partitioning of siderophile elements: A high pressure and temperature terrestrial magma ocean and core formation. Earth and Planetary Science Letters 171, 383-399

Righter, K., Humayun, M., Danielson, L. (2008) Partitioning of palladium at high pressures and temperatures during core formation. Nature 1, 321-323

Righter, K., Pando, K.M., Danielson, L., Lee, C.T. (2010) Partitioning of Mo, P and other siderophile elements (Cu, Ga, Sn, Ni, Co, Cr, Mn, V, and W) between metal and silicate melt as a function of temperature and silicate composition. Earth and Planetary Science Letters 291, 1-9

Righter, K. (2011) Prediction of metal-silicate partition coefficients for siderophile elements: An update and assessment of PT conditions for metal-silicate equilibrium during accretion of the Earth. Earth and Planetary Science Letters 304, 158-167

Ringwood, A.E. (1966) Chemical evolution of the terrestrial planets. Geochimica et Cosmochimica Acta 30, 41-104

Rubie, D.C., Gessmann, C.K., Frost, D.J. (2004) Partitioning of oxygen during core formation on the Earth and Mars. Nature 429, 58-61

Rubie, D.C., Frost, D.J., Mann, U., Asahara, Y., Nimmo, F., Tsuno, K., Kegler, P., Holzheid, A., Palme, H. (2011) Heterogeneous accretion, composition and core-mantle differentiation of the Earth. Earth and Planetary Science Letters 301, 31-42

Siebert, J., Corgne, A., Ryerson, F.J. (2011) Systematics of metal-silicate partitioning for many siderophile elements applied to Earth's core formation. Geochimica et Cosmochimica Acta 75, 1451-1489

Stevenson, D.J. (1990) Fluid dynamics of core formation. In: Newsom, H.E. and Jones, J.H. Eds., *Origin of the Earth*. Oxford University Press, New York, 231-249

Tankins, E.S., Thomas, M.K., Erthal, J.F., Williams, F.S. (1965) The activity of oxygen in liquid iron-molybdenum and iron-tungsten alloys. Transactions of the American Society of Metals 58, 245-252

Tonks, W.B., Melosh, H.J. (1993) Magma ocean formation due to giant impacts. Journal of Geophysical Research 98, 5319-5333

Toplis, M.J. (2005) The thermodynamics of iron and magnesium partitioning between olivine and liquid: Criteria for assessing and predicting equilibrium in natural and experimental systems. Contributions to Mineralogy and Petrology 149, 22-39

Tuff, J., Wood, B.J., Wade, J. (2011) The effect of Si on metal-silicate partitioning of siderophile elements and implications for the conditions of core formation. Geochimica et Cosmochimica Acta 75, 673-690

Ulmer, P. (1989) The dependence of the Fe^{2+}-Mg cation-partitioning between olivine and basaltic liquid on pressure, temperature and composition. Contributions to Mineralogy and Petrology 101, 261-273

Wade, J., Wood, B.J. (2001) The Earth's 'missing' niobium may be in the core. Nature 409, 75-78

Wade, J., Wood, B.J. (2005) Core formation and the oxidation state of the Earth. Earth and Planetary Science Letters 236, 78-95

Walter, M.J., Thibault, Y. (1995) Partitioning of tungsten and molybdenum between metallic liquid and silicate melt. Science 270, 1186-1189

Wänke, H. (1981) Constitution of terrestrial planets. Philosophical Transactions of the Royal Society of London A 303, 287-302

Wetherill, G.W. (1985) Occurrence of giant impacts during the growth of the terrestrial planets. Science 228, 877-879

Wood, B.J., Wade, J., Kilburn, M.R. (2009) Core formation and the oxidation state of the Earth: Additional constraints from Nb, V, and Cr partitioning. Geochimica et Cosmochimica Acta 72, 1415-1426

Zhang, J., Herzberg, C. (1994) Melting experiments on anhydrous peridotite KLB-1 from 5.0 to 22.5 GPa. Journal of Geophysical Research 99, 17729-17745

3.0 Molybdenum Metal-Silicate Partitioning Behavior: Constraining the Magma Ocean Models for Core Formation

Abstract

We report 20 new molybdenum metal-silicate partitioning experiments performed at pressures of up to 20 GPa, temperatures of 2173-2673 K, and variable silicate compositions. The molybdenum metal-silicate partition coefficients, D_{Mo}, measured from constant P-T experiments span three orders of magnitude, demonstrating the strong effect silicate composition has on the partitioning behavior of molybdenum. We find that increasing pressure causes D_{Mo} to decrease significantly, similar to the partitioning behavior of Ni. Increasing temperature also causes a significant decrease in D_{Mo}. Additionally, we present the most comprehensive parameterization of Mo to date, using our data and literature data, and show that the observed mantle abundance of Mo can be explained by single- and multi-stage core formation. We also present a comprehensive Ni parameterization and by combining the Mo and Ni results, we show that single-stage core formation is still the simplest, most unique way of explaining the mantle abundance of these two elements, and we suggest magma ocean conditions of 35-37 GPa and 2950-3000 K with 1.8 wt.% C, 3.0 wt.% S, and 3.4 wt.% Si.

3.1 Introduction

The magma ocean hypothesis, as outlined by Stevenson (1990), states that terrestrial core formation occurred through metal droplets separating out of a layer of liquid silicate. These droplets, which are estimated to have been ~1 cm in diameter (Rubie et al. 2003), would equilibrate with the surrounding silicate and sink to the silicate

liquidus where equilibration would stop and the metal would pond, forming a layer at the base of the magma ocean. Due to density instabilities this metal would then sink through the solid silicate to the core in the form of large diapirs (Karato and Murthy 1997). A driving force behind this model was the suggestion that large impacts are likely during the late stages of planetary accretion (Wetherill 1985, Canup and Agnor 2000). The energy released from these impacts would produce enough heat to partially, or completely, melt a growing planet, thus causing one or more magma oceans (Melosh 1990, Tonks and Melosh 1993). An example of such a high energy impact is the collision thought to be responsible for producing the Moon. The giant impact hypothesis states that when Earth was 90% accreted, a Mars-sized body collided with Earth and the ejected debris formed the Moon (Hartmann and Davis 1975, Cameron and Ward 1976, Canup and Asphaug 2001). Analysis of lunar samples brought back from the Apollo missions show quite convincingly that lunar evolution involved a magma ocean, from which the plagioclase floatation crust (anorthositic highlands) and complementary Eu anomaly between the highlands plagioclase and mare pyroxenes developed (Smith 1970, Wood et al. 1970, Schnetzler and Philpotts 1971, Warren 1985).

The likelihood of giant impacts in the inner solar system and a magma ocean on the Moon has lead to the search for evidence of magma oceans on other planetary bodies. Besides Earth and the Moon, magma oceans have been suggested for Mars, Mercury, and Vesta (e.g. Li and Agee 1996, Righter and Drake 1996, Righter and Drake 1997, Klein et al. 2004, Greenwood et al. 2005, Riner et al. 2009, Brown and Elkins-Tanton 2009). However, unlike the Moon, the evidence for a magma ocean on Earth is not as straightforward. If a global floatation crust once existed on Earth, any remnants of it have

long since been erased through geologic activity. Yet core formation did leave a chemical signature on Earth's mantle that can be used to investigate the magma ocean hypothesis. The siderophile (iron-loving) elements in the mantle are depleted relative to bulk Earth (chondritic) values (Ringwood 1966) due to their preference for the metal phase during core separation. By conducting equilibrium metal-silicate partitioning experiments, Li and Agee (1996) determined that at ~28 GPa and 2000 °C, the partition coefficients [$D_i = c_i(\text{metal})/c_i(\text{silicate})$] for Ni and Co equal the values required to explain the mantle depletions of these elements. They suggested that these conditions correspond to the point of final metal-silicate equilibration during core formation and thus provide strong evidence for a deep magma ocean on Earth.

The evidence for a magma ocean on Earth became even stronger when further experimental studies determined that other siderophile elements would reach their required D values at similar high pressure (P) and temperature (T) conditions. The D values for V, Cr, and Mn are too low at modest temperatures (1260 °C) and atmospheric pressure (Drake 1989), but their depletions can be explained by the high T and reducing conditions suggested for a terrestrial magma ocean (Gessmann and Rubie 2000, Chabot and Agee 2003). Furthermore, at low P-T conditions, the D values for W and Mo are too high to be explained by equilibrium between metal and silicate, but decrease considerably at high P-T conditions (e.g. Walter and Thibault 1995, Cottrell et al. 2009, Cottrell et al. 2010, Burkemper et al. 2012, Wade et al. 2012).

Based on the idea that accretion was a dynamic process and core formation probably started when Earth was only 10% of its current size (Melosh 1990), Wade and Wood (2005) developed a model where core formation occurred through a series of

magma oceans in which pressure increased as the size of Earth increased. With temperature constrained to be on the peridotite liquidus and allowing oxygen fugacity to increase from -4 to -2 log units below the iron-wüstite buffer (-2ΔIW) as accretion progressed, their model can explain the mantle abundances of V, Ni, Co, W, P, Mn, Ga, and Si. Rubie et al. (2011) developed a similar multi-stage model but invoked disequilibrium at the end of accretion in order to successfully explain Fe, Ni, Co, W, Cr, V, Nb, Ta, and Si. In contrast to the multi-stage models, Righter (2011) proposed a single-stage model where 11 elements (Ni, Co, Mo, W, P, Cu, Ga, Pd, Mn, Cr, and V) can be explained by magma ocean conditions of 27-33 GPa, 3300-3600 K, and -1ΔIW. Single-stage core formation, as endorsed by Righter (2011), suggests that these conditions represent the final magma ocean conditions after a large impact re-equilibrated and erased the mantle signature of any previous magma oceans. What all these models have in common is that they are dependent on the experimental datasets used to create them; therefore constraining the partitioning behavior of all the elements involved as much as possible is essential.

The literature contains an extensive experimental database for Ni and Co, over 300 each; whereas, data for Mo are not as abundant, less than 200, most of which are at low pressures (< 2 GPa). Additionally, the Mo solubility data of Burkemper et al. (2012) showed a negligible pressure effect (their Figure 3b), whereas Siebert et al. (2011) showed D_{Mo} to decrease with increasing pressure (their Figure 8). The present study specifically addresses this discrepancy by performing a systematic investigation of the effect of pressure on D_{Mo}. It is especially important to have tight constraints for the effect of pressure on partitioning because extrapolations to deep magma ocean conditions

typically extend well beyond the pressure range investigated experimentally. Therefore, not only is a large dataset essential, but one at high pressure is a necessity. This study increases the number of high pressure Mo data in the literature by presenting results from 20 new metal-silicate partitioning experiments covering a pressure range of 3-20 GPa, a temperature range of 1900-2400 °C, with variable silicate and metal composition. This work is the second part of a comprehensive study investigating the behavior of Mo in silicate melts that involves both solubility and partitioning experiments, and began with the solubility study of Burkemper et al. (2012).

3.2 Methods

3.2.1 Strategy

The experimental strategy employed was to design experiments that would best represent terrestrial core formation. The metal phases used consisted of both an Fe-rich and FeNi-rich alloy, and magnesia capsules were used to avoid unwanted sample contamination. The capsule did significantly increase the MgO concentration of the silicate, but since Earth's mantle is ultramafic this was not considered a drawback. This is in contrast to the often used graphite capsules which add a significant (typically 5 wt.% or greater, Metal Activity Calculator described in Wade et al. 2012) carbon component to the metal phase, much higher than is suggested for Earth's core based on cosmochemical abundance (McDonough 2003). Our experiments were doped with 10 wt.% Mo which caused the concentration in the metal and silicate phases to be higher than in the core and mantle, respectively; however, this was done so the run products could be analyzed with an electron microprobe and we show that the partitioning still obeys Henry's law at these

concentrations, Section 3.2.2. Additionally, Earth's core contains ~10% light elements (Birch 1952), but we chose not to add light elements to our experiments in order to focus on the effects of P, T, and silicate composition.

3.2.2 Starting materials

Four different starting silicate compositions were employed in this study, including both natural and synthetic materials, in order to investigate the effects of silicate composition on partitioning. The natural compositions included a powdered basalt, NB219, from southeastern Oregon (Draper 1991) and the USGS andesite standard, AGV-2, that was fired at 1000 °C for 1 hour to remove water. Synthetic compositions included a peridotitic composition and a high FeO, high TiO_2 ultramafic composition (Apollo 14 black glass). The synthetic compositions were prepared from reagent grade oxide/silicate powders at the Institute of Meteoritics. The powders were mixed under ethanol, which was then evaporated off in a 100 °C oven. Magnesia capsules were machined at Arizona State University from high purity rods (Saint-Gobain). Due to the magnesia capsules, the starting compositions are significantly altered during the experiment so that all final run product compositions are ultramafic with MgO concentrations between 28-47 wt.%.

The pure metals consisted of metal shavings obtained by filing >99.5% pure Fe, Ni, and Mo rods. The pure metals were used to make two metal mixtures, one with 50 wt.% Fe, 40% Mo, and 10% Ni and the other with 60 wt.% Fe and 40% Mo. These metal mixtures were then mixed with the silicate compositions in a 3:1 silicate to metal ratio so that the final Mo concentration in all cases was 10 wt.%. This is the same Mo concentration used previously by Walter and Thibault (1995) in which they showed no

apparent deviations from Henry's law. Additionally, we performed one experiment with 12 wt.% Mo at 2100 °C and 5 GPa to compare with experiment #7. The D_{Mo} value for the 12 wt.% experiment, when adjusted to the same oxygen fugacity, is 737±85 which is within error of the D value for experiment #7 of 645±76 and suggests that Henry's law extends over a wide range of Mo concentrations, similar to W (Ertel et al. 1996). Due to the high P-T conditions of experiment #19, W from the W-Re thermocouple wire infiltrated the sample and became a significant component of the metal phase.

3.2.3 Experimental and analytical techniques

The metal-silicate mixtures were loaded into magnesia capsules that were sealed with a friction fit lid. The 3-8 GPa experiments were performed on Walker-type multi-anvil presses at the Institute of Meteoritics using the same cell assembly, procedures, and pressure calibrations described in Agee et al. (1995). Briefly, octahedra cast from Aremco Ceramacast® 584 ceramic were used as the pressure medium. They were fitted with rhenium heaters and temperature was measured with W/Re thermocouple wires inserted perpendicular to the rhenium heater and temperature was monitored with a Eurotherm 3504 controller. The octahedron assembly was surrounded by eight tungsten-carbide cubes with 8 mm truncated edges. The 15-20 GPa experiments were performed on a 1500T multi-anvil press at the Geophysical Laboratory (Carnegie Institute of Washington) using the COMPRES sponsored 8/3 assembly described in Bertka and Fei (1997) and Leinenweber et al. (2012). In both the low and high pressure set-ups, the experiments were quenched by cutting power to the system. Run times were between one and five minutes depending on the temperature of the experiment. Short run times are necessary when using magnesia capsules to limit the capsule reaction with the silicate. A

duplicate of experiment #11 (1900 °C, 3 GPa) was held for 10 minutes and significant magnesiowüstite and olivine formation occurred. These run times are comparable to previous experiments conducted with magnesia capsules in which a steady state was obtained (e.g. Righter et al. 2010).

All run products were analyzed on the JEOL 8200 Electron Probe Microanalyzer at the Institute of Meteoritics. The metal phase was analyzed using a 15 kV accelerating voltage and 20 nA beam current. Quench texture was commonly observed in the metal phase (Figure 3-1a), therefore a 20 μm spot size was employed. The silicate phase was analyzed using a 20 kV accelerating voltage and 60 nA beam current. The Mo concentration in the silicate was as low as 180 ppm, therefore Mo was analyzed on two spectrometers and the peak counts were combined in order to get a detection limit of ~50 ppm, an order of magnitude below the lowest measured Mo concentration. Quench textures can be seen in the silicate phase of all the run products (Figure 3-1b), very similar to those seen in Li and Agee (2001). A 20 μm broad beam was used to take into account the compositional variation between the quench crystals and melt pockets, and obtain an average concentration; however, some run products contained more prominent quench textures (e.g. exp. #2) and required a 50 μm spot size.

3.3 Results

3.3.1 Phase relations

An image of a typical run product can be seen in Figure 3-1b. All experiments were performed in the stability fields of liquid silicate and liquid metal. When power was cut to the experimental set-up, the liquid silicate and liquid metal quenched to produce

the textures seen in Figure 3-1. Separation between metal and silicate was very distinct in all run products. In most cases the metal phase formed one large metal sphere, as shown in Figure 3-1b; however, sometimes the metal phase would be separated into multiple smaller spheres. In this case, microprobe analyses were taken on all the spheres, and the compositional variation between the spheres was found to be minimal. Olivine was present in three of the run products due to the temperature of those runs being close to the silicate liquidus, and magnesiowüstite formed in some experiments due to the reaction of the silicate with the capsule (Table 3-1). Table 3-1 lists the metal and silicate compositional data, and Table 3-2 summarizes the measured D_{Mo} values and run conditions.

3.3.2 Oxygen fugacity

The oxygen fugacities listed in Table 3-2 were calculated relative to the iron-wüstite buffer. The large amounts of Fe metal in our experiments and the high solubility of FeO in the silicate phase make iron-wüstite the dominant oxygen buffer, and therefore the most reliable way to estimate oxygen fugacity. Oxygen exchange between iron species is controlled by the buffer reaction

$$Fe + \frac{1}{2}O_2 \leftrightarrow FeO \tag{3-1}$$

therefore, oxygen fugacity relative to the iron-wüstite buffer can be calculated according to,

$$\Delta IW = 2\log\frac{a_{FeO}^{silicate}}{a_{Fe}^{metal}} \tag{3-2}$$

where a is the activity of FeO in the silicate and Fe in the metal. Activity is related to mole fraction according to $a=X\gamma$, where X is mole fraction and γ is activity coefficient.

The activity coefficient of FeO in silicate melts has been shown to be slightly dependent on silicate composition, varying from 0.88-2.26 for the CMAS compositions employed by O'Neill and Eggins (2002), and has not been determined for the ultramafic compositions used in this study. Therefore, we assume ideal behavior in which the activity coefficient is equal to one, making $a_{FeO}^{silicate}$ equal to X_{FeO}. The activity coefficient of Fe in the metal phase is also compositionally dependent. However, the Metal Activity Calculator program described in Wade et al. (2012) uses interaction parameters for elements in liquid iron alloys found in the Steelmaking Data Sourcebook to calculate γFe for specific metal compositions. Therefore we used this program to calculate γFe for our experiments and the values can be found in Table 3-2.

All of the experiments presented here were performed under reducing conditions, from -2.37 to -1.07ΔIW. These oxygen fugacities are similar to the -2.2ΔIW suggested for terrestrial core formation based on the current concentrations of Fe in the core and FeO in the mantle (McDonough 2003). Experiments #1-11 had Ni in the metal phase and experiment 19 contained W. The addition of these elements will slightly change the oxygen fugacity of the experiment (as opposed to just an Fe-metal phase) by providing another oxygen buffer. A plot showing the high pressure oxygen buffers relevant to this study can be seen in Figure 3-2. Both the Ni-NiO and W-WO_2 buffers are at higher oxygen fugacities than iron-wüstite at the P-T conditions of our experiments.

3.3.3 Effect of pressure

Experiments #5-9 were performed using the same peridotite starting composition and at a constant temperature of 2100 °C over a pressure range of 3-7.5 GPa. The results can be seen in Figure 3-3. At constant relative oxygen fugacity, increasing pressure

causes D_{Mo} to decrease. This result is in contrast to the solubility experiments of Burkemper et al. (2012), which showed a negligible effect over the same pressure range. However, Siebert et al. (2011) performed partitioning experiments, also using magnesia capsules, and determined a decreasing pressure trend, similar to that shown in Figure 3-3. Furthermore, Wade et al. (2012) concluded that pressure has a strong effect on Mo partitioning, and Walter and Thibault (1995) and Ohtani et al. (1997) found that D_{Mo} decreases with increasing P-T conditions. As suggested by Burkemper et al. (2012), their lack of an observable pressure trend is probably due to the scatter in their isothermal data sets.

The data point at 3 GPa (exp #5) in Figure 3-3 is an obvious outlier, falling much lower than the decreasing trend would predict. This could indicate a bimodal pressure trend, like that shown in Cottrell et al. (2009) for W, where increasing pressure would cause D_{Mo} to increase to a certain point (in this case ~3 GPa) and any further increase in pressure would cause D_{Mo} to decrease. However, the bimodal trend of Cottrell et al. (2009) was refuted by Righter (2011) and, in regards to exp #3, we believe it is more likely an outlier due to the high T, low P conditions of that experiment. At these conditions, the capsule reacts significantly with the silicate causing considerable magnesiowüstite formation, which could be affecting the partitioning behavior. This explanation is further supported by the parameterization performed in Section 3.4.1, which successfully predicts all the partitioning data, including experiments below 3 GPa, with a single decreasing pressure trend.

Due to the fact that some of our experiments contained Ni metal, D_{Ni} could be calculated and the results can be seen in Figure 3-4. The data from this study are plotted

with data from Thibault and Walter (1995) and Li and Agee (1996), and the data are in excellent agreement. D_{Ni} has been known for quite some time to decrease with increasing pressure, and our data display this trend well. The D_{Ni} value for the data point at 8 GPa is slightly higher than the two at 4.5 and 6 GPa because the starting silicate for this experiment was basalt, whereas the rest were peridotite. This is in agreement with previous work that showed D_{Ni} to have a slight compositional dependence (e.g. Righter 2011), with D_{Ni} increasing with decreasing NBO/T (ratio of non-bridging oxygens to tetrahedrally coordinated cations, Mysen 1983). Also shown in Figure 3-4 is a comparison of the decreasing trend shown in Figure 3-3 for D_{Mo} with that observed for D_{Ni}. Both elements become significantly less siderophile as pressure is increased. However, even the D_{Mo} values determined from our highest pressure experiments, 15 and 20 GPa (2300 and 2400 °C, respectively, Figure 3-3) are too large to explain the mantle depletion (relative to chondritic) of Mo. The D_{Mo} value required to explain this depletion is between 40 and 100, calculated by assuming a CI chondrite bulk Earth and using mass balance to determine the concentration of Mo in the core (Newsom 1995, McDonough and Sun 1995, Palme and O'Neill 2003, McDonough 2003). This indicates that a shallow magma ocean (≤ 600 km) cannot explain the observed mantle abundance of molybdenum.

3.3.4 Effect of silicate composition and temperature

Seven experiments were performed at 1950 °C and 4 GPa in order to investigate the effect of silicate composition. The D_{Mo} values for these experiments span three orders of magnitude (Figure 3-5). This large compositional dependence is similar to that found for other high valence cations. High valence cations require more oxygens to stabilize

them in silicate melts than do low valence cations (i.e. Ni and Co); therefore their compositional dependence is generally greater (e.g. Jana and Walker 1997a, Cottrell et al. 2009, Righter et al. 2010, Siebert et al. 2011). Overall, the data in Figure 3-5 show that increasing the concentration of network formers (i.e. Si, Al) in the silicate melt caused D_{Mo} to increase, whereas network modifiers (i.e. Fe, Mg, Ca) caused a decrease in D_{Mo}. A notable exception to this is the experiment with NBO/T = 2.35 (exp #1). Based on the calculated NBO/T, the D_{Mo} value for this experiment is expected to be much higher compared to the rest of the experiments with larger NBO/T values. A possible explanation for this is the ~2 wt.% K in experiment #1. Burkemper et al. (2012) suggested that the large K cation may open up additional sites in the silicate melt favorable to Mo, thus decreasing D_{Mo} more than is accounted for by NBO/T. As a result, the parameterization performed in Section 3.4.1 employs the mole fractions of individual oxides to account for changes in silicate composition instead of a universal melt parameter, such as NBO/T. This is the same approach used by Righter et al. (2010) and Burkemper et al. (2012), who further demonstrated that individual oxides have unique effects on molybdenum partitioning (see also O'Neil and Eggins 2002 and Wade et al. 2012).

When using magnesia capsules, the effect of temperature is unavoidably linked to silicate composition because MgO infiltration increases with increasing temperature (e.g. Righter et al. 2010), making it difficult to separate the two effects. Previous work has consistently shown that D_{Mo} decreases with increasing temperature over a wide temperature range (Holzheid et al. 1994, Walter and Thibault 1995, Righter et al. 2010, Siebert et al. 2011, Burkemper et al. 2012). All of these studies employed solubility

experiments or partitioning experiments in graphite capsules, and were therefore able to hold silicate composition constant as temperature was increased. This decreasing trend is suggested by our data shown in Figure 3-3, in which the experiments at the highest temperatures (and highest pressures, experiments #19-20) have the lowest D_{Mo} values (see the parameterization in Section 3.4.1 for more details on the effect of temperature).

3.3.5 W partitioning

W is in the same column of the periodic table as Mo, therefore they are considered to be 'geochemical twins' and expected to have similar chemical properties. Yet, W is significantly less depleted in Earth's mantle than Mo. The D_W required to explain the observed mantle abundance of tungsten is 15-22 (McDonough 2003, Palme and O'Neill 2003). As shown in Table 3-2, experiment #19 contained both Mo and W, giving a D_{Mo} of 173 and D_W of 50. This result is in agreement with the observation that W is less depleted in the mantle than Mo, but the D_W value is too large to explain the W mantle abundance. Although a thorough comparison with the literature data on W partitioning is needed before concrete conclusions can be made, this result suggests that the conditions of experiment #19 (15 GPa and 2300 °C) are not the magma ocean conditions that imparted the W abundance to the mantle.

3.4 Discussion

3.4.1 Parameterization of Mo and Ni data

In order to elucidate the effects of specific variables from an expansive experimental database, partitioning data can be parameterized using a multiple linear regression. Righter (2011) compared two different approaches for accounting for trace

elements in the metal phase, one that uses empirical terms that mimic the Margules parameter (as in Righter et al. 1997), and another that uses epsilon interaction parameters (as in Wade and Wood 2005). Both methods were shown to produce the same results. Additionally, Burkemper et al. (2012) compared two different approaches for accounting for silicate composition, one that uses oxide mole fractions (an empirical approach first performed in Righter et al. 1999), and another that uses a regular solution model that obeys the Gibbs-Duhem equation (as in O'Neill and Eggins 2002). Burkemper et al. (2012) found that the empirical approach does better at reproducing the data used in the regression so we chose to adopt the empirical approaches to account for metal and silicate composition and parameterized the Mo data according to

$$\log D_{Mo} = a\Delta IW + b\frac{1}{T} + c\frac{P}{T} + \sum d_i X_i + e\log(1 - X_C) + f\log(1 - X_S) + g\log(1 - X_{Si}) + j \quad (3\text{-}3)$$

where D_{Mo} is the metal-silicate partition coefficient, ΔIW is the oxygen fugacity relative to the iron-wüstite buffer, T is temperature in Kelvin, P is pressure in GPa, X_i is the mole fraction of oxide i in the silicate phase, X_C, X_S, and X_{Si} are the mole fraction of carbon, sulfur, and silicon in the metal phase, respectively, and a-j are linear regression coefficients. The data included in the parameterization include 112 partitioning and 78 solubility experiments from the literature (Hillgren 1993, Holzheid et al. 1994, Walter and Thibault 1995, Hillgren et al. 1996, Ohtani et al. 1997, Righter et al. 1997, Jana and Walker 1997a, Jana and Walker 1997b, Wade and Wood 2001, O'Neill and Eggins 2002, Holzheid and Palme 2007, Righter et al. 2010, Siebert et al. 2011, Tuff et al. 2011, Wade et al. 2012, Burkemper et al. 2012) and the 20 new partitioning experiments presented here. The regression coefficients are shown in Table 3-3 and how well the

parameterization fits the data can be seen in Figure 3-6. The R^2 value is 0.91, and the parameterization predicts data determined over a wide range of experimental conditions and both solubility and partitioning data well. Additionally, the parameterization does not include a term for Ni in the metal phase, yet it is able to predict data with up to 99 wt.% Ni in the metal phase (Hillgren 1993), suggesting Ni does not have an effect on Mo partitioning other than that caused by the change in oxygen fugacity.

The *a* coefficient of -1.00 indicates a Mo valence of 4+ in the silicate. Holzheid et al. (1994) and O'Neill and Eggins (2002) determined that the valence state of Mo changes from dominantly 4+ to dominantly 6+ around -1ΔIW using an anorthite-diopside eutectic composition at 1 bar. All but nine of the experiments included in the parameterization are below the iron-wüstite buffer, and the majority are at -1ΔIW or below, so a 4+ valence is expected. Multiple studies included in the parameterization examined the effect of silicate composition at constant pressure and temperature (Walter and Thibault 1995, Hillgren et al. 1996, Jana and Walker 1997a, O'Neill and Eggins 2002, Siebert et al. 2011, Wade et al. 2012, Burkemper et al. 2012). The regression coefficients determined here for SiO_2 and TiO_2 are larger than those for Al_2O_3, MgO, FeO, and CaO; indicating SiO_2 and TiO_2 behave similarly in silicate melts with regards to Mo, and increasing the concentration of SiO_2 and TiO_2 relative to the other oxides would cause a significant increase in D_{Mo}. This is in agreement with the general trend of increasing D_{Mo} with decreasing NBO/T, shown in Figure 3-5. Additionally, because of the large number of studies that have investigated silicate composition, the parameterization can easily separate the effect of temperature from silicate composition. The positive *b* coefficient indicates D_{Mo} will decrease with increasing temperature, in

agreement with the raw data of Holzheid et al. (1994), Walter and Thibault (1995), Righter et al. (2010), Siebert et al. (2011), and Burkemper et al. (2012). The negative *c* coefficient indicates that increasing pressure causes D_{Mo} to decrease, in agreement with our raw data (Figure 3-3).

The regression coefficients *e*, *f*, and *g* indicate the effects the light elements C, S, and Si have on molybdenum partitioning, respectively. All three light elements have significant effects on D_{Mo}, but especially Si. The parameterization predicts that increasing the Si content of the metal phase will cause D_{Mo} to decrease strongly, in agreement with the study of Tuff et al. (2011). The same trend is predicted with increasing S content, but the decrease in D_{Mo} is not as strong. This is in agreement with data from Lodders and Palme (1991) who determined that D_{Mo} decreases with increasing sulfur content of the Fe-rich metal phase. In contrast, the negative $\log(1-X_C)$ coefficient indicates that increasing C content of the metal phase will cause an increase in D_{Mo}, presumably due to the formation of Mo-carbide species (Jana and Walker 1997b).

In order to place further constraints on core formation, we also performed a Ni parameterization that includes the D_{Ni} values determined in the present study and the abundant literature data (Hillgren 1993, Peach and Mathez 1993, Walker et al. 1993, Hillgren et al. 1994, Holzheid et al. 1994, Agee et al. 1995, Thibault and Walter 1995, Hillgren et al. 1996, Holzheid and Palme 1996, Li and Agee 1996, Gaetani and Grove 1997, Jana and Walker 1997a, Jana and Walker 1997b, Ohtani et al. 1997, Righter et al. 1997, Gessmann and Rubie 1998, Ito et al. 1998, Seifert et al. 1998, Li et al. 2001, Wade and Wood 2001, O'Neill and Eggins 2002, Bouhifd and Jephcoat 2003, Chabot et al. 2005, Wade and Wood 2005, Holzheid and Palme 2007, Corgne et al. 2008, Kegler et al.

2008, Righter et al. 2010, Bouhifd and Jephcoat 2011, Siebert et al. 2011, Siebert et al. 2012). The parameterization equation used for Ni was similar to Equation 3-3 except that instead of using individual oxide mole fractions to account for silicate compositions, NBO/T was employed (see Table 3-3), which has been shown to be a sufficient parameter for Ni because D_{Ni} is not strongly affected by changes in silicate melt composition (e.g. Jana and Walker 1997a, Righter 2011). One other difference is the addition of a $\log(1-X_O)$ term to account for the oxygen content of the metal phase. The data included in the Ni parameterization extend to much higher pressures than for Mo, and the amount of oxygen soluble in the metal phase increases with increasing pressure (Figure 3-7), so that at the highest pressure of 74 GPa, the amount of oxygen in the metal is significant. The regression coefficients determined are presented in Table 3-3 and how well the regression fits the data is shown in Figure 3-8. The partitioning behavior of Ni has been extensively studied and the results of our parameterization agree with previous work. It is very interesting that the $\log(1-X_O)$ coefficient is larger than the coefficients for the other light element terms, indicating that O has a greater effect on D_{Ni} than S, Si, and C, thus emphasizing the importance of taking the O content of the metal phase into account in future parameterizations.

3.4.2 Implications for core formation

The parameterization performed in Section 3.4.1 is the most comprehensive Mo parameterization to date, and can be used to constrain the magma ocean models for core formation. Assuming a chondritic bulk Earth composition, the D_{Mo} value required to explain the observed mantle abundance of Mo is between 40 and 100 (Newsom 1995, McDonough and Sun 1995, Palme and O'Neill 2003, McDonough 2003). In order to

solve for a set of P-T conditions that can explain the Mo abundance, these numbers were put into Equation 3-3. In addition, silicate composition was set to KLB-1 peridotite (NBO/T = 2.7, Davis et al. 2009) and oxygen fugacity was kept constant at -2.2ΔIW. According to the Stevenson (1990) magma ocean model, the last point of metal-silicate equilibration is at the base of the liquid silicate; therefore, by assuming no metal entrainment, a further constraint on the P-T conditions is that they must lie on the peridotite liquidus. If no light elements are considered, the P-T conditions that satisfy these criteria are 34-46 GPa and 2900-3200 K. The same procedure was followed for the Ni parameterization in order to obtain a set of conditions where D_{Ni} equals 23-27, the range of values required to explain the observed Ni mantle abundance (McDonough 2003 gives D = 25, range given by Wood et al. 2006). The P-T conditions that satisfy these criteria are 33-36 GPa and 2900-3000 K, which directly overlap with the conditions determined for Mo. These conditions are also similar to those suggested by previous studies on other elements. Gessmann and Rubie (2000) and Chabot and Agee (2003) showed that at very hot (~3500 K), reducing conditions (-2.3ΔIW), somewhat similar to those determined here, the mantle depletions of V, Cr, and Mn can be explained by equilibrium core formation. However, Righter (2011) suggested that these elements may also be housed in lower mantle minerals, thus negating the need to find compatible magma ocean conditions. In a unique study, Mann et al. (2009) examined the partitioning behavior of lithophile and weakly siderophile elements and determined that magma ocean pressures >30 GPa are required to explain certain elements' relative mantle abundances. Finally, Cottrell et al. (2010) suggested magma ocean conditions of 10-40 GPa along the peridotite liquidus in order to explain the W mantle abundance, in agreement with our

suggested conditions. However, the parameterization of Cottrell et al. (2010) determined an insignificant temperature effect on W partitioning, in opposition to Righter et al. (2010), who determined a significant increase in D_W with temperature. These contradictory results must be remedied before the implications of the partitioning behavior of W can be accurately compared to Mo and Ni.

These suggested conditions may be indicative of single-stage core formation. As Earth's accretion progressed, the impacting bodies became larger (e.g. Canup and Agnor 2000) and single-stage core formation models suggest that the very large late stage impacts would cause extensive re-equilibration and erase any chemical signature of previous smaller impacts (e.g. Righter 2011). Therefore, the conditions determined above would represent the last major impact and equilibration event. However, Earth's core is known to have ~10% of a light element present from measurements of a density deficit between the liquid outer core and liquid iron (Birch 1952). Three of the most likely candidates are S, Si, and C (Hillgren et al. 2000). Since the light elements affect D_{Ni} and D_{Mo} to varying degrees, there is a limited number of light element combinations and P-T conditions that are able to explain the mantle abundances of both elements. Still keeping oxygen fugacity fixed at -2.2ΔIW and a KLB-1 silicate composition, the mantle abundances of Ni and Mo can be explained by magma ocean conditions of 35-37 GPa and 2950-3000 K with $X_C = 0.07$, $X_S = 0.05$, and $X_{Si} = 0.06$ (approximately equal to 1.8, 3.0, and 3.4 wt.%, respectively), Figure 3-9. No oxygen metal phase contents were reported for the Mo experiments, so it was not taken into account in the parameterization, and therefore was not considered a possible solution. However, using Figure 3-7 as a guide, at the suggested pressures of around 35-37 GPa, an oxygen mole fraction in the

metal phase of ~0.1 is possible, which could significantly alter the suggested magma ocean conditions.

Besides the single-stage model for core formation, recent studies have also proposed multi-stage models in which the P-T conditions of core formation increase as accretion progresses (e.g. Rubie et al. 2011, Wade et al. 2012). In contrast to the single-stage model, multi-stage models suggest that the final impacts of accretion did not completely erase the chemical signature from previous equilibration events. Therefore, the elemental abundances observed in the mantle are the combined result of multiple equilibration events. Two such multi-stage models are shown in Figure 3-10, one at a constant oxygen fugacity and one with progressive oxidation. Both models use the Mo and Ni parameterizations performed in Section 3.4.1 and show that multi-stage core formation, with or without progressive oxidation, can explain both the Mo and Ni mantle abundances. As determined by Burkemper et al. (2012), it is the final impacts of accretion, where the D_{Mo} value is significantly low, that impart the majority of Mo to the mantle. Therefore, going from constant oxygen fugacity to progressive oxidation during the early stages of accretion does not change the final D_{Mo} value of 84 (Figure 3-10) because the last few impacts in both models are at the same oxygen fugacity of -2.2ΔIW. The same is true for Ni; a final D_{Ni} value of 25 is achieved in both the constant and progressive oxygen fugacity models. Therefore, any number of progressive oxidation paths could explain the Mo and Ni mantle abundances. However, adding light elements (as in Wade et al. 2012) and modifying the depth of equilibration (as in Burkemper et al. 2012) alters the final D values significantly because these changes affect the final equilibration events. Thus, multi-stage models offer a number of different pathways to

end at the final D values required to explain the observed mantle depletions. Figure 3-10 shows but two of those pathways.

3.5 Conclusions

The 20 new experiments presented here have further constrained the effect of pressure, temperature, and silicate melt composition on molybdenum partitioning. Our study and the recent studies of Wade et al. (2012) and Burkemper et al. (2012) have greatly expanded the Mo dataset in the literature and furthered our understanding of Mo partitioning behavior. Our parameterization includes our 20 new experiments and 190 experiments from the literature and is the most comprehensive parameterization of Mo performed to date, thus allowing for more accurate constraints on core formation. Our parameterization indicates that the Mo abundance in the upper mantle can be explained by both single- and multi-stage magma ocean models. By combining the Mo parameterization with our comprehensive Ni parameterization and taking into account the light element(s) in the core, we suggest magma ocean conditions of 35-37 GPa and 2950-3000 K with 1.8 wt.% C, 3.0 wt.% S, and 3.4 wt.% Si for the single-stage model. For most multi-stage models, D_{Mo} and D_{Ni} are only low enough to dramatically affect the mantle abundance of Mo and Ni during the final impacts of accretion, granting the models extreme flexibility (e.g. in terms of oxygen fugacity) in the early stages of accretion and allowing for many different accretion pathways.

Compilation of the literature data on Ni metal-silicate partitioning revealed that O in the metal phase has a non-trivial effect on D_{Ni} and may be a significant metal phase component at high pressures, yet it is frequently left out of core formation models.

Further studies investigating the effect of O in the metal phase on siderophile element partitioning behavior would be useful. Additionally, like Mo, W is a high valence, refractory, moderately siderophile element and can therefore provide valuable constraints on core formation. The D_W calculated in exp #19 is too high to explain the observed mantle abundance of W, and based on the literature data, it is unclear if this value would decrease sufficiently with increasing P-T conditions. This demonstrates the need for more data on W metal-silicate partitioning, especially on the effect of temperature.

Table 3-1. Compositional data for the metal and silicate phases from the electron microprobe in wt.%. Numbers in parentheses are standard deviations of the probe measurements. Some experiments have relatively large standard deviations due to prominent quench textures, see text. qs – quenched silicate, qm – quenched metal, mw – magnesiowüstite, ol – olivine, np – not probed.

Exp #	1	2	3	4	5	6	7
Metal							
Fe	38.86 (2.31)	39.82 (0.46)	35.78 (0.63)	41.50 (8.29)	46.60 (3.05)	29.66 (4.24)	42.61 (0.74)
Ni	16.31 (3.70)	8.85 (0.70)	11.41 (1.23)	10.78 (1.80)	9.78 (0.45)	8.98 (2.04)	7.97 (0.15)
Mo	44.06 (3.15)	50.22 (0.45)	52.12 (1.95)	45.55 (9.33)	42.36 (2.55)	59.70 (3.61)	48.38 (1.05)
W	np	np	np	np	np	np	np
TOTAL	99.23 (0.53)	98.90 (0.44)	99.31 (0.54)	97.83 (0.81)	98.74 (1.13)	98.35 (1.33)	98.96 (0.37)
n	8	20	17	12	11	11	6
Silicate							
SiO_2	38.32 (1.02)	28.07 (1.54)	36.80 (1.32)	36.97 (2.03)	38.75 (0.99)	37.88 (2.96)	38.96 (1.13)
TiO_2	0.75 (0.27)	9.77 (0.43)	0.46 (0.17)	np	np	np	np
Al_2O_3	11.14 (2.95)	3.41 (0.26)	10.80 (2.77)	7.23 (3.61)	4.80 (1.13)	5.21 (2.73)	5.06 (2.48)
FeO	4.66 (0.78)	14.61 (0.58)	4.27 (0.56)	9.08 (1.90)	4.98 (0.80)	6.21 (1.56)	7.51 (1.04)
MgO	37.47 (7.12)	37.56 (2.08)	36.86 (6.43)	43.70 (4.05)	47.34 (2.02)	47.21 (3.27)	45.17 (3.30)
CaO	3.50 (1.46)	3.65 (0.27)	8.77 (3.36)	3.65 (1.58)	3.87 (1.04)	3.56 (1.66)	2.92 (1.28)
K_2O	2.21 (0.99)	np	np	np	np	np	np
MnO	0.05 (0.01)	0.22 (0.03)	np	np	np	np	np
Na_2O	2.92 (1.48)	np	1.38 (0.72)	np	np	np	np
SrO	np	0.19 (0.03)	np	np	np	np	np
ZrO_2	np	2.33 (0.14)	np	np	np	np	np
P_2O_5	0.04 (0.01)	np	np	np	np	np	np
Cr_2O_3	np	np	np	np	np	np	np
NiO	np	np	np	0.063 (0.008)	0.023 (0.015)	np	np
WO_2	np	np	np	np	np	np	np
MoO_2	0.074 (0.028)	0.790 (0.070)	0.064 (0.023)	0.190 (0.096)	0.043 (0.013)	0.205 (0.118)	0.100 (0.060)
TOTAL	101.14 (1.01)	100.61 (1.08)	99.41 (1.01)	100.89 (0.80)	99.81 (0.94)	100.27 (1.13)	99.71 (0.98)
n	22	20	35	30	26	30	30
phases	qs, qm	qs, qm	mw, qs, qm	qs, qm	mw, qs, qm	mw, qs, qm	qs, qm

Table 3-1 (con't). Compositional data for the metal and silicate phases from the electron microprobe in wt.%. Numbers in parentheses are standard deviations of the probe measurements. Some experiments have relatively large standard deviations due to prominent quench textures, see text. qs – quenched silicate, qm – quenched metal, mw – magnesiowüstite, ol – olivine, np – not probed.

Exp #	8	9	10	11	12	13	14
Metal							
Fe	44.77 (2.04)	45.29 (2.31)	46.79 (0.95)	48.86 (0.14)	70.32 (1.33)	45.89 (5.17)	60.34 (0.33)
Ni	8.79 (0.67)	9.56 (0.71)	10.12 (1.00)	8.48 (0.05)	np	np	np
Mo	45.56 (2.24)	43.37 (2.99)	42.58 (2.06)	41.52 (0.44)	26.29 (2.67)	51.77 (4.84)	39.14 (0.28)
W	np	np	np	np	np	np	np
TOTAL	99.12 (0.82)	98.22 (1.05)	99.49 (0.43)	98.87 (0.51)	96.69 (1.43)	97.71 (0.55)	99.47 (0.23)
n	19	21	14	6	8	12	13
Silicate							
SiO_2	40.04 (1.10)	38.13 (0.42)	38.47 (0.68)	35.93 (2.13)	34.30 (0.80)	35.54 (0.78)	35.85 (0.88)
TiO_2	np	np	0.47 (0.11)	np	np	np	0.47 (0.11)
Al_2O_3	5.17 (2.14)	7.14 (0.91)	11.56 (0.86)	8.82 (3.36)	10.39 (1.20)	8.67 (1.25)	12.30 (1.22)
FeO	7.45 (1.05)	9.50 (0.37)	5.10 (0.71)	9.14 (2.08)	11.84 (0.91)	9.63 (0.53)	5.29 (0.54)
MgO	44.08 (3.96)	40.21 (1.52)	32.38 (2.26)	40.48 (5.80)	36.52 (1.95)	34.16 (2.67)	36.03 (4.10)
CaO	3.74 (1.55)	4.57 (0.62)	8.71 (0.99)	6.33 (2.71)	7.28 (0.91)	11.17 (1.56)	8.65 (2.60)
K_2O	np	np	np	np	np	np	np
MnO	np	np	np	np	np	np	np
Na_2O	np	np	1.47 (0.30)	np	np	np	1.48 (0.53)
SrO	np	np	np	np	np	np	np
ZrO_2	np	np	np	np	np	np	np
P_2O_5	np	np	np	np	np	np	np
Cr_2O_3	np	np	np	np	np	np	np
NiO	0.055 (0.007)	np	0.032 (0.013)	0.025 (0.010)	np	np	np
WO_2	np	np	np	np	np	np	np
MoO_2	0.114 (0.053)	0.187 (0.028)	0.055 (0.016)	0.177 (0.091)	0.112 (0.034)	0.164 (0.022)	0.024 (0.012)
TOTAL	100.65 (0.87)	99.73 (0.39)	98.24 (1.16)	100.91 (0.95)	100.44 (0.42)	99.33 (0.57)	100.09 (1.05)
n	48	29	23	31	17	20	28
phases	qs, qm	ol, qs, qm	qs, qm	qs, qm	ol, qs, qm	qs, qm	qs, qm

Table 3-1 (con't). Compositional data for the metal and silicate phases from the electron microprobe in wt.%. Numbers in parentheses are standard deviations of the probe measurements. Some experiments have relatively large standard deviations due to prominent quench textures, see text. qs – quenched silicate, qm – quenched metal, mw – magnesiowüstite, ol – olivine, np – not probed.

Exp #	15	16	17	18	19	20
Metal						
Fe	70.38 (0.26)	55.79 (0.22)	55.41 (0.24)	47.22 (0.69)	35.41 (1.24)	58.85 (1.77)
Ni	np	np	np	np	np	np
Mo	28.98 (0.48)	43.14 (0.58)	43.39 (0.49)	50.94 (0.80)	32.67 (2.09)	36.97 (0.97)
W	np	np	np	np	27.87 (2.96)	np
TOTAL	99.36 (0.27)	98.97 (0.54)	98.80 (0.55)	98.16 (0.62)	95.94 (0.65)	95.82 (1.01)
n	5	13	8	5	5	4
Silicate						
SiO_2	34.98 (3.98)	38.89 (0.65)	37.63 (1.53)	36.51 (0.99)	39.33 (0.59)	38.79 (0.31)
TiO_2	np	np	np	np	0.37 (0.02)	0.45 (0.02)
Al_2O_3	7.34 (1.13)	6.25 (1.12)	7.14 (2.90)	7.26 (1.62)	12.11 (0.35)	14.29 (0.18)
FeO	8.61 (0.94)	9.52 (0.98)	9.01 (1.50)	10.90 (0.85)	7.64 (0.42)	8.26 (0.13)
MgO	46.76 (4.85)	40.65 (2.46)	42.42 (3.85)	40.42 (1.87)	29.86 (1.07)	27.62 (0.50)
CaO	3.54 (0.78)	5.04 (1.03)	4.94 (1.50)	5.82 (0.80)	8.62 (0.31)	9.24 (0.14)
K_2O	np	np	np	np	np	np
MnO	np	np	np	np	np	np
Na_2O	np	np	np	np	0.64 (0.07)	0.90 (0.05)
SrO	np	np	np	np	np	np
ZrO_2	np	np	np	np	np	np
P_2O_5	np	np	np	np	np	np
Cr_2O_3	np	np	np	np	0.02 (0.01)	np
NiO	np	np	np	np	np	np
WO_2	np	np	np	np	0.659 (0.325)	np
MoO_2	0.113 (0.049)	0.127 (0.038)	0.092 (0.040)	0.189 (0.036)	0.251 (0.018)	0.135 (0.012)
TOTAL	101.35 (0.32)	100.48 (0.48)	101.23 (0.66)	101.10 (0.47)	99.49 (0.32)	99.69 (0.50)
n	19	23	23	27	29	14
phases	qs, qm	qs, qm	ol, qs, qm	qs, qm	mw, qs, qm	qs, qm

Table 3-2. P-T and oxygen fugacity conditions, run times, and D_{Mo} values for all experiments.

Exp #	P (GPa)	T (K)	NBO/T	Time (s)	γFe	ΔIW	D_{Mo}
1	4	2223	2.35	300	0.80	-2.11	792
2	4	2223	3.56	300	0.73	-1.07	85
3	4	2223	2.52	300	0.70	-2.02	1081
4	4	2223	3.18	300	0.78	-1.62	320
5	3	2373	3.42	240	0.83	-2.29	1322
6	4	2373	3.47	240	0.59	-1.49	389
7	5	2373	3.28	240	0.76	-1.79	645
8	6.5	2373	3.16	300	0.80	-1.87	535
9	7.5	2373	2.95	240	0.82	-1.66	310
10	8	2373	2.15	300	0.83	-2.17	1030
11	3	2173	3.00	300	0.83	-1.76	313
12	4	2223	2.84	300	0.94	-1.89	312
13	4	2223	2.88	300	0.70	-1.54	421
14	4	2223	2.43	300	0.86	-2.37	2162
15	3	2373	3.50	120	0.94	-2.20	341
16	7.5	2373	3.04	240	0.83	-1.85	455
17	4.5	2273	3.12	240	0.82	-1.89	629
18	4.5	2273	3.17	240	0.72	-1.50	360
19	15	2573*	1.99	60	0.86	-1.82	173
20	20	2673*	1.80	60	0.89	-2.00	366

* Temperature estimated from power-temperature regression

Table 3-3. Multiple linear regression coefficients from the Mo and Ni parameterizations. N/A = not applicable.

Parameter	Mo coefficient	Standard error	Ni coefficient*	Standard error
ΔIW	-1.00	0.04	-0.44	0.01
1/T	6526	598	4918	228
P/T	-65.96	16.15	-82.95	5.42
SiO_2	13.32	2.01	N/A	-
Al_2O_3	9.35	2.33	N/A	-
FeO	8.08	2.02	N/A	-
MgO	9.45	1.95	N/A	-
CaO	7.78	1.98	N/A	-
TiO_2	13.26	2.67	N/A	-
NBO/T	N/A	-	-0.07	0.01
log(1-Xc)	-7.56	0.67	-2.15	0.28
log(1-Xs)	6.96	1.30	-2.19	0.13
log(1-Xsi)	13.48	2.31	1.98	0.85
log(1-Xo)	N/A	-	-4.13	0.77
Intercept	-12.49	1.90	-0.07	0.15

* Parameterization equation:

$$\log D = a\Delta IW + b\frac{1}{T} + c\frac{P}{T} + d(NBO/T) + e\log(1 - X_C) + f\log(1 - X_S) + g\log(1 - X_{Si}) + h\log(1 - X_O) + j$$

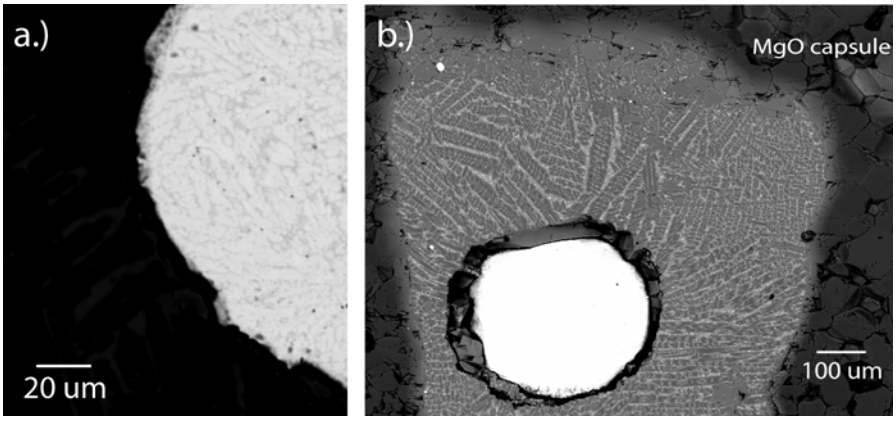

Figure 3-1. a.) Close-up back scattered electron image of the metal phase of experiment #1 showing quench texture. The contrast has been adjusted to show the metal phase texture, the brighter metal phase is more molybdenum rich and formed upon quench. The dark area to the left is the silicate phase. b.) Back scattered electron image of a typical run product showing distinct separation between the metal (bright white) and silicate (gray) phases and quench texture in the silicate phase.

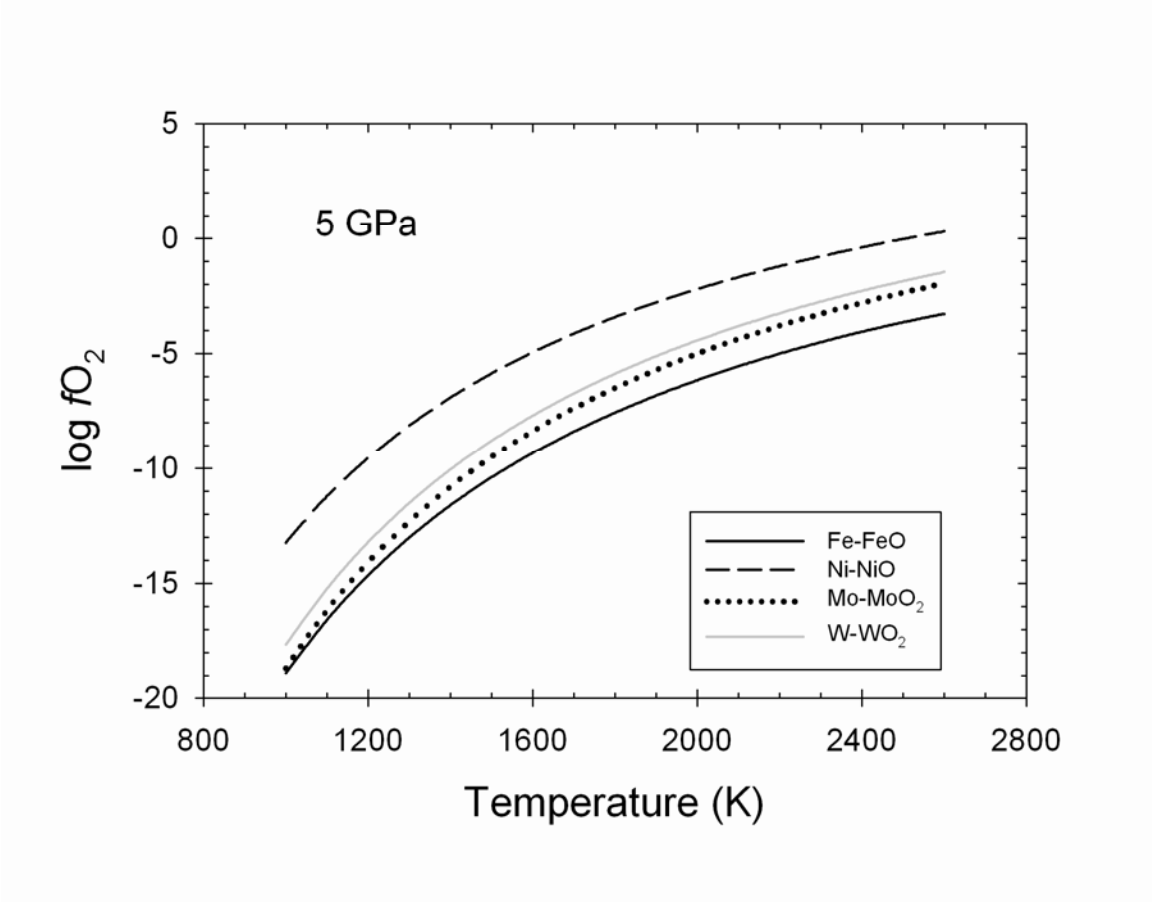

Figure 3-2. Plot of logfO_2 vs. temperature for the oxygen buffers relevant to the present study, all at 5 GPa. The iron-wüstite and nickel-nickel oxide buffers are from Campbell et al. (2009) and the molybdenum-molybdenum oxide (MMO) buffer is from Burkemper et al. (2012). The high pressure tungsten-tungsten oxide buffer was calculated using the same method as for MMO described in Burkemper et al. (2012) using the 1 bar buffer from O'Neill and Pownceby (1993) and the Murnaghan equation of state parameters from Fried et al. (2002) to calculate ΔV. Parameters include: $V_o(W) = 9.55$ mL/mol, $V_o(WO_2) = 17.82$; $B_o(W) = 315$ GPa, $B_o(WO_2) = 302$; $B_o'(W) = 3.9$, $B_o'(WO_2) = 5.0$.

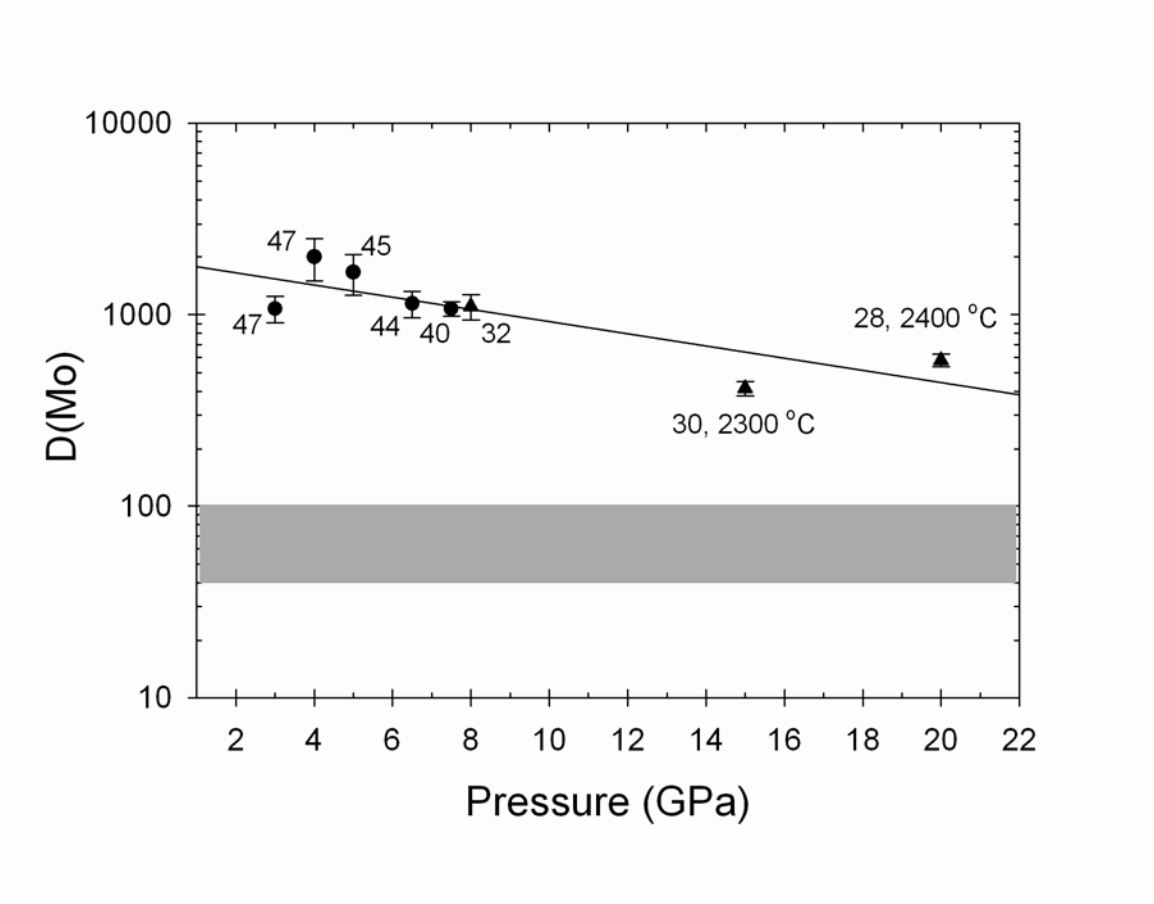

Figure 3-3. Plot of D_{Mo} vs. pressure. All the data have been adjusted to -2.2ΔIW using the relationship between oxygen fugacity and D_{Mo}, on a plot of logD_{Mo} vs. logfO_2 the slope is equal -x/4, where x is the valence of the element in the silicate, for Mo, x is equal to +4. All the experiments in the plot were performed at 2100 °C unless otherwise noted. Circular symbols indicate the starting composition was peridotite and triangles indicate a basaltic starting composition. The numbers next to the data points are the run product MgO concentrations (wt.%). The plot clearly shows that MgO infiltration from the capsule decreases slightly with increasing pressure, the effect this has on Mo partitioning is discussed in Section 3.4.1. The gray shaded region is the D_{Mo} range required to explain the observed mantle abundance of Mo. Error bars are two times the standard error from the probe measurements.

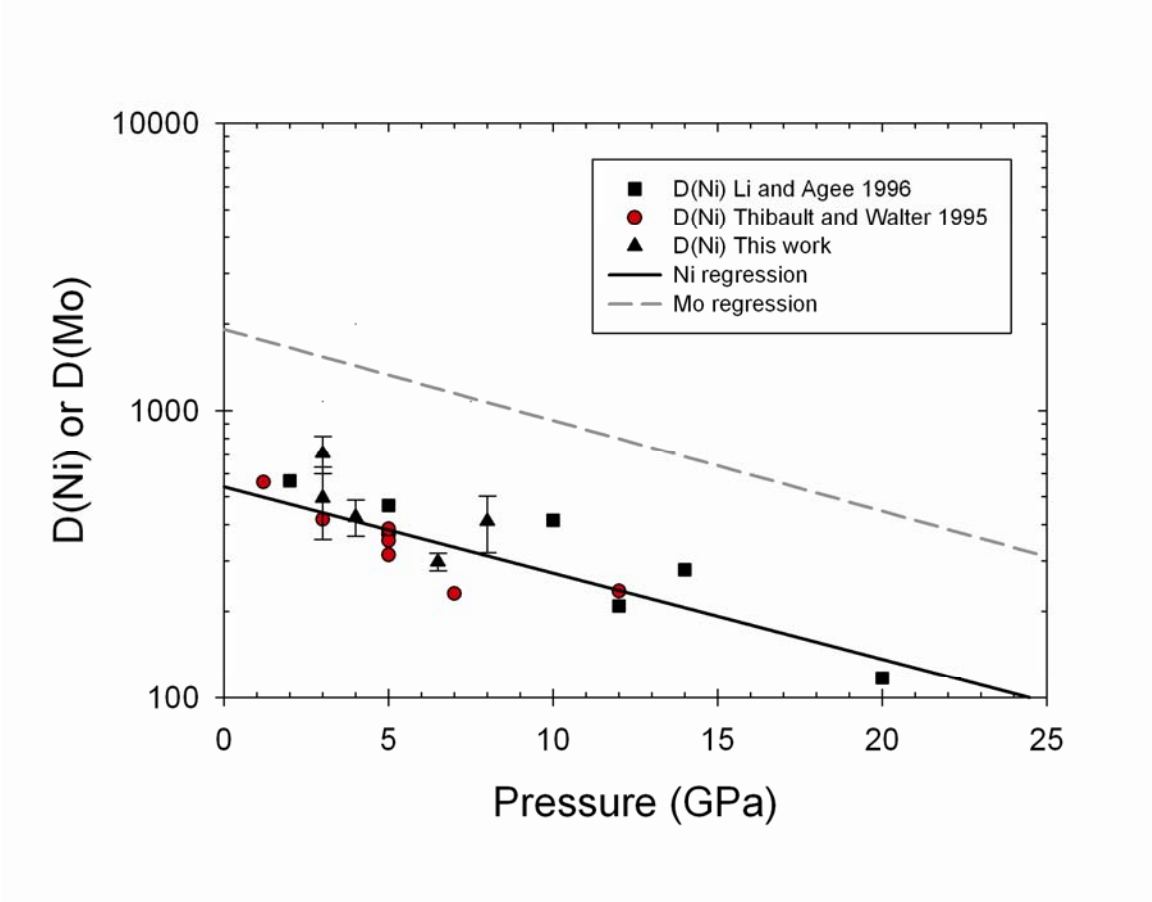

Figure 3-4. Plot of D vs. pressure. All the Ni data have been adjusted to -2.2ΔIW according to $\log D_2 = 0.5(\Delta IW_1 - \Delta IW_2) + \log D_1$. The Mo regression line is the same as that shown in Figure 2. The Ni regression line is a least squares regression for the previous data of Li and Agee (1996) and Thibault and Walter (1995), it does not include the data from the present study. No temperature or compositional corrections were applied to the data in this plot. Previous work has shown that the effects of temperature and silicate composition on D_{Ni} are weak compared to the effect of pressure (e.g. Thibault and Walter 1995, Chabot et al. 2005). Error bars are two times the standard error from the probe measurements.

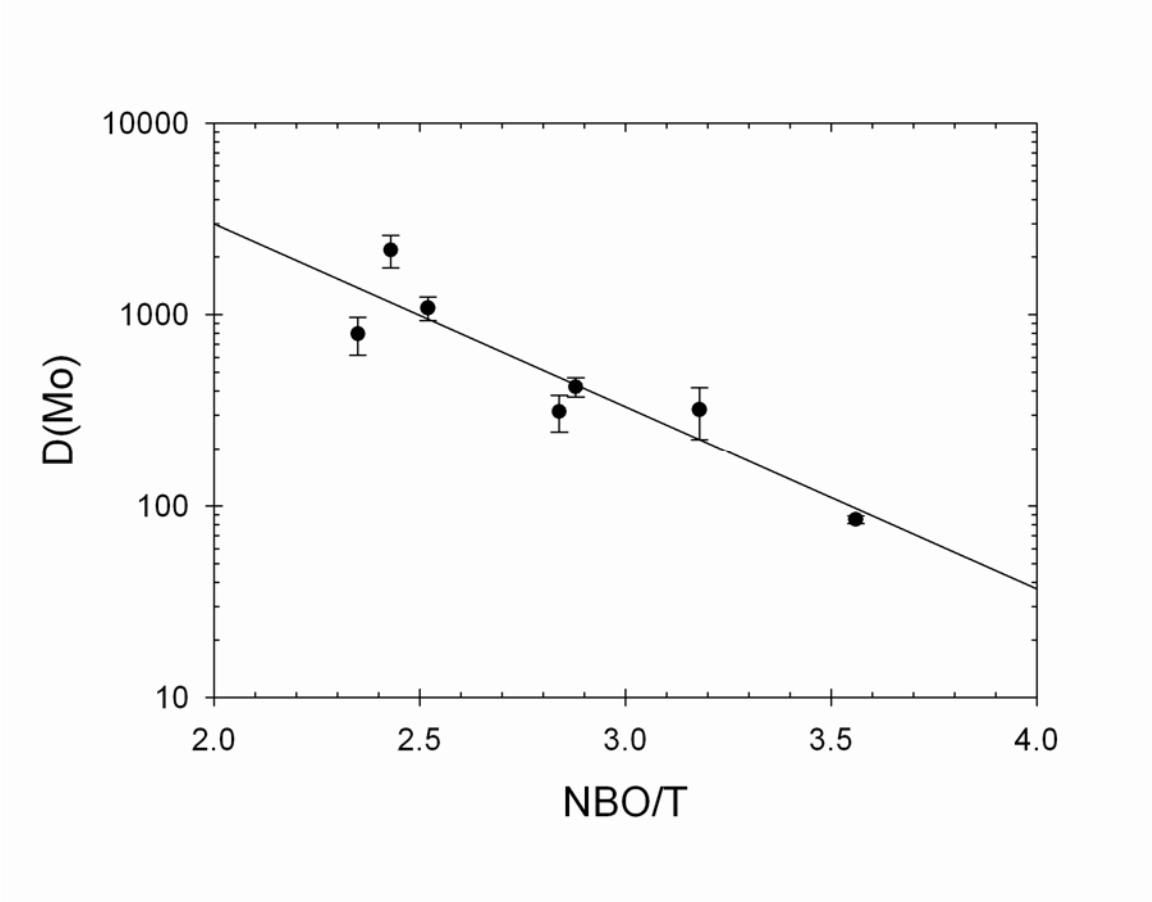

Figure 3-5. Plot of D_{Mo} vs. the ratio of non-bridging oxygens to tetrahedrally coordinated cations, NBO/T (Mysen 1983). All of the data are from experiments at 2223 K and 4 GPa. Network modifiers increase the number of non-bridging oxygens whereas, network formers increase the number of tetrahedrally coordinated cations. D_{Mo} decreases with increasing NBO/T and a similar decrease was seen by Walter and Thibault (1995), Hillgren et al. (1996), Jana and Walker (1997a), Siebert et al. (2011), and Wade et al. (2012). Error bars are two times the standard error from the probe measurements.

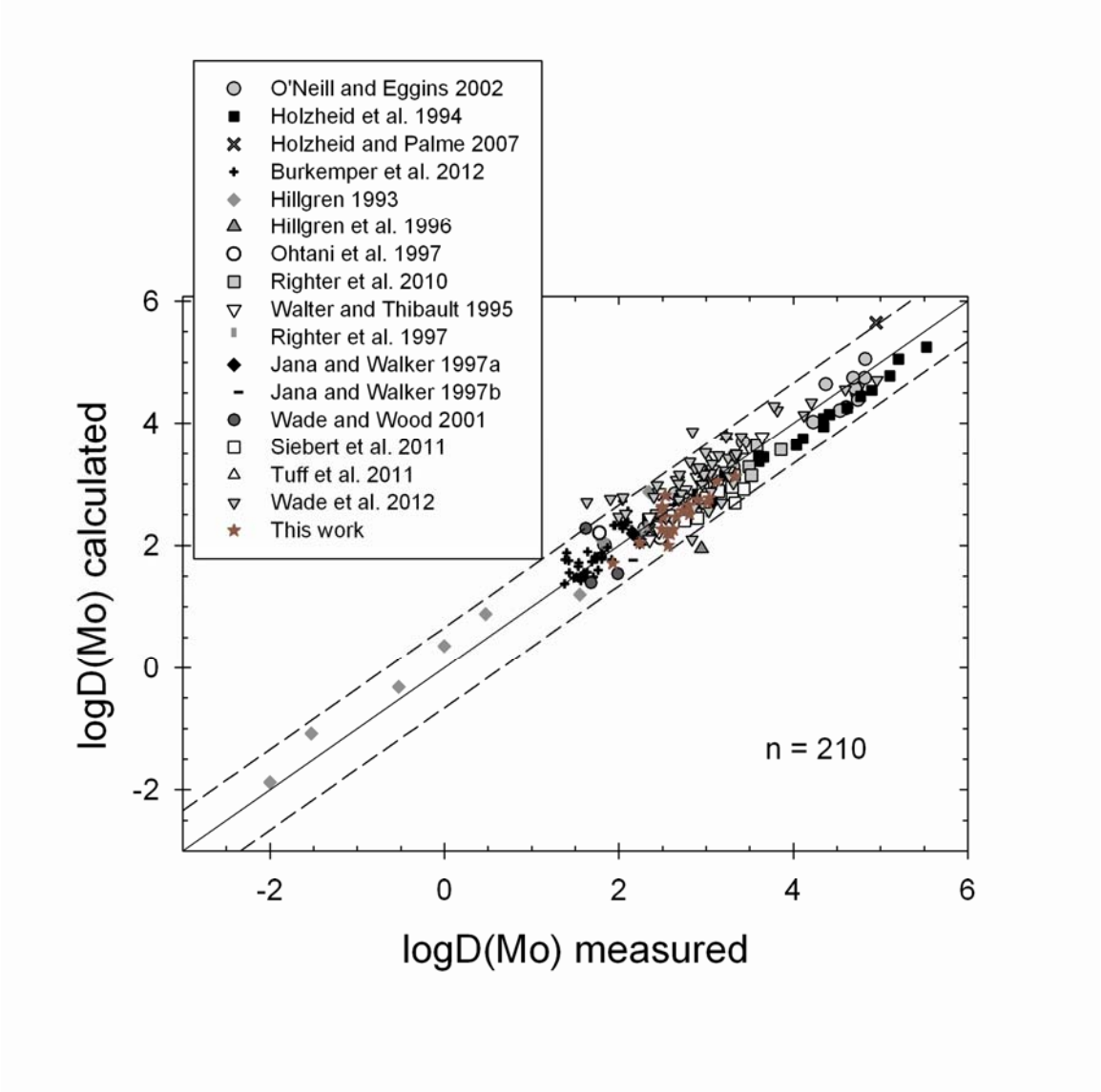

Figure 3-6. Plot of $logD_{Mo}$ calculated using the parameterization vs. $logD_{Mo}$ measured for all the data points used in the multiple linear regression. In order not to bias the regression with low pressure data, only a fraction of the O'Neill and Eggins (2002) data set was used; those at -11.63 log fO_2 for their AD and A-F melts, and those at -10.20 log fO_2 for their MAS and CAS melts. The graphite capsule experiments of Siebert et al. (2011) were also left out of the regression, due to the uncertain amount of carbon in the metal phase. As were the Si-containing experiments of Tuff et al. (2011) because the regression breaks down when they are included. It is unclear why this occurs since the data of Wade and Wood (2001) and Wade et al. (2012) are predicted well and contain up to 16.4 wt.% Si in the metal, but it is presumably due to the strong interactions between Mo and Si in the metal phase. The R^2 value for the parameterization is 0.91 with a standard error of 0.33. The solid black line is a 1:1 line and the dashed line indicates two times the standard error.

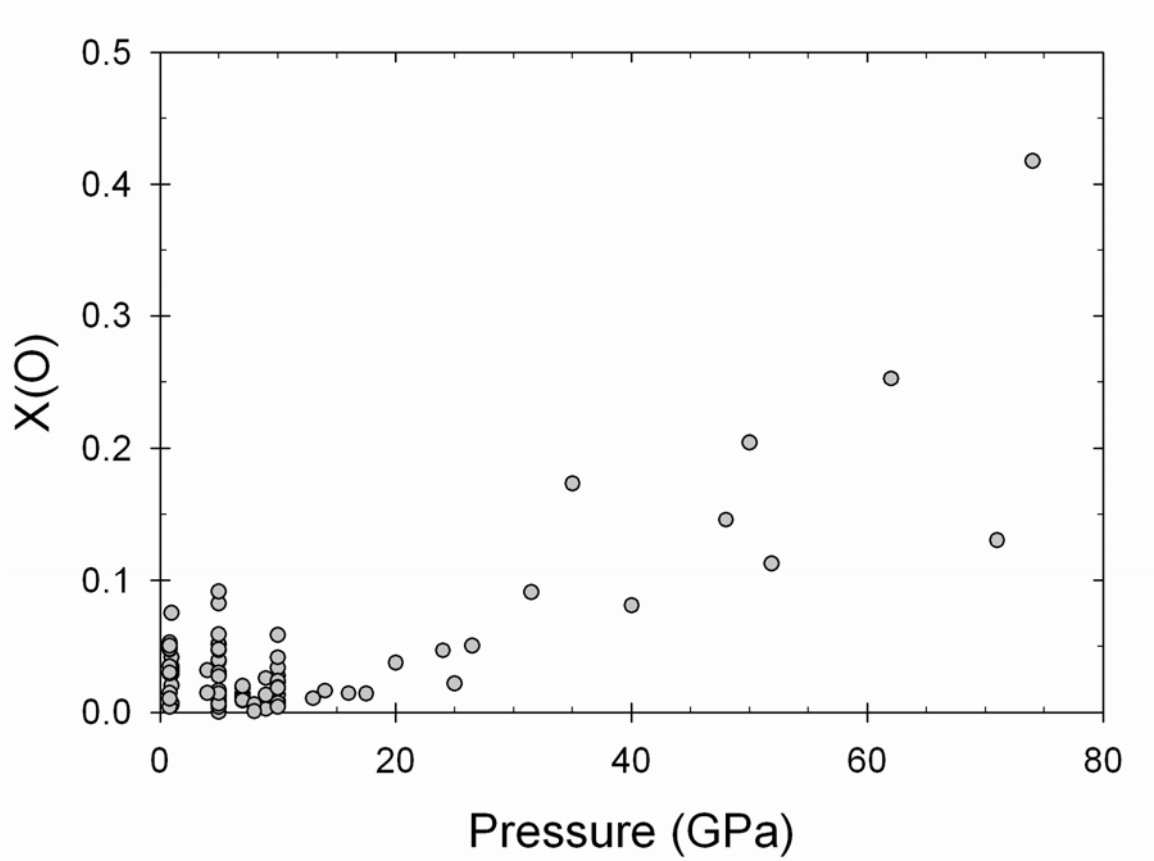

Figure 3-7. Plot of oxygen mole fraction in the metal phase vs. pressure for the Ni partitioning experiments from the literature. The plot shows no correlation at pressures below 20 GPa, but above 20 GPa, X(O) increases as pressure increases. Data are from Bouhifd et al. 2011, Siebert et al. 2011, Chabot et al. 2005, Ito et al. 1998, Li and Agee 2001, Gessmann and Rubie 1998, Jana and Walker 1997b, Jana and Walker 1997c, Walker et al. 1993, Hillgren et al. 1996, Peach and Mathez 1993, Agee et al. 1995, and Corgne et al. 2008.

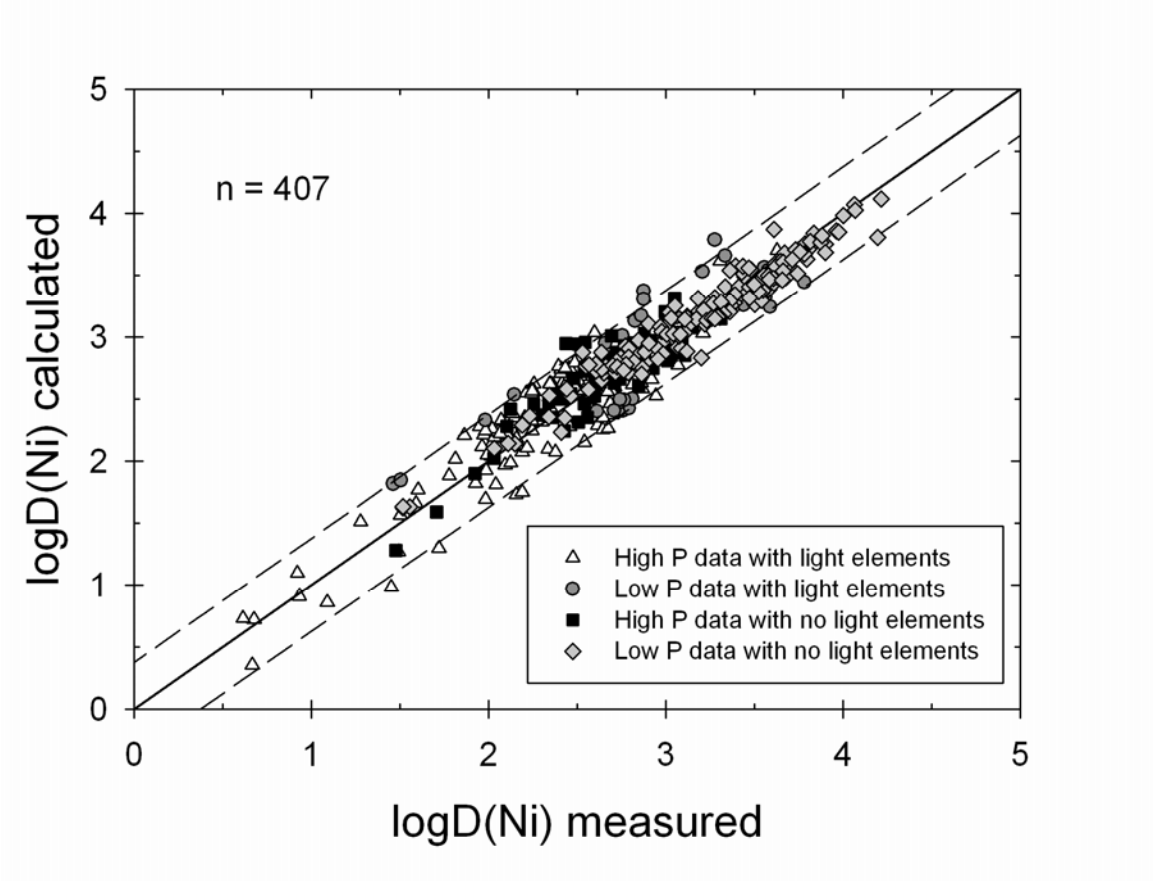

Figure 3-8. Plot of $logD_{Ni}$ calculated using the parameterization vs. $logD_{Ni}$ measured for all the data points used in the multiple linear regression. Due to the large number of studies that report D_{Ni} values, using separate graph symbols for each study caused the graph to be too cluttered. Therefore, we opted to separate the data by pressure and the presence of any light elements in order to show that the parameterization does not better predict the effects of one variable over the other. High pressure data is any experiment done at greater than 1 GPa. The plot shows a similar spread for each of the four datasets indicating that the parameterization does well predicting both the effects of pressure and light elements. The data included in the parameterization are from the present study, Wade and Wood 2001, Wade and Wood 2005, Righter et al. 2010, Holzheid and Palme 2007, Kegler et al. 2008, Bouhifd and Jephcoat 2003, Bouhifd and Jephcoat 2011, Siebert et al. 2012, Chabot et al. 2005, Ito et al. 1998, Li and Agee 1996, Li et al. 2001, Gessmann and Rubie 1998, Jana and Walker 1997a, Jana and Walker 1997b, Thibault and Walter 1995, Gaetani and Grove 1997, Walker et al. 1993, Righter et al. 1997, Hillgren 1993, Hillgren et al. 1994, Hillgren et al. 1996, Peach and Mathez 1993, Holzheid et al. 1994, Holzheid and Palme 1996, O'Neill and Eggins 2002, Siebert et al. 2011, Agee et al. 1995, Seifert et al. 1998, Corgne et al. 2008, and Ohtani et al. 1997. The R^2 value for the parameterization is 0.91 with a standard error of 0.19. The solid black line is a 1:1 line and the dashed line indicates two times the standard error.

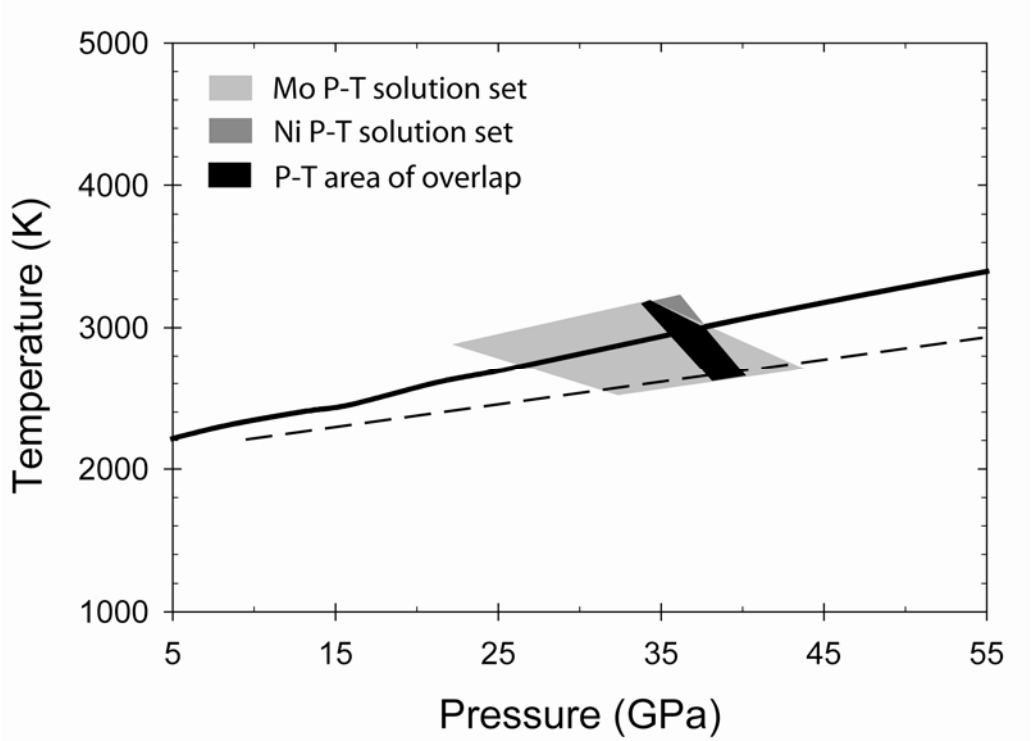

Figure 3-9. Pressure-temperature solution sets for single-stage core formation determined from the Mo and Ni parameterizations. Oxygen fugacity was kept constant at -2.2ΔIW and silicate composition was also kept constant using KLB-1 peridotite (Davis et al. 2009). Light element concentrations in the metal phase were X_c = 0.07, X_S = 0.05, and X_{Si} = 0.06. A set of conditions was considered a solution if they gave D_{Mo} = 40-100 or D_{Ni} = 23-27, and were near the peridotite liquidus. The solid line is the peridotite liquidus from Zhang and Herzberg (1994) for pressures of 0-23 GPa and from Andrault et al. (2011) for >23 GPa, and the dashed line is the mantle solidus from Andrault et al. (2011). The light gray shaded area is the P-T solution set that can explain the observed mantle abundance of Mo, the dark gray is for Ni, and the black shaded area is the where the two solution sets overlap.

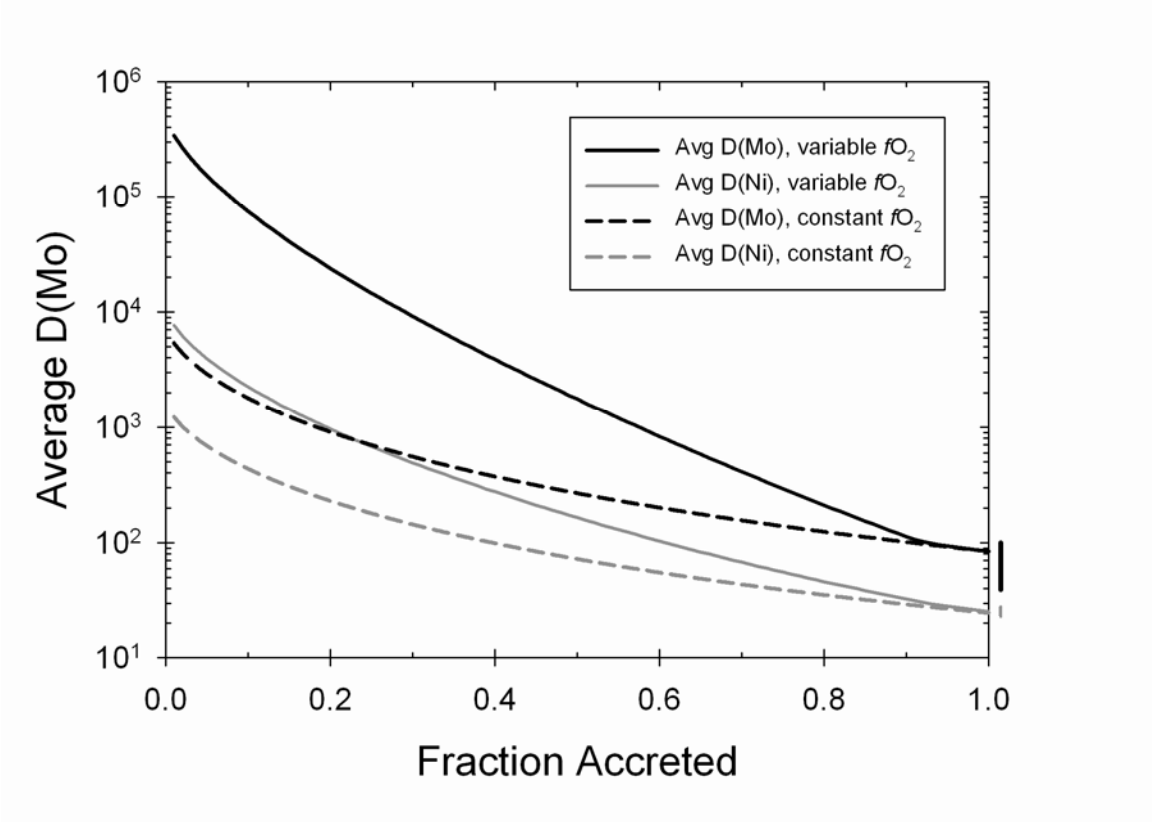

Figure 3-10. Average D_{Ni} and D_{Mo} values vs. fraction accreted for two different multi-stage models, one with progressive oxidation and one at a constant oxygen fugacity of -2.2ΔIW. The models are similar to those put forth by Wade and Wood (2005) in which Earth is accreted in 1% steps and the incoming metal equilibrates with the entire mantle before being segregated to the core, where no further equilibration occurs. The pressure of equilibration was kept constant at the base of a magma ocean that is 27% of the depth to the core-mantle boundary (135 GPa). Temperature increases with pressure along the peridotite liquidus (from Andrault et al. 2011). For the progressive oxidation model, oxygen fugacity increases at a constant rate of 0.02 log units from -4.00ΔIW at 1% accretion to -2.22ΔIW at 90% accretion, and then stays at -2.20ΔIW for the rest of accretion. For the constant oxygen fugacity model, fO_2 remains at -2.20ΔIW throughout accretion. The lines to the right of the graph indicate the D_{Ni} and D_{Mo} values required to explain the observed mantle abundance of Ni (gray) and Mo (black).

3.6 References

Agee, C.B., Li, J., Shannon, M.C. (1995) Pressure-temperature phase diagram for the Allende meteorite. Journal of Geophysical Research 100, 17725-17740

Andrault, D., Bolfan-Casanova, N., Lo Nigro, G., Bouhifd, M.A., Garbarino, G., Mezouar, M. (2011) Solidus and liquidus profiles of chondritic mantle: Implication for melting of Earth across its history. Earth and Planetary Science Letters 304, 251-259

Bertka, C.M., Fei, Y. (1997) Mineralogy of the martian interior up to core-mantle boundary pressures. Journal of Geophysical Research 102, 5251-5264

Birch, F. (1952) Elasticity and constitution of the Earth's interior. Journal of Geophysical Research 57, 227-286

Bouhifd, M.A., Jephcoat, A.P. (2003) The effect of pressure on partitioning of Ni and Co between silicate and iron-rich metal liquids: a diamond-anvil cell study. Earth and Planetary Science Letters 209, 245-255

Bouhifd, M.A., Jephcoat, A.P. (2011) Convergence of Ni and Co metal-silicate partition coefficients in the deep magma-ocean and coupled silicon-oxygen solubility in iron melts at high pressures. Earth and Planetary Science Letters 307, 341-348

Brown, S.M., Elkins-Tanton, L.T. (2009) Compositions of Mercury's earliest crust from magma ocean models. Earth and Planetary Science Letters 286, 446-455

Burkemper, L.K., Agee, C.B., Garcia, K.A. (2012) Constraints on core formation from molybdenum solubility in silicate melts at high pressure. Earth and Planetary Science Letters 335-336, 95-104

Cameron, A.G.W., Ward, W.R. (1976) The origin of the Moon. Lunar Science VII, 120-122

Campbell, A.J., Danielson, L., Righter, K., Seagle, C.T., Wang, Y., Prakapenka, V.B. (2009) High pressure effects on the iron-iron oxide nickel-nickel oxide oxygen fugacity buffers. Earth and Planetary Science Letters 286, 556-564

Canup, R.M., Agnor, C.B. (2000) Accretion of the terrestrial planets and the Earth-Moon system. In: Canup, R. M. and Righter, K. eds. *Origin of the Earth and Moon*. The University of Arizona Press, Tucson AZ, pp. 113-129

Canup, R.M., Asphaug, E. (2001) Origin of the Moon in a giant impact near the end of Earth's formation. Nature 412, 708-712

Chabot, N.L., Agee, C.B. (2003) Core formation in the Earth and Moon: new experimental constraints from V, Cr, and Mn. Geochimica et Cosmochimica Acta 67, 2077-2091

Chabot, N.L., Draper, D.S., Agee, C.B. (2005) Conditions of core formation in the Earth: constraints from nickel and cobalt partitioning. Geochimica et Cosmochimica Acta 69, 2141-2151

Corgne, A., Keshav, S., Wood, B.J., McDonough, W.F., Fei, Y. (2008) Metal-silicate partitioning and constraints on core composition and oxygen fugacity during Earth accretion. Geochimica et Cosmochimica Acta 72, 574-589

Cottrell, E., Walter, M.J., Walker, D. (2009) Metal-silicate partitioning of tungsten at high pressure and temperature: implications for equilibrium core formation in Earth. Earth and Planetary Science Letters 281, 275-287

Cottrell, E., Walter, M.J., Walker, D. (2010) Erratum to "Metal-silicate partitioning of tungsten at high pressure and temperature: Implications for equilibrium core formation in Earth" [Earth and Planetary Science Letters 281 (2009) 275-287]. Earth and Planetary Science Letters 289, 631-634

Davis, F.A., Tangeman, J.A., Tenner, T.J., Hirschmann, M.M. (2009) The composition of KLB-1 peridotite. American Mineralogist 94, 176-180

Drake, M.J., Newsom, H.E., Capobianco, C.J. (1989) V, Cr, and Mn in the Earth, Moon EPB, and SPB and the origin of the Moon: Experimental studies. Geochimica et Cosmochimica Acta 53, 2101-2111

Draper, D.S. (1991) Late Cenozoic bimodal magmatism in the northern Basin and Range Province of southeastern Oregon. Journal of Volcanology and Geothermal Research 47, 299-328

Ertel, W., O'Neill, H.St.C., Dingwell, D.B., Spettel, B. (1996) Solubility of tungsten in a haplobasaltic melt as a function of temperature and oxygen fugacity. Geochimica et Cosmochimica Acta 60, 1171-1180

Fried, L.E., Howard, W.M., Souers, P.C. (2002) EXP6: A new equation of state library for high pressure thermochemistry. 12th International Detonation Symposium, San Diego, CA

Gaetani, G.A., Grove, T.L. (1997) Partitioning of moderately siderophile elements among olivine, silicate melt, and sulfide melt: Constraints on core formation in the Earth and Mars. Geochimica et Cosmochimica Acta 61, 1829-1846

Gessmann, C.K., Rubie, D.C. (1998) The effect of temperature on the partitioning of nickel, cobalt, manganese, chromium, and vanadium at 9 GPa and constraints on formation of the Earth's core. Geochimica et Cosmochimica Acta 62, 867-882

Gessmann, C.K., Rubie, D.C. (2000) The origin of the depletions of V, Cr, and Mn in the mantles of the Earth and Moon. Earth and Planetary Science Letters 184, 95-107

Greenwood, R.C., Franchi, I.A., Jambon, A., Buchanan, P.C. (2005) Widespread magma oceans on asteroidal bodies in the early Solar System. Nature 435, 916-918

Hartmann, W.K., Davis, D.R. (1975) Satellite-sized planetesimals and lunar origin. Icarus 24, 504-515

Hillgren, V.J. (1993) Partitioning behavior of moderately siderophile elements in Ni-rich systems: implications for the Earth and Moon. PhD thesis. University of Arizona, 423 pp

Hillgren, V.J. Drake, M.J., Rubie, D.C. (1994) High-pressure and high-temperature experiments on core-mantle segregation in the accreting Earth. Science 264, 1442-1445

Hillgren, V.J., Drake, M.J., Rubie, D.C. (1996) High pressure and high temperature metal-silicate partitioning of siderophile elements: The importance of silicate liquid composition. Geochimica et Cosmochimica Acta 60, 2257-2263

Hillgren, V.J., Gessmann, C.K., Li, J. (2000) An experimental perspective on the light element in Earth's core. In: Canup, R. M. and Righter, K. eds. *Origin of the Earth and Moon*. The University of Arizona Press, Tucson AZ, 245-263

Holzheid, A., Borisov, A., Palme, H. (1994) The effect of oxygen fugacity and temperature on solubilities of nickel, cobalt, and molybdenum in silicate melts. Geochimica et Cosmochimica Acta 58, 1975-1981

Holzheid, A., Palme, H. (1996) The influence of FeO on the solubilities of cobalt and nickel in silicate melts. Geochimica et Cosmochimica Acta 60, 1181-1193

Holzheid, A., Palme, H. (2007) The formation of eucrites: Constraints from metal-silicate partition coefficients. Meteoritics and Planetary Science 42, 1817-1829

Ito E., Katsura, T., Suzuki, T. (1998) Metal/silicate partitioning of Mn, Co, and Ni at high-pressures and high temperatures and implications for core formation in a deep magma ocean. Geophysical monograph 101, American Geophysical Union, Washington, DC, 215-225

Jana, D., Walker, D. (1997a) The influence of silicate melt composition on distribution of siderophile elements among metal and silicate liquids. Earth and Planetary Science Letters 150, 463-472

Jana, D., Walker, D. (1997b) The impact of carbon on element distribution during core formation. Geochimica et Cosmochimica Acta 61, 2759-2763

Jana, D., Walker, D. (1997c) The influence of sulfur on partitioning of siderophile elements. Geochimica et Cosmochimica Acta 61, 5255-5277

Karato, S., Murthy, V.R. (1997) Core formation and chemical equilibrium in the Earth – I. Physical considerations. Physics of the Earth and Planetary Interiors 100, 61-79

Kegler, P., Holzheid, A., Frost, D.J., Rubie, D.C., Dohmen, R., Palme, H. (2008) New Ni and Co metal-silicate partitioning data and their relevance for an early terrestrial magma ocean. Earth and Planetary Science Letters 268, 28-40

Kleine, T., Mezger, K., Munker, C., Palme, H., Bischoff, A. (2004) ^{182}Hf-^{182}W isotope systematics of chondrites, eucrites, and martian meteorites: Chronology of core formation and early mantle differentiation in Vesta and Mars. Geochimica et Cosmochimica Acta 68, 2935-2946

Leinenweber, K.D., Tyburczy, J.A., Sharp, T.G., Soignard,E., Diedrich, T., Petuskey, W.B., Wang, Y., Mosenfelder, J.L. (2012) Cell assemblies for reproducible multi-anvil experiments (the COMPRES assemblies). American Mineralogist 97, 353-369

Li, J., Agee, C.B. (1996) Geochemistry of mantle-core differentiation at high pressure. Nature 381, 686-689

Li, J., Agee, C.B. (2001) The effect of pressure, temperature, oxygen fugacity, and composition on partitioning of nickel and cobalt between liquid Fe-Ni-S alloy and liquid silicate: Implications for the Earth's core formation. Geochimica et Cosmochimica Acta 65, 1821-1832

Lodders, K., Palme, H. (1991) On the chalcophile character of molybdenum: determination of sulfide/silicate partition coefficients of Mo and W. Earth and Planetary Science Letters 103, 311-324

Mann, U., Frost, D.J., Rubie, D.C. (2009) Evidence for high-pressure core-mantle differentiation from the metal-silicate partitioning of lithophile and weakly-siderophile elements. Geochimica et Cosmochimica Acta 73, 7360-7386

McDonough, W.F., Sun, S.-s. (1995) The composition of the Earth. Chemical Geology 120, 223-253

McDonough, W.F., (2003) Compositional model for the Earth's core. In: Carlson, R.W. ed. *Treatise on Geochemistry, Vol. 2, The Mantle and Core.* Elsevier Ltd, 547-568

Melosh, H.J. (1990) Giant impacts and the thermal state of the early Earth. In: Newsom, H.E. and Jones, J.H. eds. *Origin of the Earth*. Oxford University Press, 69-83

Mysen, B.O. (1983) The structure of silicate melts. Annual Review of Earth and Planetary Science 11, 75-97

Newsom, H. E. (1995) Composition of the solar system, planets, meteorites, and major terrestrial reservoirs. In: Ahrens, T.J. ed. *Global Earth Physics: A Handbook of Physical Constants*. AGU Reference Shelf, 159-189

Ohtani, E., Yurimoto, H., Seto, S. (1997) Element partitioning between metallic liquid, silicate liquid, and lower-mantle minerals: Implications for core formation of the Earth. Physics of the Earth and Planetary Interiors 100, 97-114

O'Neill, H.S.C., Pownceby, M.I. (1993) Thermodynamic data from redox reactions at high temperatures. I. An experimental and theoretical assessment of the electrochemical method using stabilized zirconia electrolytes, with revised values for the Fe-"FeO", Co-CoO, Ni-NiO and Cu-Cu_2O oxygen buffers, and new data for the W-WO_2 buffer. Contributions to Mineralogy and Petrology 114, 296-314

O'Neill, H.S.C., Eggins, S.M., (2002) The effect of melt composition on trace element partitioning: an experimental investigation of the activity coefficient of FeO, NiO, CoO, MoO_2, MoO_3 in silicate melts. Chemical Geology 186, 151-181

Palme, H., O'Neill, H.S.C. (2003) Cosmochemical estimates of mantle composition. In: Carlson, R.W. ed. *Treatise on Geochemistry, Vol. 2, The Mantle and Core.* Elsevier Ltd, pp. 1-38

Peach, C.L., Mathez, E.A. (1993) Sulfide melt-silicate melt distribution coefficients for nickel and iron and implications for the distribution of other chalcophile elements. Geochimica et Cosmochimica Acta 57, 3013-3021

Righter, K., Drake, M.J. (1996) Core formation in Earth's Moon, Mars, and Vesta. Icarus 124, 513-529

Righter, K., Drake, M.J. (1997) A magma ocean on Vesta: Core formation and petrogensis of eucrites and diogenites. Meteoritics and Planetary Science 32, 929-944

Righter, K., Drake, M.J., Yaxley, G. (1997) Prediction of siderophile element metal-silicate partition coefficients to 20 GPa and 2800 ^{o}C: the effects of pressure, temperature, oxygen fugacity, and silicate and metallic melt compositions. Physics of the Earth and Planetary Interiors 100, 115-134

Righter, K., Drake, M.J. (1999) Effect of water on metal-silicate partitioning of siderophile elements: A high pressure and temperature terrestrial magma ocean and core formation. Earth and Planetary Science Letters 171, 383-399

Righter, K., Pando, K.M., Danielson, L., Lee, C.T. (2010) Partitioning of Mo, P and other siderophile elements (Cu, Ga, Sn, Ni, Co, Cr, Mn, V, and W) between metal and silicate melt as a function of temperature and silicate composition. Earth and Planetary Science Letters 291, 1-9

Righter, K. (2011) Prediction of metal-silicate partition coefficients for siderophile elements: An update and assessment of PT conditions for metal-silicate equilibrium during accretion of the Earth. Earth and Planetary Science Letters 304, 158-167

Riner, M.A., Lucey, P.G., Desch, S.J., McCubbin, F.M. (2009) Nature of opaque components on Mercury: Insights into a Mercurian magma ocean. Geophys. Res. Lett. 36, L02201, doi: 10.1029/2008GL036128

Ringwood, A.E. (1966) Chemical evolution of the terrestrial planets. Geochimica et Cosmochimica Acta 30, 41-104

Rubie, D.C., Melosh, H.J., Reid, J.E., Liebske, C., and Righter, K. (2003) Mechanisms of metal-silicate equilibration in the terrestrial magma ocean. Earth and Planetary Science Letters 205, 239-255

Rubie, D.C., Frost, D.J., Mann, U., Asahara, Y., Nimmo, F., Tsuno, K., Kegler, P., Holzheid, A., Palme, H. (2011) Heterogeneous accretion, composition and core-mantle differentiation of the Earth. Earth and Planetary Science Letters 301, 31-42

Schnetzler, C.C., Philpotts, J.A. (1971) Alkali, alkaline earth, and rare-earth element concentrations in some Apollo 12 soils, rocks, and separated phases. Proc. Second Lunar Sci. Con. 2, 1101-1122

Siebert, J., Corgne, A., Ryerson, F.J. (2011) Systematics of metal-silicate partitioning for many siderophile elements applied to Earth's core formation. Geochimica et Cosmochimica Acta 75, 1451-1489

Siebert, J., Badro, J., Antonangeli, D., Ryerson, F.J. (2012) Metal-silicate partitioning of Ni and Co in a deep magma ocean. Earth and Planetary Science Letters 321-322, 189-197

Seifert, S., O'Neill, H.S.C., Brey, G. (1988) The partitioning of Fe, Ni and Co between olivine, metal, and basaltic liquid: An experimental and thermodynamic investigation, with application to the composition of the lunar core. Geochimica et Cosmochimica Acta 52, 603-616

Smith, J.V., Anderson, A.T., Newton, R.C., Olsen, E.J., Wyllie, P.J. (1970) A petrologic model for the Moon based on petrogenesis, experimental petrology, and physical properties. The Journal of Geology 78, 381-405

Stevenson, D.J. (1990) Fluid dynamics of core formation. In: Newsom, H.E. and Jones, J.H. Eds., *Origin of the Earth*. Oxford University Press, New York, pp. 231-249

Thibault, Y., Walter, M.J. (1995) The influence of pressure and temperature on the metal-silicate partition coefficients of nickel and cobalt in a model C1 chondrite and implications for metal segragation in a deep magma ocean. Geochimica et Cosmochimica Acta 59, 991-1002

Tonks, W.B., Melosh, H.J. (1993) Magma ocean formation due to giant impacts. Journal of Geophysical Research 98, 5319-5333

Tuff, J., Wood, B.J., Wade, J. (2011) The effect of Si on metal-silicate partitioning of siderophile elements and implications for the conditions of core formation. Geochimica et Cosmochimica Acta 75, 673-690

Wade, J., Wood, B. J. (2001) The Earth's 'missing' niobium may be in the core. Nature 409, 75-78

Wade, J. Wood, B.J. (2005) Core formation and the oxidation state of the Earth. Earth and Planetary Science Letters 236, 78-95

Wade, J., Wood, B.J., Tuff, J. (2012) Metal-silicate partitioning of Mo and W at high pressures and temperatures: Evidence for late accretion of sulphur to the Earth. Geochimica et Cosmochimica Acta 85, 58-74

Walker, D., Norby, L., Jones, J.H. (1993) Superheating effects on metal-silicate partitioning of siderophile elements. Science 262, 1858-1861

Walter, M.J., Thibault, Y. (1995) Partitioning of tungsten and molybdenum between metallic liquid and silicate melt. Science 270, 1186-1189

Warren, P.H. (1985) The magma ocean concept and lunar evolution. Ann. Rev. Earth Planet. Sci. 13, 201-240

Wetherill, G.W. (1985) Occurrence of giant impacts during the growth of the terrestrial planets. Science 228, 877-879

Wood, J.A., Dickey Jr, J.S., Marvin, U.B., Powell, B.N. (1970) Lunar anorthosites and a geophysical model of the moon. Proc. Apollo 11 Lunar Sci. Conf. 1, 965-988

Wood, B.J., Walter, M.J., Wade, J. (2006) Accretion of the Earth and segregation of its core. Nature 441, 825-833

Zhang, J., Herzberg, C. (1994) Melting experiments on anhydrous peridotite KLB-1 from 5.0 to 22.5 GPa. Journal of Geophysical Research 99, 17729-17745

4.0 Late-stage Equilibrium Core Formation on Earth

Abstract

We present the results of 12 new high pressure metal-silicate partitioning experiments examining the effect of oxygen fugacity, temperature, sulfur, and carbon on W partitioning, and 2 new Mo metal-silicate partitioning experiments examining the effect of sulfur and carbon. Through the investigation of the effect of oxygen fugacity on D_W, we determined that W dissolves as W^{6+} in silicate melts, over the oxygen fugacity range investigated. Over the 250 degree temperature range studied, there is no discernable temperature effect on D_W, but parameterization of our data and an extensive amount of data from the literature (over a wider temperature range) shows temperature to have a slight increasing effect. The addition of carbon to the metal phase causes both W and Mo to become more siderophile; whereas, sulfur causes both elements to become less siderophile, especially W. By combining our W parameterization with an updated Mo expression and a Ni parameterization from the literature, we show that these three elements' mantle abundances can be explained by a single set of magma ocean conditions, 35-37 GPa (~1100 km depth) and 2950-3000 K with $X_C = 0.07$, $X_S = 0.05$, and $X_{Si} = 0.06$ in the metal phase. This metal phase composition is in agreement with isotope and light element-iron alloy studies. The fact that a single set of conditions was able to be determined for three key elements suggests that a large impact during the late stages of Earth's accretion caused extensive metal-silicate re-equilibration and the siderophile element signature imparted to the mantle was the result of final equilibration at the base of the resulting magma ocean.

4.1 Introduction

Numerical modeling of terrestrial planet accretion suggests that large impacts between planetary embryos are likely during the late stages of accretion (Wetherill 1985, Canup and Agnor 2000). The large amount of heat released from these impacts, along with heat produced from the gravitational energy of accretion, would cause extensive melting of the growing Earth and the formation of one or more magma oceans (Melosh 1990, Tonks and Melosh 1993). In the magma ocean model, core formation occurs by Fe-rich metal separating out of, and equilibrating with, a layer of liquid silicate. The metal would sink to the silicate liquidus where it would pond, equilibration would stop, and the metal would sink through the solid silicate to the center of the planet as large diapirs (e.g. Stevenson 1990). The first geochemical evidence in support of this theory came from high pressure partitioning experiments on the moderately siderophile elements Ni and Co. The siderophile elements are depleted in the mantle (relative to chondritic abundances) due to core formation and partition coefficients [$D_i = c_i(\text{metal})/c_i(\text{silicate})$] from experiments at 1 bar determined D values that were too high to explain the observed upper mantle abundance of Ni and Co (Ringwood 1966, see review in Jones and Drake 1986). However, both elements become less siderophile with increasing pressure and reach the required D values at pressures > 25 GPa, suggesting core formation out of a magma ocean of ~750 km depth (Li and Agee 1996).

Further studies showed that the partitioning behavior of other siderophile elements are also affected by pressure; however, the magma ocean conditions during core formation (i.e. pressure, temperature, oxygen fugacity) are still not agreed upon (e.g. Gessmann and Rubie 2000, Chabot and Agee 2003, Chabot et al. 2005, Kegler et al.

2008, Wood et al. 2009). For example, Wade and Wood (2005) suggested a multi-stage core formation model with the oxygen fugacity and the P-T conditions of core formation increasing as accretion progressed and impactors grew in size. Each impact would cause a magma ocean of specific depth and the chemical signature imparted to the mantle would be the combined result of each equilibration event. The progressive oxidation multi-stage models are exceptional in their ability to explain the mantle abundances of V and Cr. Nevertheless, Righter (2011) showed that V, Cr, and Mn are more compatible in deep mantle minerals than metal, thus eliminating the need to find metal-silicate equilibrium (magma ocean) conditions that explain these elements. As a result, Righter (2011) was able to determine a set of single-stage magma ocean conditions (~30 GPa, ~3500 K, -1ΔIW, $X_S = 0.04$, $X_C = 0.11$) that can explain Ni, Co, Mo, W, Ga, Cu, P, and Pd, indicating extensive metal-silicate re-equilibration after a large impact late in accretion which erased the chemical signature of previous equilibration events. Using an expanded experimental database, Burkemper et al. (2013) suggested magma ocean conditions of 35-37 GPa, 2950-3000 K and -2.2ΔIW (2.2 log units below the iron-wüstite buffer) with $X_C = 0.07$, $X_S = 0.05$, and $X_{Si} = 0.06$ in the core metal in order to explain the mantle abundances of Mo and Ni.

In order to come to a consensus on the conditions of core formation, tighter constraints need to be placed on the models. Therefore more experiments are needed, especially for sparsely examined elements and for the effect of light elements in the metal phase which, in comparison to the effects of pressure and temperature, has not been as extensively investigated. There has been debate over the identity of the light element, or combination of light elements, in the core since Birch (1952) noticed a density deficit

between the outer core and pure liquid iron. The most probable elements are H, C, O, Si, and S (Hillgren et al. 2000) and for any core formation model to be complete it must take into account the light element(s) in the core, therefore potentially providing insight into the composition of the core.

Tungsten is an ideal element for studying core formation. It is refractory, hence it should not be depleted in the bulk Earth relative to its chondritic abundance. It is moderately siderophile so it partitions strongly into the metal phase, but enough remains in the silicate to measure with relative accuracy, as opposed to the highly siderophile elements. Furthermore, the tungsten partitioning data in the literature are not in agreement. Cottrell et al. (2009) showed temperature to have a negligible effect on D_W but the data of Righter et al. (2010) showed a significant increasing effect. Additionally, the valence state of W when it is dissolved in silicate melts at relevant core formation oxygen fugacities (around -2ΔIW) has been argued to be predominantly 4+ (Ertel et al. 1996), predominantly 6+ (O'Neill et al. 2008), and to show a change in valence upon increasing pressure (Cottrell et al. 2009). In this study we present new data on the effect of oxygen fugacity (related to valence state) and temperature on D_W, and examine the effect of S and C on the partitioning behavior of W and Mo.

4.2 Experimental and analytical techniques

Starting silicate materials consisted of two different synthetic compositions, a peridotite and basalt, and one natural basalt (NB219, Draper 1991). Metal materials consisted of Fe and Mo metal shavings obtained by filing >99.5% pure metal rods, and powdered W (99.9%, Alfa Aesar). Two metal mixtures were made, one with 60% Fe and

40% W, and the other with 60% Fe and 40% Mo. These mixtures where then added to the silicate starting material in a 3:1 silicate to metal ratio so that the final bulk W (or Mo) abundance was 10 wt.%. This is the same concentration used by Burkemper et al. (2013) for their Mo experiments which showed no apparent deviations from Henry's Law. Additionally, W has been shown to obey Henry's Law behavior up to very high silicate concentrations, 14 wt.% at 1500 °C (Ertel et al. 1996). For the light element experiments, 2.3 wt.% S was added to the bulk silicate-metal mixtures for the two sulfur experiments, and 1.3 wt.% C for the two carbon experiments. All of the experiments were run on a 2000T Walker-type multi-anvil press at the Institute of Meteoritics (IOM), using the same calibration methods described in Agee et al. (1995). The experimental set-up was the same as that described in Burkemper et al. (2013) except for the use of graphite capsules as well as magnesia capsules. All capsules were machined at Arizona State University as part of the COMPRES Multi-Anvil Cell Assembly Initiative. The cell assembly consisted of a ceramic octahedron fitted with a Re heater and a W/Re thermocouple perpendicular to the heater. A Eurotherm 3504 controller was used to monitor the temperature.

Each experiment was rapidly quenched by terminating power to the system. Upon termination, the liquid metal and liquid silicate quenched to produce the distinct phases and textures shown in Figure 4-1. A JEOL 8200 electron probe microanalyzer (IOM) was employed to obtain compositional analyses of all run product phases. A 15 keV accelerating voltage, 20 nA beam current, and 20 μm spot size were used to analyze the metal phase. The silicate phase in the magnesia capsule experiments consisted of elongated quench crystals and melt pockets and was therefore analyzed with a 35 μm

spot size. The W concentration in the silicate phase of the graphite capsule experiments was quite low due to the effect of carbon in the metal phase on D_W, therefore a 20 keV accelerating voltage and 60 nA beam current were used to analyze these experiments. Also, to obtain a lower limit of detection, W was analyzed on two spectrometers and the peak counts were combined (LOD ~100 ppm).

4.3 Results

4.3.1 Partition coefficients and oxygen fugacity

The compositional data for each experiment can be seen in Table 4-1; run conditions, partition coefficients (by weight) and oxygen fugacities in Table 4-2. Oxygen fugacity was calculated relative to the iron-wüstite (IW) buffer according to

$$\Delta IW = 2\log\frac{a_{FeO}^{silicate}}{a_{Fe}^{metal}} \quad (4\text{-}1)$$

where a is the activity of FeO in the silicate and Fe in the metal. Activity is related to phase composition according to $a=X_i\gamma_i$, where X_i is the mole fraction of i and γ_i is the activity coefficient of i. Activity coefficients of FeO in silicate melts have been determined for polymerized melts and were shown to be slightly compositionally dependent, varying from 0.88-2.26 at 1400 °C (O'Neill and Eggins 2002). These melts are quite different from the high temperature, depolymerized melts in the present study; therefore, we assumed ideal behavior, $a_{FeO} = X_{FeO}$. The activity coefficient of Fe in the metal was determined using the Metal Activity Calculator, which takes into account the temperature of the experiment and the composition of the metal alloy (Wade et al. 2012a).

4.3.2 Valence state of tungsten

Experiment #10 was performed at the same P-T conditions as experiment #8 (2100 °C, 3 GPa), but more of the Fe in experiment #10 was added as FeO to increase the oxygen fugacity, Table 4-2. The results of these two experiments are shown in Figure 4-2, along with data from O'Neill et al. (2008). The slopes of the lines in Figure 4-2 are equal to cation valence/-4, therefore both the data of O'Neill et al. (2008) and our data suggest that W dissolves in the silicate melt as dominantly W^{6+}. The previous work of Rammensee and Wänke (1977) and Ertel et al. (1996) indicated that W^{4+} was the dominant valence state of W in silicate melts. Conversely, the partitioning data of Hillgren (1991), Walter and Thibault (1995), and Siebert et al. (2011) implied a higher valence, and O'Neill et al. (2008) suggested that the low valence determined by Ertel et al. (1996) could have been due to micronugget formation or incorrect fO_2 measurements. Cottrell et al. (2009) determined that W dissolves in silicate melts as dominantly 6+ at low pressure (0.5 GPa) but as mainly 4+ at higher pressures (11-18 GPa). An even lower valence of 3+ is suggested by the parameterization of Righter (2011) which includes both high and low pressure data. However, Wade et al. (2012a) combined their W partitioning data with that of Cottrell et al. (2009) and showed that both datasets are compatible with a W^{6+} valence state. Therefore, because our data agree with those of O'Neill et al. (2008) and because Wade et al. (2012a) refuted the idea of the valence being pressure dependant, we conclude that 6+ is the dominant valence of W in silicate melts at relevant core formation oxygen fugacities (see also the recent paper by Wade et al. 2012b).

4.3.3 Effect of temperature

Four of our experiments (#6-9) were performed at constant pressure, oxygen fugacity, and composition in order to determine the effect of temperature on D_W, Figure

4-3. Over the 250 degree range investigated here, there is no discernable temperature effect. Cottrell et al. (2009) also suggested that the effect of temperature is insignificant, but the data of Righter et al. (2010) show D_W increases with increasing temperature. Siebert et al. (2011) report a negligible or very weak increasing temperature effect, as do Wade et al. (2012a). In Section 4.4.1, we parameterize the data from the present study and an extensive amount of literature data obtained over a wide range of temperatures (1190-2427 °C), and the parameterization determined that D_W increases slightly with increasing temperature. This suggests that D_W does have a slight dependence on temperature, but it is only discernable over a wide range of temperatures.

4.3.4 Effect of carbon and sulfur

In order to better constrain the effect of light elements on D_W and D_{Mo} we performed constant P-T experiments in magnesia capsules. Two experiments (one with Mo in the metal and one with W) performed at 4.5 GPa, 2000 °C, and the same starting silicate composition contained ~7 wt.% carbon. These two experiments were compared with experiments done at the same conditions without carbon in the metal phase, and the effect of carbon on D_W and D_{Mo} can be seen in Figure 4-4. Both W and Mo become more siderophile upon the addition of carbon to the metal phase, as also shown by Jana and Walker (1997a), Cottrell et al. (2009), and Siebert et al. (2011).

The same procedure was followed to investigate the effect of S on D_W and D_{Mo} and the results are also shown in Figure 4-4. Both W and Mo become less siderophile upon the addition of sulfur to the metal phase, as previously shown by Lodders and Palme (1991), Hillgren (1993), Jana and Walker (1997b), Ohtani et al (1997), and Wade et al. (2012a). The Mo experiment (#14) had roughly 7 wt.% S dissolved in the metal

phase, Table 4-1 and Figure 4-1b. Interestingly, adding the same amount of S to the bulk composition for the W experiment (#12) caused the formation of a sulfur-rich phase and a separate sulfur-poor alloy, Figure 4-1c. As a result, the sulfur content of the D_W data point (calculated using the sulfur-rich phase) in Figure 4-4 is 26 wt.%, much higher than for the Mo experiment, hence why D_W is so much lower. The separation of a sulfur-rich phase and sulfur-poor alloy was also seen in the experiments of Hillgren (1993) and Jana and Walker (1997b), the latter study suggesting that this phase separation is dependant on the temperature of the experiment and the concentrations (and identity) of the solutes in the metal phase. Our results agree with the observation that W exhibits strong S avoidance, and the effect of S on Mo is less extreme (Jana and Walker 1997b, Wade et al. 2012a).

4.4 Discussion

4.4.1 W and Mo parameterization

A predictive expression for tungsten partitioning data was determined by parameterizing the data following the method of Burkemper et al. (2013), which used an equation similar to Righter et al. (1997) and Righter et al. (1999). Due to the conflicting literature data on the valence state of W, and the unusually low valence predicted in some high pressure parameterizations (e.g. Righter 2011), we chose to fix the oxygen fugacity term to -1.5 (indicating a 6+ valence) and parameterized the data according to

$$\log D_W + 1.5\Delta IW = b\frac{1}{T} + c\frac{P}{T} + \sum d_i X_i + e\left(\log 1 - X_C\right) + f\left(\log 1 - X_S\right) + h \qquad (4.2)$$

where X_i is the mole fraction of oxide i in the silicate, X_C and X_S are the mole fraction of carbon and sulfur in the metal phase, respectively, and b-h are multiple linear regression

coefficients. The $\log(1-X_{Si})$ term of Burkemper et al. (2013) was not included because there is not enough data on the effect of Si on W partitioning to obtain accurate results for that parameter. A total of 200 experiments were parameterized including the data from the present study and literature data from Newsom and Drake (1982), Jana and Walker (1997a), Jana and Walker (1997c), O'Neill et al. (2008), Cottrell et al. (2009), Righter et al. (2010), Tuff et al. (2011), Wade et al. (2012a), and Burkemper et al. (2013). The coefficients determined by the multiple linear regression can be seen in Table 4-3. The R^2 value of the parameterization is 0.92 and how well the expression fits the data can be seen in Figure 4-5. Additionally, our two Mo partitioning experiments were added to the experimental database used in Burkemper et al. (2013), and those data were also parameterized and the results can be seen in Table 4-3 and Figure 4-6.

The negative 1/T term in the W parameterization indicates that D_W increases as temperature increases. Although the magnitude of this term suggests only a slight increase, it is not insignificant. This is in contrast to what our data in Figure 4-3 show, but agrees with the data of Righter et al. (2010) and Siebert et al. (2011). As previously mentioned, this discrepancy can be explained by the wide range of temperatures examined in the parameterization's experimental database, over which a slight effect of temperature is predicted. Our investigation of the effect of temperature covered a 250 degree range, which may not have been large enough to discern a temperature dependence. The negative P/T term indicates that D_W decreases with increasing pressure, in agreement with the data of Siebert et al. (2011), Wade et al. (2012a), and the high pressure data of Cottrell et al. (2009). The large and very different silicate melt terms indicate that silicate melt composition has a strong effect on D_W (similar to that on D_{Mo})

as previously determined by Walter and Thibault (1995), Hillgren et al. (1996), Jana and Walker (1997c), Jaeger and Drake (2000), O'Neill et al. (2008), Siebert et al. (2011), and Wade et al. (2012a). The negative $\log(1-X_C)$ term and positive $\log(1-X_S)$ term indicates that increasing the amount of carbon in the metal phase will cause D_W to increase and that increasing the amount of sulfur in the metal phase with cause D_W to decrease, in agreement with our data in Figure 4-4.

The parameterization results shown in Table 4-3 for D_{Mo} are within error of that determined by Burkemper et al. (2013), suggesting excellent consistency among molybdenum partitioning studies. For the purposes of the core formation modeling in Section 4.4.2, the $\log(1-X_{Si})$ coefficient determined in the multiple linear regression of the molybdenum data was also used to account for the effect of Si in the metal phase on D_W, since not enough data were available to determine an accurate coefficient in the W parameterization. Tuff et al. (2011) showed that Si in the metal phase has a very strong and very similar effect on D_{Mo} and D_W, therefore we feel this assumption is justified.

4.4.2 Implications for core formation

The expression determined in Section 4.4.1 can be used to model core formation in an attempt to explain the observed upper mantle abundance of W. Assuming a chondritic bulk Earth, mass balance calculations show that the D_W value required to explain the mantle abundance of W is between 15 and 22 (Palme and O'Neill 2003, McDonough 2003, range given by Wood et al. 2006). Assuming single-stage core formation, a set of P-T conditions that produces these D values can be determined by setting silicate composition to KLB-1 peridotite (Davis et al. 2009) and oxygen fugacity to -2.2ΔIW (based on the current amount of Fe in the core and FeO in the mantle,

McDonough 2003). A further constraint on the P-T conditions can be placed by assuming that final metal-silicate equilibration occurred at the base of the magma ocean, thus constraining the P-T conditions to be near the peridotite liquidus. If no light elements are considered, the P-T conditions that can explain the observed mantle abundance of W are not reached until >50 GPa. This would suggest that the core formed out of a magma ocean with a depth greater than 1500 km. However, we know that the outer core contains roughly 10% of an element, or multiple elements, lighter than iron and Burkemper et al. (2013) suggested a core composition that contained $X_C = 0.07$, $X_S = 0.05$, and $X_{Si} = 0.06$ (approximately 1.8 wt.% C, 3.0 wt.% S, and 3.4 wt.% Si). When this combination of light elements is considered, the P-T conditions required to explain the mantle abundance of W become 30-43 GPa and 2800-3150 K. The P-T range is quite large due to the opposing effects of pressure and temperature on D_W. Burkemper et al. (2013) originally suggested the above light element combination and P-T conditions of 35-37 GPa and 2950-3000 K to explain the mantle abundance of Mo and Ni. Applying our updated Mo parameterization to this model does not change the required P-T conditions, and our suggested W conditions directly overlap with those determined for Mo and Ni. Therefore, all three elements can be explained by single-stage, equilibrium core formation out of a magma ocean of 35-37 GPa and 2950-3000 K with $X_C = 0.07$, $X_S = 0.05$, and $X_{Si} = 0.06$, see Figure 4-7.

The single-stage magma ocean model states that although core formation probably started when Earth was just 10% of its current size (due to significant melting, Melosh 1990), large impacts during the later stages of Earth's accretion were energetic enough to cause extensive melting and re-equilibration so that the mantle signature we

observe today is a record of only the final equilibration event (e.g. Righter 2011). The single-stage model described above is able to explain three key refractory, moderately siderophile elements, using the most comprehensive experimental databases to date. Furthermore, it is compatible with the current FeO content of the mantle, and is in agreement with light element cosmochemical abundances (McDonough 2003, Hillgren et al. 2000 and references within). Finally, recent isotope and light element-iron alloy studies agree that Si is most likely a significant component in the outer core (Georg et al. 2007, Badro et al. 2007, Shahar et al. 2009, Sata et al. 2010), in agreement with our results.

Light element-iron alloy studies have also determined that there may be a significant amount of O in Earth's core (e.g. Badro et al. 2007), and Burkemper et al. (2013) suggested that significant O may be possible at the suggested P-T conditions. However, there is not currently enough partitioning data that incorporates oxygen in the metal phase to take its effect into account in the modeling. Additionally, since the current literature data on W partitioning behavior is not fully in agreement, more W partitioning data would greatly improve the accuracy of the proposed model, especially on the effect of Si in the metal phase.

4.5 Conclusions

Over the past 20 years, the geophysical and geochemical evidence for a magma ocean (or oceans) early in Earth's history has become irrefutable. However, the conditions within the magma ocean and how it influenced core formation and mantle composition remain debated. The refractory moderately siderophile elements are ideal for

studying core formation because their bulk Earth abundances do not require a volatility correction and their observed upper mantle abundances are relatively well known. Our investigation of the metal-silicate partitioning behavior of the moderately siderophile element W determined that it dissolves as dominantly W^{6+} in silicate melts, there is a slight temperature effect on D_W that is only discernable over a wide range of temperatures, and carbon in the metal phase causes D_W to increase whereas sulfur causes D_W to decrease dramatically. By combining the experimental databases used in Burkemper et al. (2013) with our new data and W data from the literature, we showed that the three key refractory moderately siderophile elements W, Mo, and Ni can be explained by late-stage equilibrium core formation after a large impact that caused a magma ocean of ~1100 km depth with Si, S, and C present in the metal phase.

Table 4-1. Compositional data (in wt.%) for each run product determined by electron microprobe. Numbers in parentheses are standard deviations. qs = quenched silicate, qm = quenched metal, ol = olivine, mw = magnesiowüsite.

Exp #	1	2	3	4	5	6	7
Metal							
Fe	65.75 (0.91)	66.81 (0.54)	55.81 (1.02)	55.14 (0.18)	65.67 (0.40)	62.91 (1.47)	63.98 (0.61)
Mo	np	np	np	np	np	np	np
W	32.34 (0.83)	32.48 (0.58)	41.71 (0.94)	41.36 (0.13)	32.76 (0.74)	30.11 (1.36)	29.37 (0.57)
S	np	np	np	np	np	np	np
C*	np	np	np	np	np	6.98	6.65
TOTAL	98.09 (0.28)	99.29 (0.26)	97.52 (0.28)	96.50 (0.23)	98.43 (0.50)	100	100
n	10	10	8	8	6	9	8
Silicate							
SiO_2	35.38 (0.92)	34.45 (0.64)	36.81 (0.58)	39.94 (0.42)	38.31 (0.66)	48.03 (0.30)	47.54 (0.27)
TiO_2	np	np	np	np	0.47 (0.03)	0.68 (0.01)	0.63 (0.01)
Al_2O_3	8.52 (1.79)	9.76 (1.29)	5.70 (0.81)	5.83 (1.29)	11.69 (0.28)	16.93 (0.10)	17.74 (0.17)
FeO	11.26 (1.04)	11.01 (0.73)	7.69 (0.49)	8.39 (0.71)	5.63 (0.27)	10.08 (0.04)	10.30 (0.12)
MgO	37.73 (2.74)	38.24 (1.63)	46.19 (0.81)	42.29 (2.34)	34.73 (0.88)	9.78 (0.11)	9.80 (0.08)
CaO	6.04 (1.17)	6.75 (1.06)	4.02 (0.36)	4.48 (0.95)	8.82 (0.47)	11.11 (0.03)	10.94 (0.04)
Na_2O	np	np	np	np	1.17 (0.11)	2.12 (0.03)	2.04 (0.03)
S	np	np	np	np	np	np	np
Mo	np	np	np	np	np	np	np
W	1.01 (0.29)	1.39 (0.38)	0.60 (0.14)	0.37 (0.15)	0.11 (0.03)	0.026 (0.016)	0.040 (0.016)
TOTAL	99.93 (0.61)	101.60 (0.86)	101.01 (0.31)	101.30 (0.43)	100.93 (0.51)	98.76 (0.38)	99.03 (0.34)
n	25	17	18	25	25	19	20
phases**	qs, qm, ol	qs, qm, ol	qs, qm, mw	qs, qm	qs, qm	qs, qm	qs, qm

* Carbon content determined by difference

** Olivine formed due to temperature of the experiment being near the liquidus, magnesiowüstite formed due to reaction of the silicate with the capsule

Table 4-1 (con't). Compositional data (in wt.%) for each run product determined by electron microprobe. Numbers in parentheses are standard deviations. qs = quenched silicate, qm = quenched metal, ol = olivine, mw = magnesiowüsite.

Exp #	8	9	10	11	12a	12b	13	14
Metal								
Fe	61.56 (2.23)	62.20 (1.60)	54.45 (5.45)	62.41 (0.29)	46.57 (3.56)	72.08 (0.62)	59.22 (2.42)	52.79 (1.69)
Mo	np	np	np	np	np	np	34.56 (2.41)	37.53 (2.62)
W	31.49 (2.27)	30.85 (1.70)	38.68 (5.34)	29.63 (0.29)	48.59 (3.91)	0.10 (0.07)	np	np
S	np	np	np	np	0.57 (0.20)	26.27 (0.67)	np	6.74 (0.98)
C*	6.95	6.95	6.87	7.96	np	np	6.22	np
TOTAL	100	100	100	100	95.72 (1.11)	98.45 (0.19)	100	97.06 (0.42)
n	14	10	7	10	6	4	7	12
Silicate								
SiO_2	47.96 (0.89)	47.90 (0.43)	45.31 (0.19)	36.42 (0.69)	35.94 (0.87)	35.94 (0.87)	35.60 (0.67)	36.39 (0.93)
TiO_2	0.64 (0.01)	0.66 (0.01)	np	np	np	np	np	np
Al_2O_3	18.24 (1.10)	17.00 (0.12)	11.24 (0.14)	6.91 (1.52)	6.69 (1.36)	6.69 (1.36)	7.90 (1.08)	7.08 (1.24)
FeO	9.84 (0.12)	10.14 (0.06)	23.52 (0.19)	8.82 (0.68)	8.32 (0.61)	8.32 (0.61)	10.22 (0.41)	9.87 (0.75)
MgO	9.69 (0.14)	9.88 (0.09)	15.65 (0.30)	41.30 (2.18)	42.43 (1.97)	42.43 (1.97)	39.01 (1.51)	41.57 (1.71)
CaO	11.04 (0.16)	11.11 (0.05)	3.30 (0.02)	5.15 (0.94)	4.92 (0.81)	4.92 (0.81)	6.39 (0.64)	5.44 (0.86)
Na_2O	2.11 (0.06)	2.11 (0.04)	np	np	np	np	np	np
S	np	np	np	np	0.18 (0.04)	0.18 (0.04)	np	0.10 (0.02)
Mo	np	np	np	np	np	np	0.043 (0.010)	0.090 (0.022)
W	0.024 (0.014)	0.043 (0.032)	0.40 (0.03)	0.66 (0.23)	1.95 (0.39)	1.95 (0.39)	np	np
TOTAL	99.55 (0.81)	98.84 (0.59)	99.42 (0.39)	99.26 (0.41)	100.43 (0.82)	100.43 (0.82)	99.16 (0.42)	100.54 (1.16)
n	25	20	13	20	20	20	15	25
phases**	qs, qm	qs, qm	qs, qm	qs, qm, ol	qs, qm, ol	qs, qm, ol	qs, qm, ol	qs, qm

* Carbon content determined by difference

** Olivine formed due to temperature of the experiment being near the liquidus, magnesiowüstite formed due to reaction of the silicate with the capsule

Table 4-2. P-T and oxygen fugacity conditions, run times, and D values for all experiments.

Exp #	Capsule	P (GPa)	T (K)	NBO/T	Time (s)	γFe	ΔIW	D(W)	D(Mo)
1	MgO	4.5	2273	2.95	150	1.02	-2.05	32	-
2	MgO	3.0	2173	2.95	300	1.02	-2.08	23	-
3	MgO	3.0	2373	3.50	120	1.03	-2.39	69	-
4	MgO	6.5	2373	3.05	300	1.03	-2.30	110	-
5	MgO	7.0	2473	2.29	60	1.02	-2.65	287	-
6	C	3.0	2173	0.79	600	0.71	-1.37	1178	-
7	C	3.0	2273	0.77	300	0.74	-1.41	734	-
8	C	3.0	2273	0.74	150	0.74	-1.42	1320	-
9	C	3.0	2423	0.79	60	0.74	-1.40	710	-
10	C	3.0	2373	1.36	150	0.80	-0.69	97	-
11	MgO	4.5	2273	3.16	300	0.63	-1.51	45	-
12a*	MgO	4.5	2273	3.26	300	1.06	-2.24	25	-
12b*	MgO	4.5	2273	3.26	300	N/A	-2.24	0.05	-
13	MgO	4.5	2273	3.07	300	0.91	-1.64	-	809
14	MgO	4.5	2273	3.21	300	0.91	-1.79	-	417

*The two D values for this experiment are from the separation of the metal into a sulfur-rich and sulfur-poor phase.

Table 4-3. Multiple linear regression coefficients from the W and Mo parameterizations. N/A = not applicable.

Parameter	*W Coefficient*	*Standard Error*	*Mo Coefficient*	*Standard Error*
Intercept	-11.28	2.92	-12.43	1.92
ΔIW	-1.50	N/A	-1.00	0.04
1/T	-3774	560	6352	602
P/T	-99.94	17.95	-71.19	16.17
SiO_2	16.79	2.88	13.38	2.03
Al_2O_3	11.01	3.23	9.27	2.35
FeO	10.77	3.10	8.19	2.04
MgO	8.92	2.92	9.46	1.97
CaO	6.50	3.03	7.83	2.00
TiO_2	15.84	4.16	13.15	2.70
log(1-Xc)	-7.12	0.61	-7.18	0.66
log(1-Xs)	9.01	2.48	6.59	1.28
log(1-Xsi)	N/A	N/A	13.35	2.33

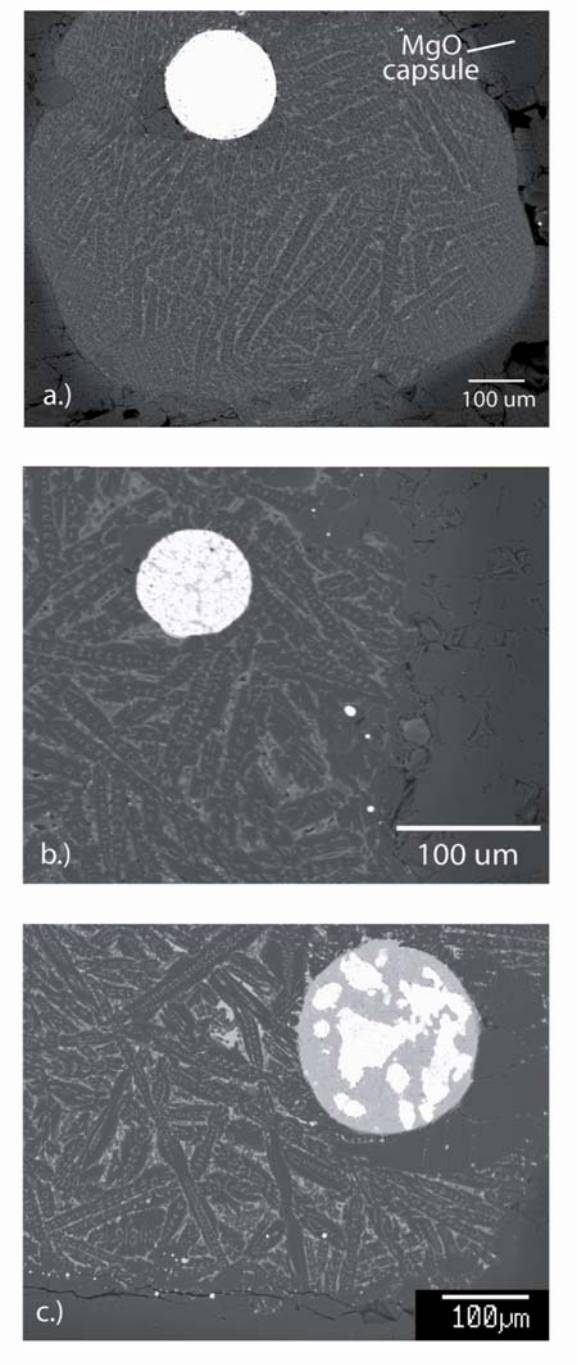

Figure 4-1. a.) Backscattered electron image of a typical run product (exp #4) showing distinct separation between the metal and silicate phases, quench texture in the silicate, and the magnesia capsule. b.) Backscattered electron image of exp #14 showing quench texture in the FeMoS metal phase. c.) Backscattered electron image of exp #12 showing phase separation between a sulfur-rich (W-poor) phase and sulfur-poor (W-rich, brighter domains) phase.

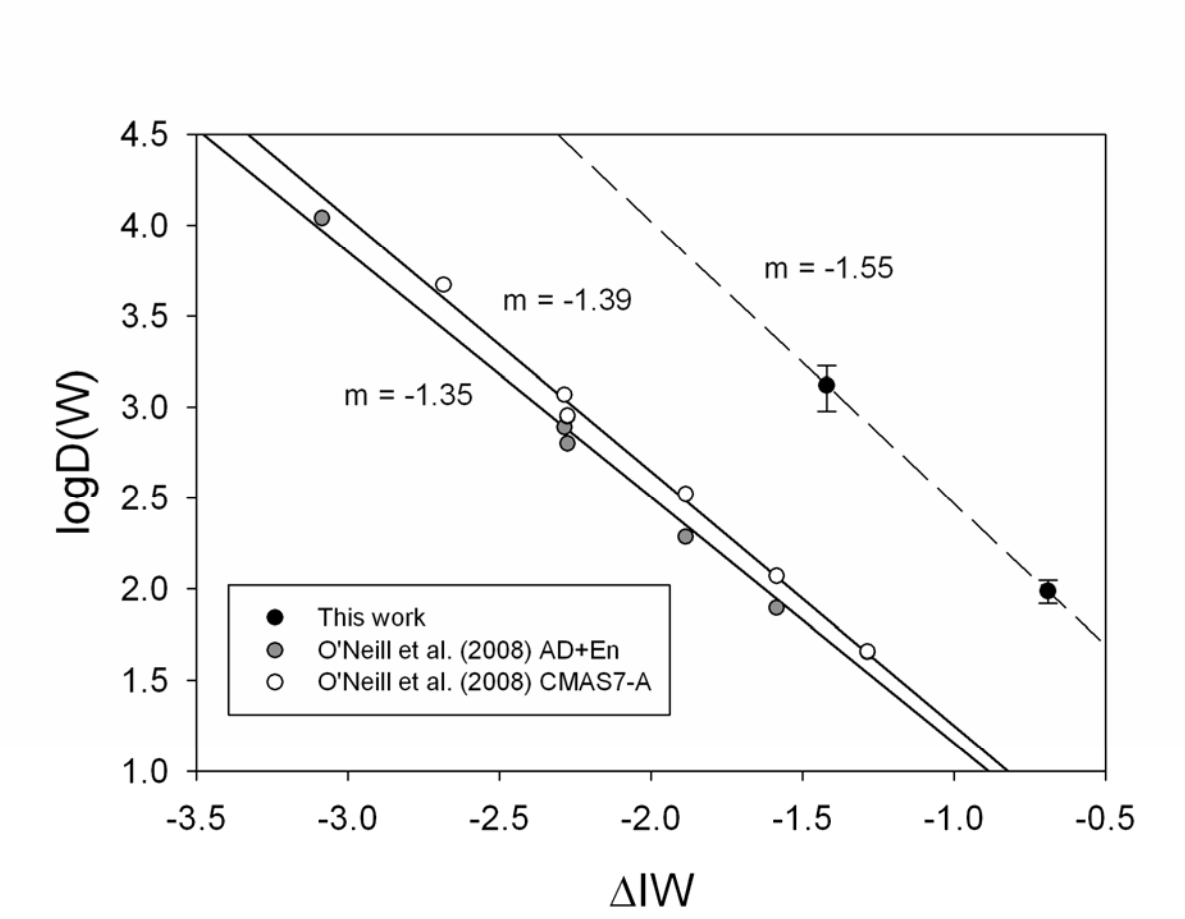

Figure 4-2. Plot of $logD_W$ versus oxygen fugacity relative to the iron-wüstite buffer. Data from O'Neill et al. (2008) are plotted with data from the present study. The data from O'Neill et al. (2008) were obtained at 1400 °C and 0.0001 GPa and the AD+En composition has an NBO/T (ratio non-bridging oxygens to tetrahedrally coordinated cations) of 1.31 and CMAS7-A has an NBO/T of 0.73. Relative oxygen fugacities were calculated from the absolute oxygen fugacity values given in O'Neill et al. (2008) using the IW buffer of O'Neill and Pownceby (1993) which gives an IW $\log fO_2$ value of -9.715 at 1673 K. The data from the present study were obtained at 2100 °C and 3 GPa and are larger than the O'Neill et al. (2008) values at the same oxygen fugacity mainly due to the use of graphite capsules. The slope of each regression line is indicated as *m* and cation valence is equal to the slope times -4. Error bars are 2x standard error.

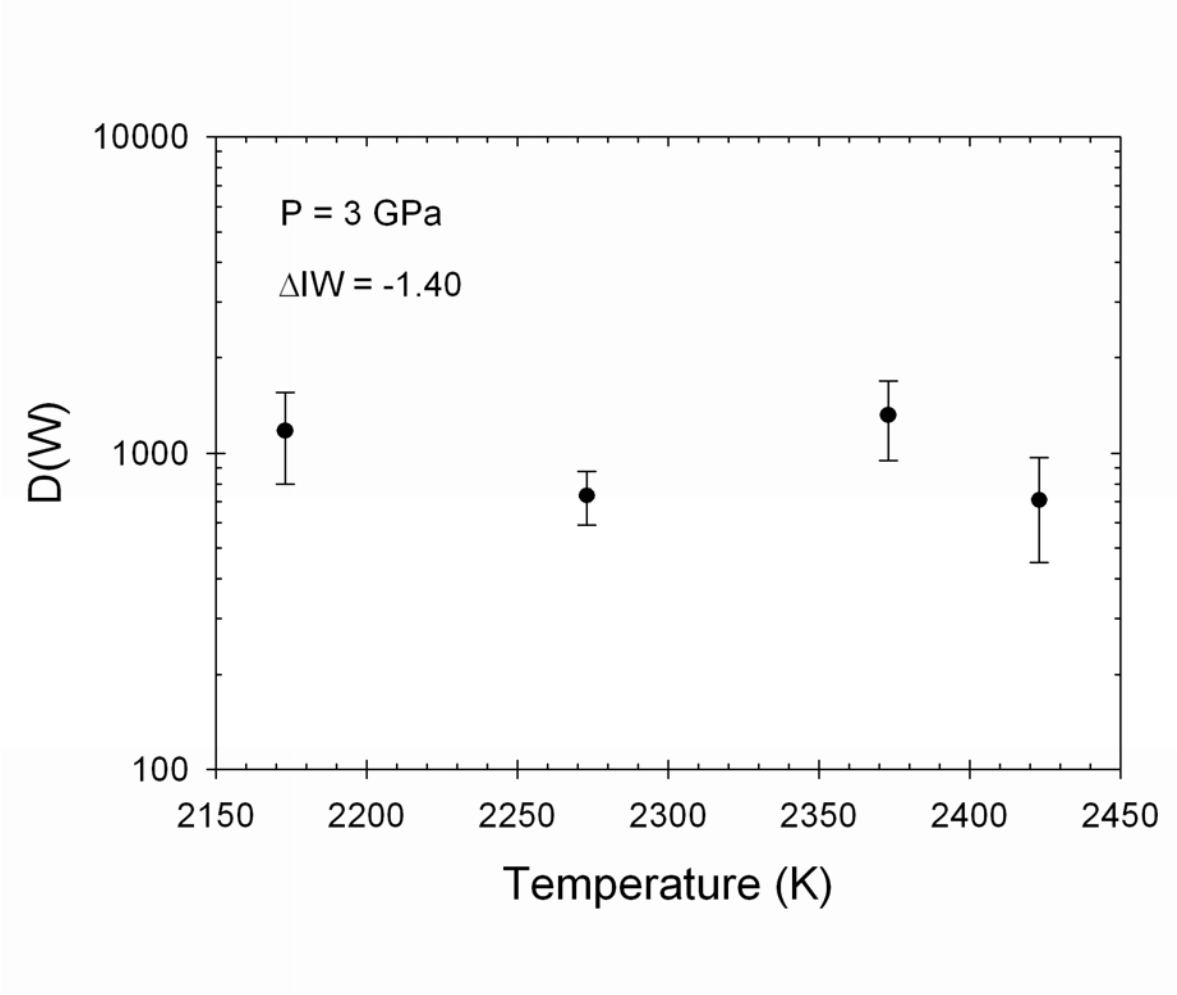

Figure 4-3. Plot of W partition coefficient versus temperature. All experiments were performed using the same starting composition, in graphite capsules, and at the same pressure. Error bars are 2x standard error.

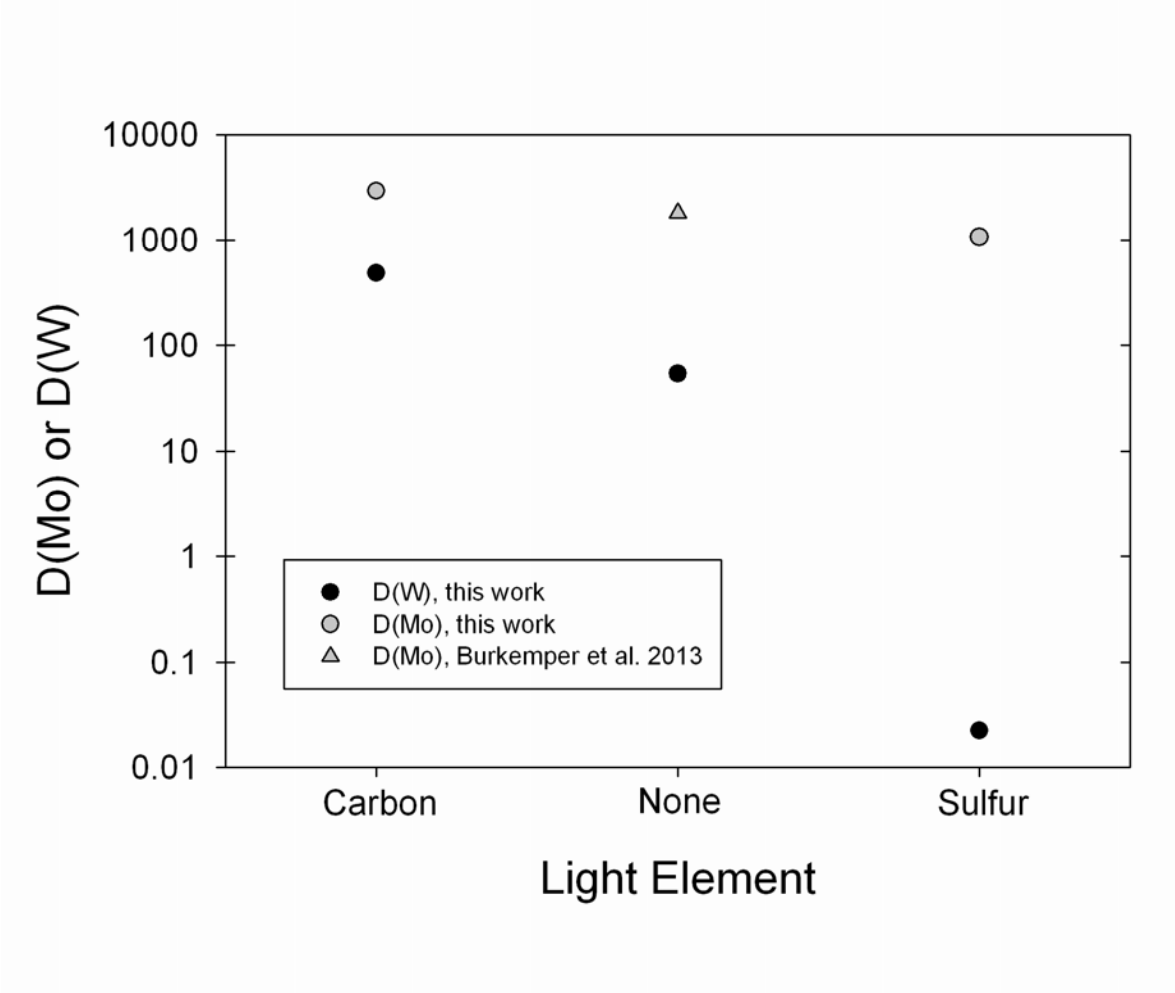

Figure 4-4. Plot showing the effect carbon and sulfur have on the partition coefficients of Mo and W. The x-axis is qualitative indicating the absence or presence of either carbon or sulfur. All experiments were performed at 4.5 GPa and 2000 °C in magnesia capsules and the D values were adjusted to be at -2.2ΔIW. Due to the large y-axis scale, errors on the D values are within the size of the data symbol.

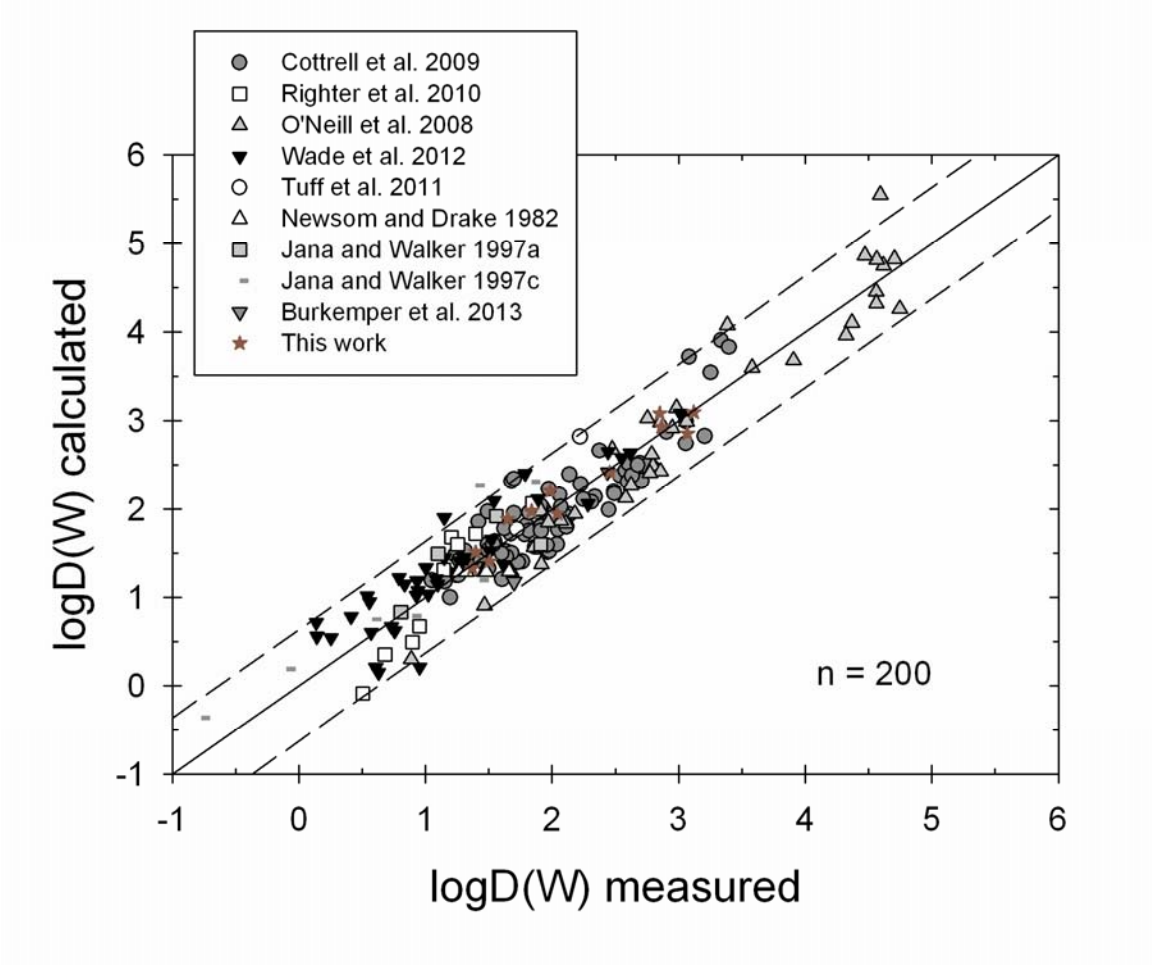

Figure 4-5. Plot of logD(W) calculated using the parameterization equation versus logD(W) measured from the experiment. The R^2 value of the fit is 0.92 with a standard error of 0.32. The solid line is a 1:1 line and the dashed lines indicate 2x standard error. All of the data from the studies listed above were included in the parameterization with the exception of the W capsule experiments of Cottrell et al. (2009) and the Si containing experiments of Tuff et al. (2011) and Wade et al. (2012). Additionally, only a subset of the O'Neill et al. (2008) data were used so as not to bias the experimental database with 1 bar data; compositions AD, AD+Fo, AD+En, AD+Wo at logfO_2 of -11.99, AD, AD+Fo, AD+En, AD+Wo, AD+Qz at logfO_2 of -13.21, CMAS7A-G at logfO_2 of -11.99, -11.30, and -13.21, MAS1-2 and CAS1-4 at logfO_2 of -11.60, and AD+TiO_2 at logfO_2 of -12.42 were included in the parameterization.

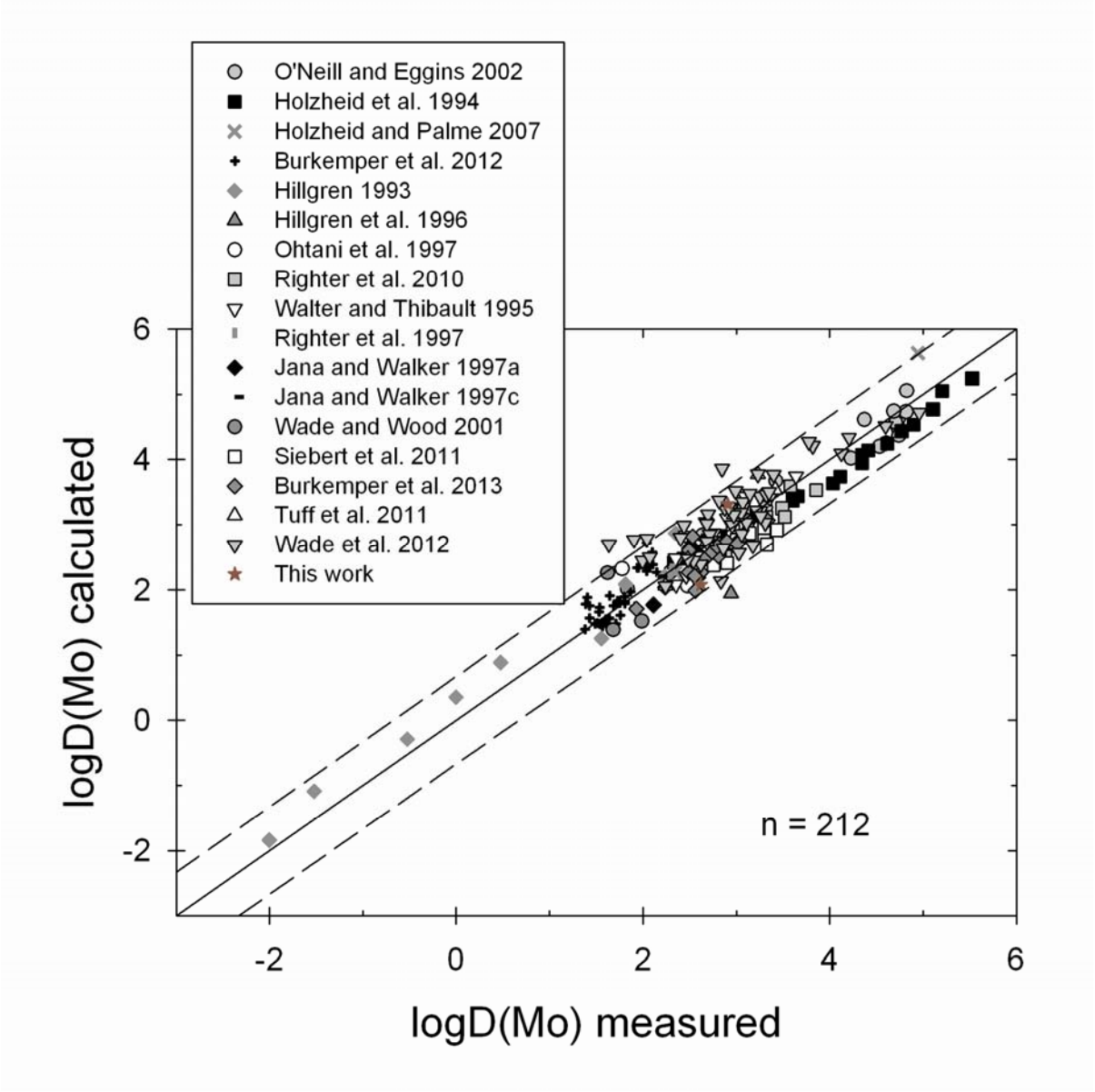

Figure 4-6. Plot of logD(Mo) calculated using the parameterization equation versus logD(Mo) measured from the experiment. The R^2 value of the fit is 0.91 with a standard error of 0.33. The solid line is a 1:1 line and the dashed lines indicate 2x standard error. All of the data from the studies listed above were included in the parameterization with the exception of the graphite capsule experiments of Siebert et al. (2011) and the Si-containing experiments of Tuff et al. (2011). Similar to the W parameterization, in order not to bias the regression with low pressure data, only a fraction of the O'Neill and Eggins (2002) data set was used; those at -11.63 log fO_2 for their AD and A-F melts, and those at -10.20 log fO_2 for their MAS and CAS melts.

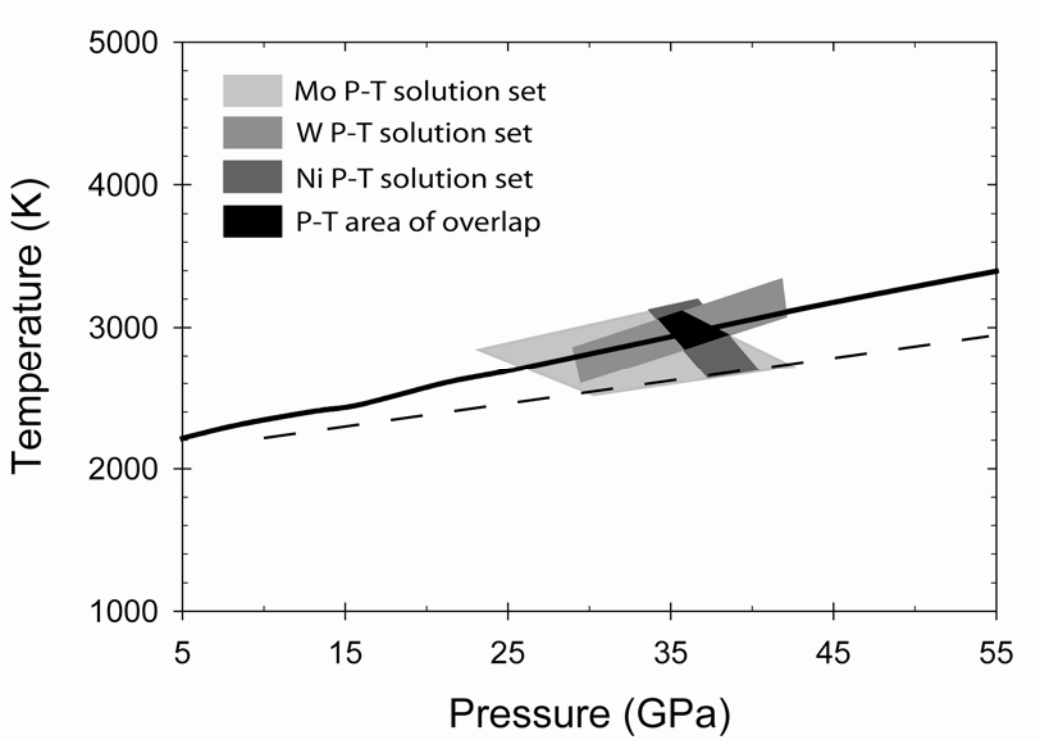

Figure 4-7. Plot of temperature versus pressure showing P-T solution sets that can explain the mantle abundances of Mo, W, and Ni. The expressions developed in Section 4.4.1 (Ni expression from Burkemper et al. 2013) were used to determine the solution sets by setting silicate composition to KLB-1 peridotite (Davis et al. 2009), oxygen fugacity to -2.2ΔIW, and light element composition to X_C = 0.07, X_S = 0.05, and X_{Si} = 0.06. This light element combination was determined by bearing in mind cosmochemical abundances (e.g. keeping carbon to a minimum), while searching for P-T conditions where all three siderophile element solution sets overlap near the peridotite liquidus (solid line). A set of conditions was considered a solution if it gave D_W = 15-22, D_{Mo} = 40-100, and D_{Ni} = 23-27. The differing effects of the light elements on W, Mo, and Ni partitioning, cause the conditions of overlap to be quite constrained, with relatively small changes in the light element combination eliminating the overlap. The peridotite liquidus (solid line) is from Zhang and Herzberg (1994) for pressures of 0-23 GPa and from Andrault et al. (2011) for >23 GPa, and the dashed line is the mantle solidus from Andrault et al. (2011).

4.6. References

Agee, C.B., Li, J., Shannon, M.C. (1995) Pressure-temperature phase diagram for the Allende meteorite. Journal of Geophysical Research 100, 17725-17740

Badro, J., Fiquet, G., Guyot, F., Gregoryanz, E., Occelli, F., Antonangeli, D., d'Astuto, M. (2007) Effect of light elements on the sound velocities in solid iron: Implications for the composition of Earth's core. Earth and Planetary Science Letters 254, 233-238

Birch, F. (1952) Elasticity and constitution of the Earth's interior. Journal of Geophysical Research 57, 227-286

Burkemper, L.K., Agee, C.B., Garcia, K.A. (2013) Molybdenum metal-silicate partitioning behavior: Constraining the magma ocean models for core formation. In prep.

Canup, R.M., Agnor, C.B. (2000) Accretion of the terrestrial planets and the Earth-Moon system. In: Canup, R. M. and Righter, K. eds. *Origin of the Earth and Moon*. The University of Arizona Press, Tucson AZ, pp. 113-129

Chabot, N.L., Agee, C.B. (2003) Core formation in the Earth and Moon: new experimental constraints from V, Cr, and Mn. Geochimica et Cosmochimica Acta 67, 2077-2091

Chabot, N.L., Draper, D.S., Agee, C.B. (2005) Conditions of core formation in the Earth: constraints from nickel and cobalt partitioning. Geochimica et Cosmochimica Acta 69, 2141-2151

Cottrell, E., Walter, M.J., Walker, D. (2009) Metal-silicate partitioning of tungsten at high pressure and temperature: implications for equilibrium core formation in Earth. Earth and Planetary Science Letters 281, 275-287

Davis, F.A., Tangeman, J.A., Tenner, T.J., Hirschmann, M.M. (2009) The composition of KLB-1 peridotite. American Mineralogist 94, 176-180

Draper, D.S. (1991) Late Cenozoic bimodal magmatism in the northern Basin and Range Province of southeastern Oregon. Journal of Volcanology and Geothermal Research 47, 299-328

Ertel, W., O'Neill, H.St.C., Dingwell, D.B., Spettel, B. (1996) Solubility of tungsten in a haplobasaltic melt as a function of temperature and oxygen fugacity. Geochimica et Cosmochimica Acta 60, 1171-1180

Georg, R.B., Halliday, A.N., Schauble, E.A., Reynolds, B.C. (2007) Silicon in the Earth's core. Nature 447, 1102-1106

Gessmann, C.K., Rubie, D.C. (2000) The origin of the depletions of V, Cr, and Mn in the mantles of the Earth and Moon. Earth and Planetary Science Letters 184, 95-107

Hillgren, V.J. (1991) Partitioning behavior of Ni, Co, Mo, and W between basaltic liquid and Ni-rich metal: Implications for the origin of the moon and lunar core formation. Geophysical Research Letters 18, 2077-2080

Hillgren, V.J. (1993) Partitioning behavior of moderately siderophile elements in Ni-rich systems: implications for the Earth and Moon. PhD thesis. University of Arizona, 423 pp

Hillgren, V.J., Drake, M.J., Rubie, D.C. (1996) High pressure and high temperature metal-silicate partitioning of siderophile elements: The importance of silicate liquid composition. Geochimica et Cosmochimica Acta 60, 2257-2263

Hillgren, V.J., Gessmann, C.K., Li, J. (2000) An experimental perspective on the light element in Earth's core. In: Canup, R. M. and Righter, K. eds. *Origin of the Earth and Moon*. The University of Arizona Press, Tucson AZ, 245-263

Jaeger, W.L., Drake, M.J. (2000) Metal-silicate partitioning of Co, Ga, and W: Dependence on silicate melt composition. Geochimica et Cosmochimica Acta 64, 3887-3895

Jana, D., Walker, D. (1997a) The impact of carbon on element distribution during core formation. Geochimica et Cosmochimica Acta 61, 2759-2763

Jana, D., Walker, D. (1997b) The influence of sulfur on partitioning of siderophile elements. Geochimica et Cosmochimica Acta 61, 5255-5277

Jana, D., Walker, D. (1997c) The influence of silicate melt composition on distribution of siderophile elements among metal and silicate liquids. Earth and Planetary Science Letters 150, 463-472

Jones, J.H., Drake, M.J. (1986) Geochemical constraints on core formation in the Earth. Nature 322, 221-228

Kegler, P., Holzheid, A., Frost, D.J., Rubie, D.C., Dohmen, R., Palme, H. (2008) New Ni and Co metal-silicate partitioning data and their relevance for an early terrestrial magma ocean. Earth and Planetary Science Letters 268, 28-40

Li, J., Agee, C.B. (1996) Geochemistry of mantle-core differentiation at high pressure. Nature 381, 686-689

Lodders, K., Palme, H. (1991) On the chalcophile character of molybdenum: determination of sulfide/silicate partition coefficients of Mo and W. Earth and Planetary Science Letters 103, 311-324

McDonough, W.F., (2003) Compositional model for the Earth's core. In: Carlson, R.W. ed. *Treatise on Geochemistry, Vol. 2, The Mantle and Core.* Elsevier Ltd, 547-568

Melosh, H.J. (1990) Giant impacts and the thermal state of the early Earth. In: Newsom, H.E. and Jones, J.H. eds. *Origin of the Earth*. Oxford University Press, 69-83

Newsom, H.E., Drake, M.J. (1982) The metal content of the eucrite parent body: Constraints from the partitioning behavior of tungsten. Geochimica et Cosmochimica Acta 46, 2483-2489

Ohtani, E., Yurimoto, H., Seto, S. (1997) Element partitioning between metallic liquid, silicate liquid, and lower-mantle minerals: Implications for core formation of the Earth. Physics of the Earth and Planetary Interiors 100, 97-114

O'Neill, H.S.C., Eggins, S.M., (2002) The effect of melt composition on trace element partitioning: an experimental investigation of the activity coefficient of FeO, NiO, CoO, MoO_2, MoO_3 in silicate melts. Chemical Geology 186, 151-181

O'Neill, H.S.C., Berry, A.J., Eggins, S.M. (2008) The solubility and oxidation state of tungsten in silicate melts: Implications for the comparative chemistry of W and Mo in planetary differentiation processes. Chemical Geology 255, 346-359

Palme, H., O'Neill, H.S.C. (2003) Cosmochemical estimates of mantle composition. In: Carlson, R.W. ed. *Treatise on Geochemistry, Vol. 2, The Mantle and Core.* Elsevier Ltd, pp. 1-38

Rammensee, W., Wänke, H. (1977) On the partition coefficient of tungsten between metal and silicate and its bearing on the origin of the moon. Proc. Lunar Sci. Conf. 8, 399-409

Righter, K., Drake, M.J., Yaxley, G. (1997) Prediction of siderophile element metal-silicate partition coefficients to 20 GPa and 2800 ^{o}C: the effects of pressure, temperature, oxygen fugacity, and silicate and metallic melt compositions. Physics of the Earth and Planetary Interiors 100, 115-134

Righter, K., Drake, M.J. (1999) Effect of water on metal-silicate partitioning of siderophile elements: A high pressure and temperature terrestrial magma ocean and core formation. Earth and Planetary Science Letters 171, 383-399

Righter, K., Pando, K.M., Danielson, L., Lee, C.T. (2010) Partitioning of Mo, P and other siderophile elements (Cu, Ga, Sn, Ni, Co, Cr, Mn, V, and W) between metal and silicate melt as a function of temperature and silicate composition. Earth and Planetary Science Letters 291, 1-9

Righter, K. (2011) Prediction of metal-silicate partition coefficients for siderophile elements: An update and assessment of PT conditions for metal-silicate equilibrium during accretion of the Earth. Earth and Planetary Science Letters 304, 158-167

Ringwood, A.E. (1966) Chemical evolution of the terrestrial planets. Geochimica et Cosmochimica Acta 30, 41-104

Sata, N., Hirose, K., Shen, G., Nakajima, Y., Ohishi, Y., Hirao, N. (2010) Compression of FeSi, Fe3C, Fe0.95O, and FeS under the core pressures and implication for light element in the Earth's core. Journal of Geophysical Research 115, doi: 10.1029/2009JB006975

Shahar, A., Ziegler, K., Young, E.D., Ricolleau, A., Schauble, E.A., Fei, Y. (2009) Experimentally determined Si isotope fractionation between silicate and Fe metal and implications for Earth's core formation. Earth and Planetary Science Letters 288, 228-234

Siebert, J., Corgne, A., Ryerson, F.J. (2011) Systematics of metal-silicate partitioning for many siderophile elements applied to Earth's core formation. Geochimica et Cosmochimica Acta 75, 1451-1489

Stevenson, D.J. (1990) Fluid dynamics of core formation. In: Newsom, H.E. and Jones, J.H. Eds., *Origin of the Earth*. Oxford University Press, New York, pp. 231-249

Tonks, W.B., Melosh, H.J. (1993) Magma ocean formation due to giant impacts. Journal of Geophysical Research 98, 5319-5333

Tuff, J., Wood, B.J., Wade, J. (2011) The effect of Si on metal-silicate partitioning of siderophile elements and implications for the conditions of core formation. Geochimica et Cosmochimica Acta 75, 673-690

Wade, J. Wood, B.J. (2005) Core formation and the oxidation state of the Earth. Earth and Planetary Science Letters 236, 78-95

Wade, J., Wood, B.J., Tuff, J. (2012a) Metal-silicate partitioning of Mo and W at high pressures and temperatures: Evidence for late accretion of sulphur to the Earth. Geochimica et Cosmochimica Acta 85, 58-74

Wade, J., Wood, B.J., Norris, C.A. (2012b) The oxidation state of tungsten in silicate at high pressures and temperatures. Chemical Geology, in press

Walter, M.J., Thibault, Y. (1995) Partitioning of tungsten and molybdenum between metallic liquid and silicate melt. Science 270, 1186-1189

Wetherill, G.W. (1985) Occurrence of giant impacts during the growth of the terrestrial planets. Science 228, 877-879

Wood, B.J., Walter, M.J., Wade, J. (2006) Accretion of the Earth and segregation of its core. Nature 441, 825-833

Wood, B.J., Wade, J., Kilburn, M.R. (2009) Core formation and the oxidation state of the Earth: Additional constraints from Nb, V, and Cr partitioning. Geochimica et Cosmochimica Acta 72, 1415-1426

5.0 Terrestrial Planet Evolution

5.1 Earth

The previous chapters showed that the Mo, Ni, and W upper mantle abundances can be explained by single-stage core formation out of a magma ocean with conditions of 35-37 GPa, 2950-3000 K, and -2.2ΔIW with 1.8 wt.% C, 3.0 wt.% S, and 3.4 wt.% Si (specifically Section 4.4.2). This does not imply that metal was separating from silicate only during the end of accretion, it implies that the final impact of accretion (possibly the Moon forming impact) was large enough to re-equilibrate the metal and the silicate so that the mantle signature observed today is the result of only this final magma ocean equilibration event. The fact that these three key siderophile elements can be explained by a single set of unique magma ocean conditions is unlikely to be coincidental; however, in order to determine if multi-stage models of core formation can also explain these elements, the W parameterization determined in Section 4.4.1 was applied to the multi-stage models described in Section 3.4.2, Figure 5-1. There are three interesting things to note in Figure 5-1. First, both the progressive oxidation and constant oxygen fugacity models produce the same final average D_W value. As with Ni and Mo, this occurs because in the progressive oxidation model, the D values are too high during the early stages of accretion (when oxygen fugacity is very low) to impact the mantle abundance to a significant degree. It is the final impacts, when both models have the same oxygen fugacity that imparts the majority of the siderophile elements to the mantle, thus producing similar D values at the end of accretion. Second, the average D_W lines for progressive oxidation and constant oxygen fugacity show the largest difference between them, compared to Ni and Mo, because W has the largest oxygen fugacity dependence

(due to its 6+ valence). Third, the final average D_W value is too large to explain the observed mantle abundance of W. This is the same qualitative result determined by the multi-stage model of Wade et al. (2012) who fixed the discrepancy by adding S to the metal phase during the last 10-20% of accretion. Due to the strong S avoidance exhibited by W, and sulfur's lesser effects on Mo and Ni, this could potentially fix the discrepancy in the present model as well; however, the timing on this late S addition is not well constrained. Wade et al. (2012) refer to the isotopic study of Schönbächler et al. (2010) as evidence for the late addition of volatiles. The multi-stage model of Rubie et al. (2011) also calls upon late volatile addition and they reference the accretion models of O'Brien et al. (2006) which suggest that as accretion progressed, terrestrial planet feeding zones increased into cooler portions of the solar nebula, bringing in more volatiles and therefore more oxidized material. However, recent work on the water content of planetary interiors suggests that volatile elements were present throughout accretion, calling into question the paradigm of late volatile addition (McCubbin et al. 2012). Finally, the progressive oxidation multi-stage models of Wade and Wood (2005) call upon mantle self-oxidation through perovskite formation and ferrous iron dissociation, yet whether this mechanism could cause the increase in oxygen fugacity (from roughly -4ΔIW to -2ΔIW) required to make the model work is still debated (Frost et al. 2008, Rubie et al. 2011, Williams et al. 2012).

Therefore, the simplest and most compelling way to explain the Mo, W, and Ni abundance in the mantle is with single-stage core formation out of a magma ocean with conditions of 35-37 GPa, 2950-3000 K, and -2.2ΔIW with 1.8 wt.% C, 3.0 wt.% S, and 3.4 wt.% Si. The following discussion puts this model in context with the big picture of

Earth's accretion history. After the gravitational collapse of the molecular cloud that would become the solar system (4.567 Ga, Allegre et al. 1995), Earth began to accrete from chondritic material within the solar nebula (the results of the previous three chapters do not preclude heterogeneous accretion or progressive oxidation). Based on Hf-W isotopes, Earth's accretion was very rapid and core formation was complete within 30 Myr after solar system formation (Kleine et al. 2002, Yin et al. 2002). The process of metal-silicate separation probably occurred throughout accretion since melting was likely when Earth had just 10% of its current mass (Melosh 1990). Large impacts near the end of Earth's accretion caused extensive melting (Wetherill 1985, Canup and Agnor 2000, Tonks and Melosh 1993) and, as suggested from the present work, the final impact of accretion was energetic enough to cause a global magma ocean and complete metal-silicate re-equilibration. This magma ocean is responsible for imparting the moderately siderophile elements' abundances to the mantle. However, this magma ocean scenario is not able to explain the highly siderophile elements, most of which are present in the mantle in too large an abundance to be explained by high pressure equilibrium core formation (e.g. Walker 2009, with the possible exception of Au, Pt, and Pd, Danielson et al. 2005, Cottrell and Walker 2006, Righter et al. 2008). These elements are most often explained be a late veneer of chondritic material accreted to Earth after core formation has ceased, thus explaining their presence in the mantle in greater than expected abundance and in chondritic proportions (e.g. Holzheid et al. 2000, Walker 2009). It has been suggested that this late addition of highly siderophile elements may have been related to the late addition of volatiles (e.g. Albarede 2009, also see above discussion). However, recent studies suggest that the addition of this late veneer material was

ubiquitous throughout the inner solar system (even on early formed planetesimals) and therefore cannot be considered a 'late' addition, but a natural consequence of continued accretion after the cessation of core formation (Day et al. 2012, Dale et al. 2012). This demonstrates the value of comparing the differentiated bodies in the solar system in order to learn more about the commonality of their evolution and important processes in the early solar system.

5.2 Mars

Metal-silicate partitioning data can be applied to core formation on other differentiated bodies in the same way it is applied to Earth, so long as something is known about the body's interior structure and bulk and mantle compositions. Mars is an excellent example because there are both hand samples (martian meteorites) and data from the surface of Mars collected by a number of missions that have visited the red planet over the past 40 years. By examining Hf-W isotope data for three shergottites, Klein et al. (2004) determined that core formation on Mars must have been completed by 15 Myr after CAI (Calcium Aluminum-rich Inclusions, oldest solids in the solar system) formation, and suggested that no further large impacts occurred since that time due to isotopic differences in the meteorite mantle source regions. Such rapid accretion and core formation would have produced extensive melting on early Mars through heat generated by impacts, gravitational energy, and metal-silicate separation. Furthermore, the martian meteorite ALH84001 has a crystallization age of 4.1 Ga indicating crust formation had to have occurred before this time (Lapen et al. 2010). The most probable explanation of these short timescales for martian differentiation is that Mars experienced a global

magma ocean early in its history (see review in Solomon et al. 2005). Additionally, models of fractional crystallization of a martian magma ocean are able to explain the different meteorite source regions that formed early and were not subsequently mixed, the low Al_2O_3 and high FeO in martian mantle, the early formed crust, and the remnant magnetic field (Elkins-Tanton et al. 2003).

Multiple studies have made estimations of the bulk and mantle compositions of Mars through the analysis of martian meteorites, and some have included siderophile element data (Wänke and Dreibus 1988, Righter et al. 1998, Kong et al. 1999), Figure 5-2. As noted in Figure 5-2, Fe is less depleted in the martian mantle compared to the terrestrial mantle, with ~18 wt.% FeO compared to 8 wt.% in Earth's mantle (Wänke and Dreibus 1988, McDonough 2003). Thus, metal-silicate equilibrium on Mars probably occurred at an oxygen fugacity of -1ΔIW (e.g. Jones 2003), compared to -2.2ΔIW on Earth. However, similar to Earth, the Mo and Ni abundances in the martian mantle are larger than expected for low pressure metal-silicate equilibrium (D values for 1 bar experiments would put the depletions around 0.001, Holzheid et al. 1994), suggesting core formation took place at relatively high pressures. Excepting the Mo data point from Kong et al. (1999), which appears to be an outlier (Figure 5-2), the relative mantle depletions of the siderophile elements examined in the present study goes Ni > Mo > W. By comparing the partitioning behavior of these three elements, Table 5-1, and applying the results to the relative depletions, insight can be gained into core formation on Mars. It has been suggested that the martian core contains large amounts of sulfur, roughly 14 wt.% (Wänke and Dreibus 1988, Lodders and Fegley 1997, Sanloup et al. 1999). Based on the different effects of S on the partitioning of Mo, W, and Ni (Table 5-1), the

presence of that much S in the core of Mars could explain the relative depletions. D_{Ni} increases upon S addition to the metal phase, which could cause a significant Ni depletion; whereas S causes D_{Mo} to decrease. The W abundance would be most affected by the presence of S in the metal phase since D_W decreases strongly upon S addition, which could explain why W is only slightly depleted in the martian mantle. Although the martian mantle composition is not well constrained, using the martian mantle composition suggested by Wänke and Dreibus (1988) and the parameterization expressions in Table 5-1, the abundances of Mo, W, and Ni are best explained by core formation out of a magma ocean with conditions of -1.7ΔIW, 16 GPa, 2453 K, with X_S = 0.13 in the metal phase. Thus, similar to what previous studies have suggested (e.g. Righter and Drake 1996), a global magma ocean of moderate depth with a significant amount of sulfur could explain the siderophile element signature in the mantle.

5.3 The Moon and differentiated asteroids

The first direct evidence of a magma ocean on any planetary body came from lunar samples brought back by the Apollo missions. Analysis of the samples showed quite irrefutably that lunar evolution involved a global magma ocean, from which the global floatation crust (anorthositic highlands) and complementary Eu anomaly between the highlands plagioclase and mare pyroxenes developed (Smith 1970, Wood et al. 1970, Schnetzler and Philpotts 1971, Warren 1985). Using metal-silicate partitioning studies to place constraints on conditions within the lunar magma ocean is difficult due to uncertainties in the bulk and mantle compositions of the Moon and the size of its core. However, by selecting best approximations for each of the mentioned parameters, Righter

and Drake (1996) suggest lunar magma ocean conditions of 3.5 GPa, 2200 K, -1.0ΔIW, and a core $X_S = 0.15$ to explain the siderophile element depletions of Ni, Co, P, Mo, and W. Additionally, crystallization of a lunar magma ocean has been used to explain the different source regions of the Mg-suite rocks, mare basalts, and picritic glasses (Elardo et al. 2011, Elkins-Tanton et al. 2011).

For comparison, Table 5-2 shows the most common estimates of bulk and mantle siderophile element abundances for the Moon, Mars, and Earth. If pressure effects dominated the partitioning behavior of Ni, Co, Mo, and W, one would expect to see depletion trends based on the size of the body alone (e.g. due to the decreasing effect pressure has on D_{Ni}, D_{Co}, D_{Mo}, and D_W the depletion factors would follow Earth > Mars > Moon). Evidence of a pressure trend is suggested in the data shown in Table 5-2 by the large difference in Ni and Co depletion factors between Earth and Mars, but then the Moon would be expected to have an even smaller depletion factor, which is not the case. This is because pressure is not the sole variable influencing metal-silicate partitioning behavior. Core formation occurred at different oxygen fugacities on the different bodies, and with different light elements in the core; both of which will affect siderophile element partitioning, as demonstrated in the previous sections. Furthermore, it is worthwhile to note that siderophile element data for the mantles of Mars and the Moon are scarce and the data shown in Table 5-2 are best estimates. Accordingly, core formation models for these bodies should be treated with a certain degree of caution.

Another planetary body for which we have some siderophile abundance estimates is the asteroid 4 Vesta. The HED (howardites, eucrites, and diogenites) basaltic meteorites represent a suite of samples from a differentiated body and are thought to be

from Vesta (McCord et al. 1970, McSween et al. 2010). Their siderophile element depletions and uniform oxygen isotopes are suggested to be from efficient mixing and core formation as a result of a magma ocean early in the asteroid's history (Righter and Drake 1996, Righter and Drake 1997, Kleine et al. 2004, Greenwood et al. 2005). However, a magma ocean crystallization model that can comprehensively explain the geochemistry of the HED suite has yet to be discovered (see reviews in McSween et al. 2010 and Zuber et al. 2011). Additionally, the uniform oxygen isotopes of angrite meteorites have been used as evidence of a magma ocean on the angrite parent body (Greenwood et al. 2005). A magma ocean may also be indicated by the remnant magnetization of certain angrites which suggests an early formed core dynamo (Weiss et al. 2008).

Thus far, the evidence points towards the ubiquity of magma oceans on differentiated solar system bodies; however, the ureilite parent body appears to have had a more complicated evolution. The siderophile elements in ureilites have been explained in different ways, first by a two stage model, with initial removal of a S-rich melt followed by the separation of Fe-metal (Warren et al. 2006), and second by high temperature separation of a S-rich liquid from a C-rich metallic liquid (Hayden et al. 2011). This suggests that although magma oceans were common occurrences in the early solar system, each differentiated body underwent a unique differentiation history.

5.4 Future perspectives

Terrestrial planet evolution remains a fascinating and worthwhile area of study. Progress in the field has led us from the relatively cold and protracted core formation

theories (e.g. Anderson et al. 1971), to the hot and rapid core formation theories suggested here, yet more remains to be discovered. As analytical techniques improve and more data is obtained through new meteorite discoveries and space missions, even more insight will be gained. For example, better compositional data from differentiated bodies will allow for better constraints to be placed on the suggested magma ocean models for solar system bodies such as Mars and Vesta. Further comparative studies on the differentiation history of the terrestrial planets (including the Moon and differentiated asteroids) is essential for obtaining a comprehensive view of terrestrial planet evolution, and understanding how heterogeneities form in the face of rapid, chaotic planetary accretion – the results of which are the truly unique planets we see today.

Table 5-1. Multiple linear regression coefficients from the Mo, W, and Ni parameterizations. N/A = not applicable.

Parameter	*Mo Coefficient*	*Standard Error*	*W Coefficient*	*Standard Error*	*Ni Coefficient*	*Standard Error*
Intercept	-12.43	1.92	-11.28	2.92	-0.07	0.15
ΔIW	-1.00	0.04	-1.50	N/A	-0.44	0.01
1/T	6352	602	-3774	560	4918	228
P/T	-71.19	16.17	-99.94	17.95	-82.95	5.41
SiO_2	13.38	2.03	16.79	2.88	N/A	N/A
Al_2O_3	9.27	2.35	11.01	3.23	N/A	N/A
FeO	8.19	2.04	10.77	3.10	N/A	N/A
MgO	9.46	1.97	8.92	2.92	N/A	N/A
CaO	7.83	2.00	6.50	3.03	N/A	N/A
TiO_2	13.15	2.70	15.84	4.16	N/A	N/A
NBO/T	N/A	N/A	N/A	N/A	-0.07	0.01
log(1-Xc)	-7.18	0.66	-7.12	0.61	-2.15	0.28
log(1-Xs)	6.59	1.28	9.01	2.48	-2.19	0.13
log(1-Xsi)	13.35	2.33	N/A	N/A	1.98	0.85
log(1-Xo)	N/A	N/A	N/A	N/A	-4.13	0.77

Table 5-2. Concentrations (in ppm) of Ni, Co, Mo, and W in the mantles of Earth, Mars, and the Moon, along with bulk planet estimates and depletion factors.

	Mantle Abundance[1]	Bulk Planet Abundance[2]	Depletion Factor[3]
Ni			
Earth	1860	10770	0.17
Mars	400	21002	0.02
Moon	470	4720	0.10
Co			
Earth	102	506	0.20
Mars	68	987	0.07
Moon	90	220	0.41
Mo			
Earth	0.039	0.928	0.04
Mars	0.118	1.810	0.07
Moon	0.002	0.068	0.03
W			
Earth	0.016	0.090	0.18
Mars	0.105	0.176	0.60
Moon	0.018	0.041	0.44

[1]Mantle abundances: Earth - Palme and O'Neill (2003), Mars - Wänke and Dreibus (1988), Moon (Ni, Co) - Delano 1986, Moon (Mo, W) - O'Neill (1991). [2]Bulk Abundances: Earth - CI chondrites, Palme and O'Neill (2003), Mars - 1.95*CI, Moon - O'Neill (1991). [3]Depletion factor = Mantle/Bulk.

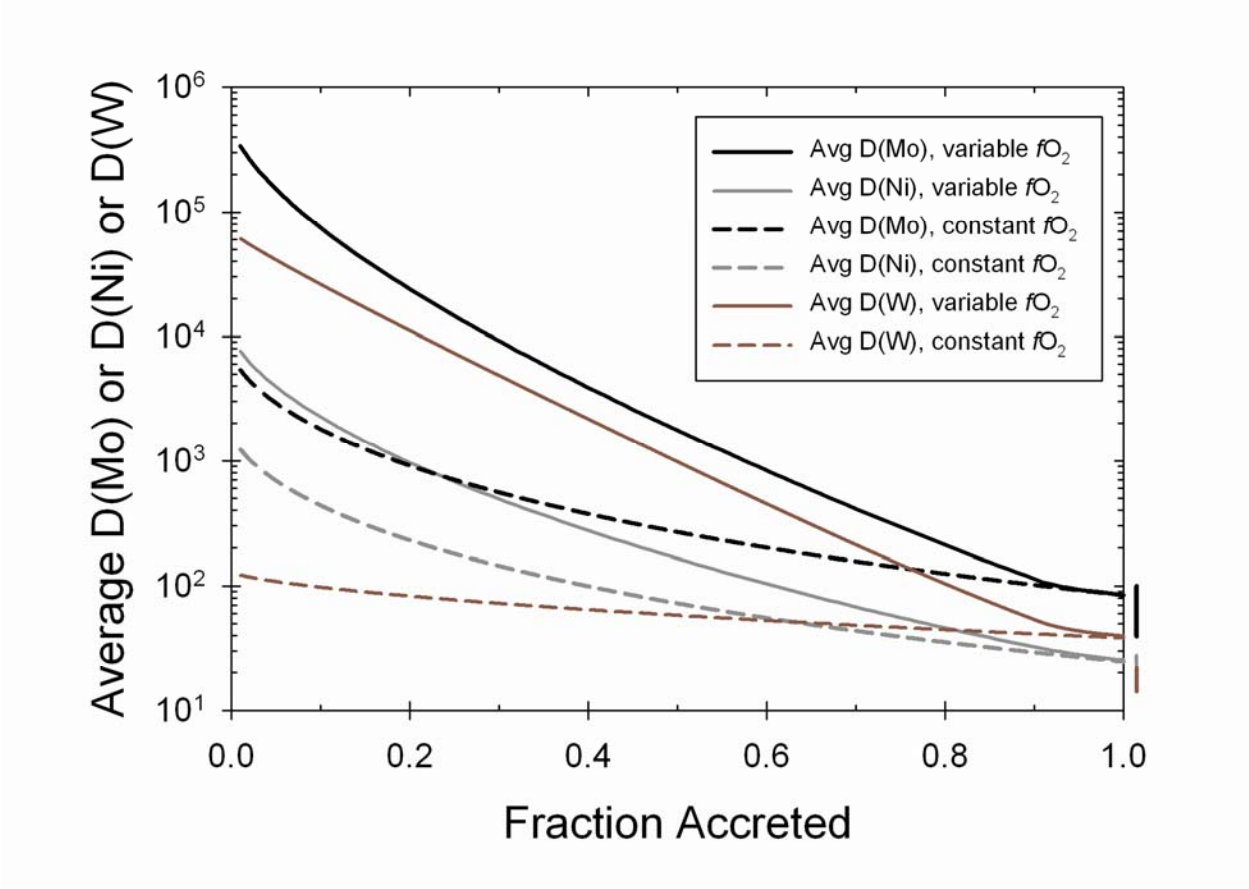

Figure 5-1. Average D(Mo), D(Ni), and D(W) values vs. fraction accreted for two different multi-stage models, one with progressive oxidation and one at a constant oxygen fugacity of -2.2ΔIW. The models are similar to that put forth by Wade and Wood (2005) in which Earth is accreted in 1% steps and the incoming metal equilibrates with the entire mantle before being segregated to the core, where no further equilibration occurs. The pressure of equilibration was kept constant at the base of a magma ocean that is 27% of the depth to the core-mantle boundary (135 GPa). Temperature increases with pressure along the peridotite liquidus (from Andrault et al. 2011). For the progressive oxidation model, oxygen fugacity increases at a constant rate of 0.02 log units from -4.00ΔIW at 1% accretion to -2.22ΔIW at 90% accretion, and then stays at -2.20ΔIW for the rest of accretion. For the constant oxygen fugacity model, fO_2 remains at -2.20ΔIW throughout accretion. The lines to the right of the graph indicate the D(Mo), D(Ni), and D(W) values required to explain the observed mantle abundance of Mo (black), Ni (gray), and W (red).

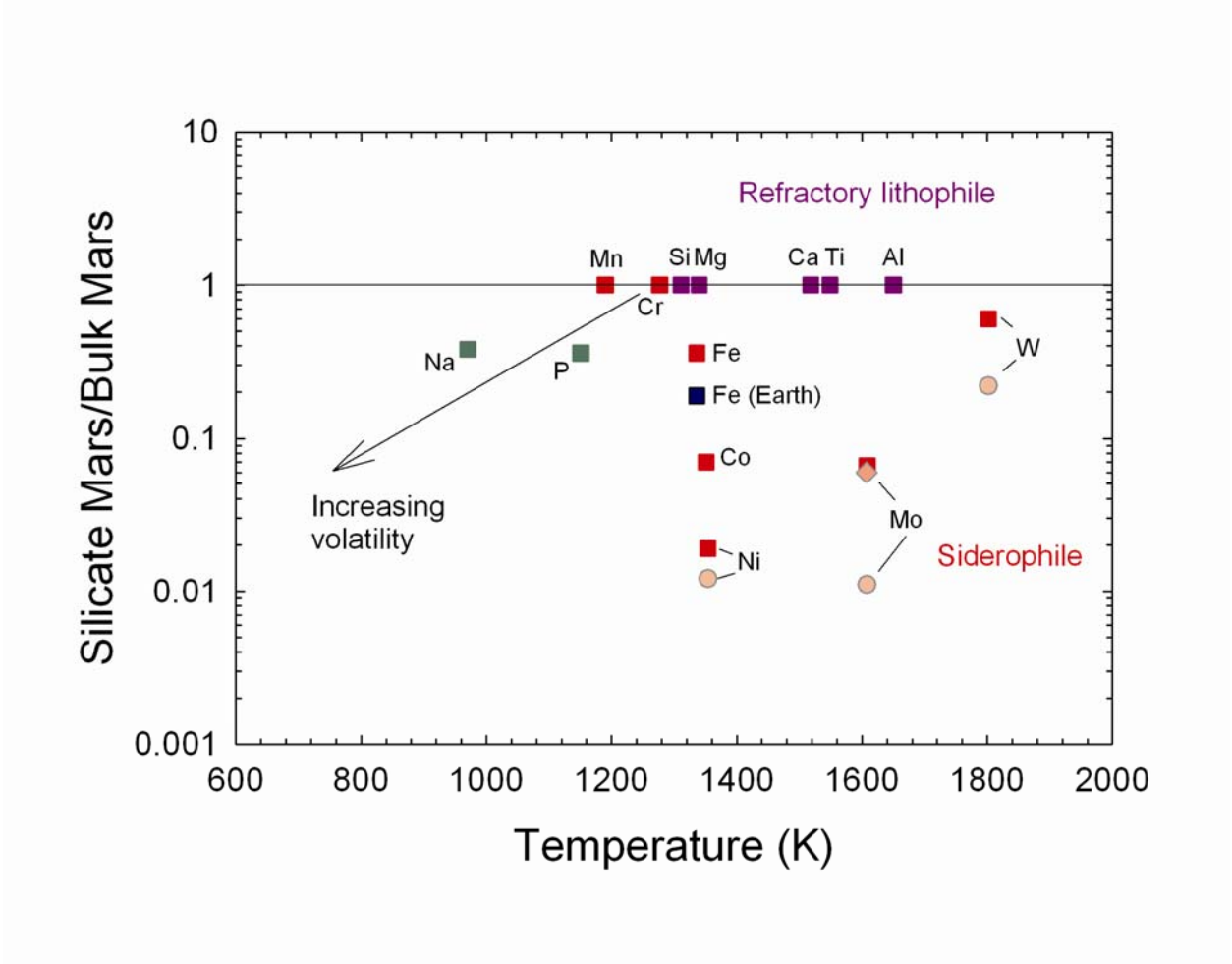

Figure 5-2. Elemental depletions in the martian mantle relative to the bulk Mars composition determined by Wänke and Dreibus (1988) for the square symbols. Diamond symbol is from Righter et al. (1998) and circle symbols are from Kong et al. (1999). Earth's iron depletion is from McDonough (2003). X-axis is the temperature at which 50% of the element would condense out of a gas of solar nebula composition at 10^{-4} bars (from Wasson 1985).

5.5 References

Albarede, F. (2009) Volatile accretion history of the terrestrial planets and dynamic implications. Nature 461, 1227-1233

Allegre, C.J., Manhes, G., Gopel, C. (1995) The age of the Earth. Geochimica et Cosmochimica Acta 59, 1445-1456

Anderson, D.L., Sammis, C., Jordan, T. (1971) Composition and evolution of the mantle and core. Science 171, 1103-1112

Canup, R.M., Agnor, C.B. (2000) Accretion of the terrestrial planets and the Earth-Moon system. In: Canup, R. M. and Righter, K. eds. *Origin of the Earth and Moon*. The University of Arizona Press, Tucson AZ, pp. 113-129

Cottrell, E., Walker, D. (2006) Constraints on core formation from Pt partitioning in mafic silicate liquids at high temperatures. Geochimica et Cosmochimica Acta 70, 1565-1580

Danielson, L.R., Sharp, T.G., Hervig, R.L. (2005) Implications for core formation of the Earth from high pressure-temperature Au partitioning experiments. LPSC XXXVI, abstract #1955

Dale, C.W., Burton, K.W., Greenwood, R.C., Gannoun, A., Wade, J., Wood, B.J., Pearson, D. G. (2012) Late accretion on the earliest planetesimals revealed by the highly siderophile elements. Science 336, 72-75

Day, J.M.D., Walker, R.J., Qin, L., Rumble III, D. (2012) Late accretion as a natural consequence of planetary growth. Nature Geoscience 5, 614-617

Delano, J.W. (1986) Abundances of cobalt, nickel, and volatiles in the silicate portion of the Moon. In: Hartmann, W.K., Phillips, R.J., and Taylor, G.J. eds. *Origin of the Earth and Moon*. Lunar and Planetary Institute, Houston, TX 231-247

Elardo, S.M., Draper, D.S., Shearer, C.K. (2011) Lunar magma ocean crystallization revisited: Bulk composition, early cumulate mineralogy, and the source regions of the highlands Mg-suite. Geochimica et Cosmochimica Acta 75, 3024-3045

Elkins-Tanton, L.T., Parmentier, E.M., Hess, P.C. (2003) Magma ocean fractional crystallization and cumulate overturn in terrestrial planets: Implications for Mars. Meteoritics and Planetary Science 38, 1753-1771

Elkins-Tanton, L.T., Burgess, S., Yin, Q.-Z. (2011) The lunar magma ocean: Reconciling the solidification process with lunar petrology and geochronology. Earth and Planetary Science Letters 304, 326-336

Frost, D.J., Mann, U., Asahara, Y., and Rubie, D.C. (2008) The redox state of the mantle during and just after core formation. Philosophical Transactions of the Royal Society of London A 366, 4315-4337

Greenwood, R.C., Franchi, I.A., Jambon, A., Buchanon, P.C. (2005) Widespread magma oceans on asteroidal bodies in the early solar system. 435, 916-918

Hayden, L.A., Van Orman, J.A., McDonough, W.F., Ash, R.D., Goodrich, C.A. (2011) Trace element partitioning in the Fe-S-C system and its implications for planetary differentiation and the thermal history of ureilites. Geochimica et Cosmochimica Acta 75, 6570-6583

Holzheid, A., Borisov, A., Palme, H. (1994) The effect of oxygen fugacity and temperature on solubilities of nickel, cobalt, and molybdenum in silicate melts. Geochimica et Cosmochimica Acta 58, 1975-1981

Jones, J.H. (2003) Constraints on the structure of the martian interior determined from the chemical and isotopic systematics of SNC meteorites. Meteoritics and Planetary Science 38, 1807-1814

Holzheid, A., Sylvester, P.J., O'Neill, H., Rubie, D.C., Palme, H. (2000) Evidence for a late chondritic veneer in the Earth's mantle from high-pressure partitioning of palladium and platinum. Nature 406, 396-399

Kleine, T., Munker, C., Mezger, K., Palme, H. (2002) Rapid accretion and early core formation on asteroids and the terrestrial planets from Hf-W chronometry. Nature 418, 952-955

Kleine, T., Mezger, K., Munker, C., Palme, H., Bischoff, A. (2004) ^{182}Hf-^{182}W isotope systematics of chondrites, eucrites, and martian meteorites: Chronology of core formation and early mantle differentiation in Vesta and Mars. Geochimica et Cosmochimica Acta 68, 2935-2946

Kong, P., Ebihara, M., Palme, H. (1999) Siderophile elements in Martian meteorites and implications for core formation in Mars. Geochimica et Cosmochimica Acta 63, 1865-1875

Lapen, T.J., Righter, M., Brandon, A.D., Debaille, V., Beard, B.L., Shafer, J.T., Peslier, A.H. (2010) A younger age for ALH84001 and its geochemical link to Shergottite sources in Mars. Science 328, 347-351

Lodders, K., Fegley Jr, B. (1997) An oxygen isotope model for the composition of Mars. Icarus 126, 373-394

McCord, T.B., Adams, J.B., Johnson, T.V. (1970) Asteroid Vesta: Spectral reflectivity and compositional implications. Science 168, 1445-1447

McCubbin, F.M., Hauri, E.H., Elardo, S.M., Vander Kaaden, K.E., Wang, J., Shearer, C.K. (2012) Hydrous melting of the martian mantle produced both depleted and enriched shergottites. Geology 40, 683-686

McDonough, W.F., (2003) Compositional model for the Earth's core. In: Carlson, R.W. ed. *Treatise on Geochemistry, Vol. 2, The Mantle and Core.* Elsevier Ltd, 547-568

McSween Jr, H.Y., Mittlefehldt, D.W., Beck, A.W., Mayne, R.G., McCoy, T.J. (2010) HED meteorites and their relationship to the geology of Vesta and the Dawn mission. Space Science Reviews 163, 141-174

Melosh, H.J. (1990) Giant impacts and the thermal state of the early Earth. In: Newsom, H.E. and Jones, J.H. eds. *Origin of the Earth*. Oxford University Press, 69-83

O'Brien, D.P., Morbidelli, A., Levison, H.F. (2006). Terrestrial planet formation with strong dynamical fiction. Icarus 184, 39-58

O'Neill, H.S.C. (1991) The origin of the Moon and the early history of the Earth – A chemical model. Part 1: The Moon. Geochimica et Cosmochimica Acta 55, 1135-1157

Palme, H., O'Neill, H.S.C. (2003) Cosmochemical estimates of mantle composition. In: Carlson, R.W. ed. *Treatise on Geochemistry, Vol. 2, The Mantle and Core.* Elsevier Ltd, 1-38

Righter, K., Drake, M.J. (1996) Core formation in Earth's Moon, Mars, and Vesta. Icarus 124, 513-529

Righter, K., Drake, M.J. (1997) A magma ocean on Vesta: Core formation and petrogensis of eucrites and diogenites. Meteoritics and Planetary Science 32, 929-944

Righter, K., Hervig, R.L., and Kring, D.A. (1998) Accretion and core formation on Mars: Molybdenum contents of melt inclusion glasses in three SNC meteorites. Geochimica et Cosmochimica Acta 62, 2167-2177

Righter, K., Humayun, M., Danielson, L. (2008) Partitioning of palladium at high pressures and temperatures during core formation. Nature 1, 321-323

Rubie, D.C., Frost, D.J., Mann, U., Asahara, Y., Nimmo, F., Tsuno, K., Kegler, P., Holzheid, A., Palme, H. (2011) Heterogeneous accretion, composition and core-mantle differentiation of the Earth. Earth and Planetary Science Letters 301, 31-42

Sanloup, C., Jambon, A., Gillet, P. (1999) A simple chondritic model of Mars. Physics of the Earth and Planetary Interiors 112, 43-54

Schnetzler, C.C., Philpotts, J.A. (1971) Alkali, alkaline earth, and rare-earth element concentrations in some Apollo 12 soils, rocks, and separated phases. Proc. Second Lunar Sci. Con. 2, 1101-1122

Schonbachler, M., Carlson, R.W., Horan, M.F., Mock, T.D., Hauri, E.H. (2010) Heterogeneous accretion and the moderately volatile element budget of Earth. Science 328, 884-887

Smith, J.V., Anderson, A.T., Newton, R.C., Olsen, E.J., Wyllie, P.J. (1970) A petrologic model for the Moon based on petrogenesis, experimental petrology, and physical properties. The Journal of Geology 78, 381-405

Solomon, S.C., Aharonson, O., Aurnou, J.M., Banerdt, W.B., Carr, M.H., Dombard, A.J., Frey, H.V., Golombek, M.P., Hauck II, S.A., Head III, J.W., Jakosky, B.M., Johnson, C.L., McGovern, P.J., Neumann, G.A., Phillips, R.J., Smith, D.E., and Zuber, M.T. (2005) New perspectives on ancient Mars. Science 307, 1214-1220

Tonks, W.B., Melosh, H.J. (1993) Magma ocean formation due to giant impacts. Journal of Geophysical Research 98, 5319-5333

Wade, J., Wood, B.J., (2005) Core formation and the oxidation state of the Earth. Earth and Planetary Science Letters 236, 78-95

Wade, J., Wood, B.J., Tuff, J. (2012) Metal-silicate partitioning of Mo and W at high pressures and temperatures: Evidence for late accretion of sulphur to the Earth. Geochimica et Cosmochimica Acta 85, 58-74

Walker, R.J. (2009) Highly siderophile elements in the Earth, Moon and Mars: Update and implications for planetary accretion and differentiation. Chemie der Erde 69, 101-125

Wänke, H., Dreibus, G. (1988) Chemical composition and accretion history of terrestrial planets. Philosophical Transactions of the Royal Society of London A 325, 545-557

Warren, P.H. (1985) The magma ocean concept and lunar evolution. Ann. Rev. Earth Planet. Sci. 13, 201-240

Warren, P.H., Ulff-Moller, F., Huber, H., Kallemeyn, G.W. (2006) Siderophile geochemistry of ureilites: A record of early stages of planetesimal core formation. Geochimica et Cosmochimica Acta 70, 2104-2126

Wasson, J.T. (1985) *Meteorites: Their record of early solar-system history.* W.H. Freeman and Company, New York, 267 pp

Weiss, B.P., Berdahl, J.S., Elkins-Tanton, L.T., Stanley, S., Lima, E.A., Carporzen, L. (2008) Magnetism on the Angrite parent body and the early differentiation of planetesimals. Science 322, 713-716

Wetherill, G.W. (1985) Occurrence of giant impacts during the growth of the terrestrial planets. Science 228, 877-879

Williams, H.M., Wood, B.J., Wade, J., Frost, D.J., Tuff, J. (2012) Isotopic evidence for internal oxidation of Earth's mantle during accretion. Earth and Planetary Science Letters 321-322, 54-63

Wood, J.A., Dickey Jr, J.S., Marvin, U.B., Powell, B.N. (1970) Lunar anorthosites and a geophysical model of the moon. Proc. Apollo 11 Lunar Sci. Conf. 1, 965-988

Yin, Q., Jacobsen, S.B., Yamashita, K., Blichert-Toft, J., Telouk, P., Albarede, F. (2002) A short timescale for terrestrial planet formation from Hf-W chronometry of meteorites. Nature 418, 949-959

Zuber, M.T., McSween Jr, H.Y., Binzel, R.P., Elkins-Tanton, L.T., Konopliv, A.S., Pieters, C.M., Smith, D.E. (2011) Origin, internal structure and evolution of 4 Vesta. Space Science Reviews 163, 77-93

Appendix

A.1 Starting materials

The "CaO" used to make the peridotite mix for experiments 20, 22-23, and 25-29 (Chapter 2) was analyzed by XRD after the experiments were performed and found to be mainly $Ca(OH)_2$ suggesting these experiments may contain up to 0.5 wt.% water. Two duplicate experiments, experiment 21 (duplicate of 20) and 24 (duplicate of 23) were performed with a starting composition that added Ca as $CaSiO_3$. As can be seen in Table 2-2, the results are within error of each other; therefore, there was either no contamination of the original peridotite mix or, more likely, the contamination had no effect on Mo solubility.

A.2 Microprobe standards

Table A-1. List of the elements analyzed by electron probe microanalysis and the standards utilized. All analyses were done with wavelength dispersive spectroscopy and ZAF corrections were applied.

Element	*Standard*
Si	almandine, pyrope, olivine
Ti	sphene
Al	almandine, pyrope, augite
Fe	olivine, almandine, pyrope
Mg	olivine, pyrope
Ca	pyrope, augite
K	orthoclase
Mn	spessartine
Na	albite
Sr	$SrBaNb_4O_{10}$
Zr	zirconia
P	apatite
Cr	doped diopside
Mo	Mo - metal
W	W - metal
Ni	Ni - metal

A.3 Error assessment on the oxygen fugacity calculation

In our calculation of oxygen fugacity in chapter 2, we assume γMoO_2 is one. O'Neill and Eggins (2002) show that γMoO_2 is very dependent on silicate melt composition, ranging from 19-446 over the compositions they studied. However, their silicate compositions were in the CMAS system, very unlike the compositions used in the present study. In all likelihood, the γMoO_2 for our experiments is not one, but since the values have not been determined for the specific compositions we used, we prefer to assume ideality, knowing γMoO_2 might be greater than one, than to estimate a higher value and add unknown error to the calculation. As a result, our method of calculating ΔIW may slightly underestimate the actual oxygen fugacity of our experiments.

Our method of calculating ΔIW is the same as that used by Cottrell et al. (2009) for their tungsten capsule experiments, except we take into account the pressure effect on the IW and MMO buffers (the difference between the buffers does not vary much with pressure so the resulting fO_2 values would not change much if the 1 bar buffers were used). Cottrell et al. (2009) state in the footnotes of their Table 1 that in their experiments with Fe in the metal phase (>30 wt.% Fe), comparison of the fO_2 calculated using the buffer difference method with the fO_2 calculated using the equation $\Delta IW = 2\log(a_{FeO}/a_{Fe})$ agree with each other within 0.5 log units. We tested the error for our Mo experiments in a similar manner. We performed an additional experiment in which Fe metal was added to the starting composition so that the run product metal phase contained 39.14 wt.% Mo and 60.34 wt.% Fe. Calculating oxygen fugacity according to $\Delta IW = 2\log(a_{FeO}/a_{Fe})$ gives -2.37ΔIW, and calculating oxygen fugacity using the buffer difference method gives -

2.65ΔIW. The results are in agreement within 0.3 log units, with the buffer difference method slightly underestimating ΔIW, as predicted above.

A.4 Calculating partition coefficients from solubility data

The method of O'Neill et al. (2008) was used to calculate partition coefficients for Mo in an iron-rich metal from our solubility data. This method is outlined below. Combining their equation (7) and (18) for a silicate melt containing only MoO_2,

$$D_{Mo}\left(metal/silicate\right) = 1/\left[\left(\gamma_{Mo}^{Feliq,\infty}\right)\left(X_{MoO_2}^{silmelt}\right)\right] \quad \text{(A-1)}$$

where $X_{MoO_2}^{silmelt}$ is the mole fraction of MoO_2 in the silicate melt and $\gamma_{Mo}^{Feliq,\infty}$ is the activity coefficient of molybdenum at infinite liquid-iron dilution relative to the standard state of the pure solid metal. From O'Neill et al. (2008) equation (22), $\gamma_{Mo}^{Feliq,\infty}$ is calculated according to

$$\gamma_{Mo}^{Feliq,\infty} = \exp\left(\frac{2957}{T} - 1.17\right) \quad \text{(A-2)}$$

where T is the temperature of the experiment in Kelvin. As mentioned in Section 2.4.1, the solubility data of Holzheid et al. (1994), O'Neill and Eggins (2002), and Holzheid and Palme (2007) were also converted to partition coefficients using the above equations. Since the $\gamma_{Mo}^{Feliq,\infty}$ values are close to one, there is not a large difference between partition coefficients calculated using the above approach and those calculated by simply using a pure Mo metal phase (e.g. $D_{Mo} = 1/X_{MoO2}$).

A.5 Parameterization equations

Equation 2-5 in the text is used to empirically fit the data to come up with a predictive expression for D_{Mo}. It is similar to the equation put forth by Righter et al. (1997) and has been criticized for violating the Gibbs-Duhem equation. In Righter (2011), it was shown that using the empirical terms of Equation 2-5 to account for light elements in the metal phase gives the same extrapolated results as using the interaction parameter approach of Wade and Wood (2005) for the siderophile elements Ni and Co. For the silicate phase, O'Neill and Eggins (2002) employ a regular solution model, which obeys Gibbs-Duhem, to take into account silicate compositional effects. There has not been a comparison of this approach to the empirical approach of Equation 2-5 which uses oxide mole fractions, therefore we perform this comparison below.

All the data regressed using Equation 2-5 were also regressed using a regular solution model (RSM) for the silicate according to

$$\log D = a\Delta IW + \frac{b}{T} + \frac{cP}{T} + d\left(X_{SiO2}\right)^2 + e\left(X_{CaO}X_{MgO}\right) + f\left(X_{Al2O3}X_{CaO}\right) + g\log(1 - X_C) + h\log(1 - X_S) + i\log(1 - X_{Si}) + j \quad \text{(A-3)}$$

where *a*-*j* are linear regression coefficients and *X* is mole fraction. The resulting coefficients are shown in Table A-2 below, along with the coefficients from the oxide mole fraction approach (from Chapter 2).

Table A-2. Linear regression coefficients for the two approaches.

RSM approach		
Parameter	Value	St. Error
Intercept	-3.12	0.30
ΔIW	-1.14	0.04
1/T	7656	602
P/T	-67.52	20.75
X(SiO2)2	3.27	0.51
X(MgOCaO)	4.23	3.01
X(Al2O3CaO)	-11.13	4.55
log(1-Xc)	-7.43	0.67
log(1-Xs)	4.41	1.41
log(1-Xsi)	15.99	2.40

Oxide approach		
Parameter	Value	St. Error
Intercept	-13.82	1.85
ΔIW	-1.12	0.03
1/T	7382	559
P/T	-56.29	18.36
SiO2	13.30	1.92
Al2O3	9.78	2.42
FeO	10.51	2.02
MgO	10.78	1.95
CaO	9.72	1.98
TiO2	12.24	2.56
log(1-Xc)	-5.87	0.70
log(1-Xs)	4.67	1.25
log(1-Xsi)	15.92	2.12

As can be seen in Table A-2, the oxygen fugacity, P, T, and light element coefficients are very similar for the two approaches. The fit is slightly better for the oxide approach than the RSM, giving R^2 values of 0.95 and 0.93, respectively. However, when the two equations are used to predict magma ocean conditions that explain the observed mantle abundance (D = 40-100), using a peridotite silicate, -2.2ΔIW, and constraining the conditions to be on the peridotite liquidus, they give quite different results. The RSM approach predicts magma ocean pressures of 28-38 GPa, whereas the oxide approach predicts 40-54 GPa.

To determine which approach gives the more accurate result, we examined how well each approach predicts the observed effect of silicate composition from the experimental data. The RSM approach predicts a strong, constant decreasing trend in D_{Mo} with increasing NBO/T. As described in the manuscript text, this is the general trend of most of the previous studies that examined the effect of silicate composition. However, our study showed that there are obvious anomalies to this (e.g. our basalt D value being higher than the andesite D value), and the data of Righter et al. (2010) actually show an

increase in D_{Mo} with increasing NBO/T. This is one reason we chose to use the oxide mole fraction approach as opposed to NBO/T, see manuscript text. Looking specifically at these experiments (our andesite and basalt experiments and the MgO capsule experiments of Righter et al. 2010), the oxide mole fraction approach predicts the experimentally determined D_{Mo} values significantly better than the RSM approach, by a factor of 2. As mentioned, the oxide mole fraction approach does not obey the Gibbs-Duhem equation, and therefore any extrapolation of the data should be treated with caution. However, we chose to use the oxide mole fraction approach because it is better at predicting the experimentally observed trends in the data, and therefore probably produces more accurate extrapolations. It will be very interesting when experimental data at the predicted high pressure magma ocean conditions becomes available to see if this is in fact correct. Our comparison demonstrates how important it is when using a predictive expression to make sure the predicted trends (e.g. the effect of silicate composition) match those observed in the experimental data, in order to ensure the predictive expression is not biasing certain variables.

List of References

Agee, C.B., Li, J., Shannon, M.C. (1995) Pressure-temperature phase diagram for the Allende meteorite. Journal of Geophysical Research 100, 17725-17740

Albarede, F. (2009) Volatile accretion history of the terrestrial planets and dynamic implications. Nature 461, 1227-1233

Allegre, C.J., Manhes, G., Gopel, C. (1995) The age of the Earth. Geochimica et Cosmochimica Acta 59, 1445-1456

Anderson, D.L., Sammis, C., Jordan, T. (1971) Composition and evolution of the mantle and core. Science 171, 1103-1112

Andrault, D., Bolfan-Casanova, N., Lo Nigro, G., Bouhifd, M.A., Garbarino, G., Mezouar, M. (2011) Solidus and liquidus profiles of chondritic mantle: Implication for melting of Earth across its history. Earth and Planetary Science Letters 304, 251-259

Badro, J., Fiquet, G., Guyot, F., Gregoryanz, E., Occelli, F., Antonangeli, D., d'Astuto, M. (2007) Effect of light elements on the sound velocities in solid iron: Implications for the composition of Earth's core. Earth and Planetary Science Letters 254, 233-238

Bertka, C.M., Fei, Y. (1997) Mineralogy of the martian interior up to core-mantle boundary pressures. Journal of Geophysical Research 102, 5251-5264

Birch, F. (1952) Elasticity and constitution of Earth's interior. Journal of Geophysical Research 57, 227-286

Bouhifd, M.A., Jephcoat, A.P. (2003) The effect of pressure on partitioning of Ni and Co between silicate and iron-rich metal liquids: a diamond-anvil cell study. Earth and Planetary Science Letters 209, 245-255

Bouhifd, M.A., Jephcoat, A.P. (2011) Convergence of Ni and Co metal-silicate partition coefficients in the deep magma-ocean and coupled silicon-oxygen solubility in iron melts at high pressures. Earth and Planetary Science Letters 307, 341-348

Brenan, J.M., McDonough, W.F. (2009) Core formation and metal-silicate fractionation of osmium and iridium from gold. Nature Geoscience 2, 798-801

Brown, S.M., Elkins-Tanton, L.T. (2009) Compositions of Mercury’s earliest crust from magma ocean models. Earth and Planetary Science Letters 286, 446-455

Burkemper, L.K., Agee, C.B., Garcia, K.A. (2012) Constraints on core formation from molybdenum solubility in silicate melts at high pressure. Earth and Planetary Science Letters 335-336, 95-104

Burkemper, L.K., Agee, C.B., Garcia, K.A. (2013) Molybdenum metal-silicate partitioning behavior: Constraining the magma ocean models for core formation. In prep.

Cameron, A.G.W., Ward, W.R. (1976) The origin of the Moon. Lunar Science VII, 120-122

Campbell, A.J., Danielson, L., Righter, K., Seagle, C.T., Wang, Y., Prakapenka, V.B. (2009) High pressure effects on the iron-iron oxide nickel-nickel oxide oxygen fugacity buffers. Earth and Planetary Science Letters 286, 556-564

Canup, R.M., Agnor, C.B. (2000) Accretion of the terrestrial planets and the Earth-Moon system. In: Canup, R. M. and Righter, K. eds. *Origin of the Earth and Moon*. The University of Arizona Press, Tucson AZ, 113-129

Canup, R.M., Asphaug, E. (2001) Origin of the Moon in a giant impact near the end of Earth's formation. Nature 412, 708-712

Chabot, N.L., Agee, C.B. (2003) Core formation in the Earth and Moon: new experimental constraints from V, Cr, and Mn. Geochimica et Cosmochimica Acta 67, 2077-2091

Chabot, N.L., Draper, D.S., Agee, C.B. (2005) Conditions of core formation in the Earth: constraints from nickel and cobalt partitioning. Geochimica et Cosmochimica Acta 69, 2141-2151

Chase Jr., M.W. (1998) NIST-JANAF Thermochemical Tables, 4th ed. Journal of Physical and Chemical Reference Data Monograph No. 9 American Institute of Physics

Corgne, A., Keshav, S., Wood, B.J., McDonough, W.F., Fei, Y. (2008) Metal-silicate partitioning and constraints on core composition and oxygen fugacity during Earth accretion. Geochimica et Cosmochimica Acta 72, 574-589

Cottrell, E., Walker, D. (2006) Constraints on core formation from Pt partitioning in mafic silicate liquids at high temperatures. Geochimica et Cosmochimica Acta 70, 1565-1580

Cottrell, E., Walter, M.J., Walker, D. (2009) Metal-silicate partitioning of tungsten at high pressure and temperature: Implications for equilibrium core formation in Earth. Earth and Planetary Science Letters 281, 275-287

Cottrell, E., Walter, M.J., Walker, D. (2010) Erratum to "Metal-silicate partitioning of tungsten at high pressure and temperature: Implications for equilibrium core formation in Earth" [Earth and Planetary Science Letters 281 (2009) 275-287]. Earth and Planetary Science Letters 289, 631-634

Danielson, L.R., Sharp, T.G., Hervig, R.L. (2005) Implications for core formation of the Earth from high pressure-temperature Au partitioning experiments. LPSC XXXVI, abstract #1955

Dale, C.W., Burton, K.W., Greenwood, R.C., Gannoun, A., Wade, J., Wood, B.J., Pearson, D. G. (2012) Late accretion on the earliest planetesimals revealed by the highly siderophile elements. Science 336, 72-75

Davis, F.A., Tangeman, J.A., Tenner, T.J., Hirschmann, M.M. (2009) The composition of KLB-1 peridotite. American Mineralogist 94, 176-180

Day, J.M.D., Walker, R.J., Qin, L., Rumble III, D. (2012) Late accretion as a natural consequence of planetary growth. Nature Geoscience 5, 614-617

Delano, J.W. (1986) Abundances of cobalt, nickel, and volatiles in the silicate portion of the Moon. In: Hartmann, W.K., Phillips, R.J., and Taylor, G.J. eds. *Origin of the Earth and Moon*. Lunar and Planetary Institute, Houston, TX 231-247

Drake, M.J., Newsom, H.E., Capobianco, C.J. (1989) V, Cr, and Mn in the Earth, Moon, EPB, and SPB and the origin of the Moon: Experimental studies. Geochimica et Cosmochimica Acta 53, 2101-2111

Draper, D.S. (1991) Late Cenozoic bimodal magmatism in the northern Basin and Range Province of southeastern Oregon. Journal of Volcanology and Geothermal Research 47, 299-328

Elardo, S.M., Draper, D.S., Shearer, C.K. (2011) Lunar magma ocean crystallization revisited: Bulk composition, early cumulate mineralogy, and the source regions of the highlands Mg-suite. Geochimica et Cosmochimica Acta 75, 3024-3045

Elkins-Tanton, L.T., Parmentier, E.M., Hess, P.C. (2003) Magma ocean fractional crystallization and cumulate overturn in terrestrial planets: Implications for Mars. Meteoritics and Planetary Science 38, 1753-1771

Elkins-Tanton, L.T., Burgess, S., Yin, Q.-Z. (2011) The lunar magma ocean: Reconciling the solidification process with lunar petrology and geochronology. Earth and Planetary Science Letters 304, 326-336

Ertel, W., O'Neill, H.S.C., Dingwell, D.B., Spettel, B. (1996) Solubility of tungsten in a haplobasaltic melt as a function of temperature and oxygen fugacity. Geochimica et Cosmochimica Acta 60, 1171-1180

Ertel, W., O'Neill, H.S.C., Sylvester, P.J., Dingwell, D.B. (1999) Solubilities of Pt and Rh in a haplobasaltic silicate melt at 1300 °C. Geochimica et Cosmochimica Acta 63, 2439-2449

Ertel, W., O'Neill, H.S.C., Sylvester, P.J., Dingwell, D.B., Spettel, B. (2001) The solubility of rhenium in silicate melts: Implications for the geochemical properties of rhenium at high temperatures. Geochimica et Cosmochimica Acta 65, 2161-2170

Ertel, W., Walter, M.J., Drake, M.J., Sylvester, P.J. (2006) Experimental study of platinum solubility in silicate melt to 14 GPa and 2273 K: Implications for accretion and core formation in Earth. Geochimica et Cosmochimica Acta 70, 2591-2602

Ertel, W., Dingwell, D.B., Sylvester, P.J. (2008) Siderophile element in silicate melts - A review of the mechanically assisted equilibration technique and the nanonugget issue. Chemical Geology 248, 119-139

Flasar, F.M., Birch, F. (1973) Energetics of core formation: A correction. Journal of Geophysical Research 78, 6101-6103

Floridis, T.P., Chipman, J. (1958) Activity of oxygen in liquid iron alloys. Transactions of the metallurgical society of AIME 212, 549-553

Fortenfant, S.S., Dingwell, D.B., Ertel-Ingrisch, W., Capmas, F., Birck, J.L., Dalpe, C. (2006) Oxygen fugacity dependence of Os solubility in haplobasaltic melt. Geochimica et Cosmochimica Acta 70, 742-756

Fried, L.E., Howard, W.M., Souers, P.C. (2002) EXP6: A new equation of state library for high pressure thermochemistry. 12th International Detonation Symposium, San Diego, CA

Frost, D.J., Mann, U., Asahara, Y., and Rubie, D.C. (2008) The redox state of the mantle during and just after core formation. Philosophical Transactions of the Royal Society of London A 366, 4315-4337

Gaetani, G.A., Grove, T.L. (1997) Partitioning of moderately siderophile elements among olivine, silicate melt, and sulfide melt: Constraints on core formation in the Earth and Mars. Geochimica et Cosmochimica Acta 61, 1829-1846

Georg, R.B., Halliday, A.N., Schauble, E.A., Reynolds, B.C. (2007) Silicon in the Earth's core. Nature 447, 1102-1106

Gessmann, C.K., Rubie, D.C. (1998) The effect of temperature on the partitioning of nickel, cobalt, manganese, chromium, and vanadium at 9 GPa and constraints on formation of the Earth's core. Geochimica et Cosmochimica Acta 62, 867-882

Gessmann, C.K., Rubie, D.C. (2000) The origin of the depletions of V, Cr, and Mn in the mantles of the Earth and Moon. Earth and Planetary Science Letters 184, 95-107

Greenwood, R.C., Franchi, I.A., Jambon, A., Buchanan, P.C. (2005) Widespread magma oceans on asteroidal bodies in the early Solar System. Nature 435, 916-918

Haack, H., McCoy, T.J. (2005) Iron and stony-iron meteorites. In: Davis, A.M. ed., *Treatise on Geochemistry, Vol. 1, Meteorites, Comets, and Planets.* Elsevier Ltd, 325-345

Hartmann, W.K., Davis, D.R. (1975) Satellite-sized planetesimals and lunar origin. Icarus 24, 504-515

Hayden, L.A., Van Orman, J.A., McDonough, W.F., Ash, R.D., Goodrich, C.A. (2011) Trace element partitioning in the Fe-S-C system and its implications for planetary differentiation and the thermal history of ureilites. Geochimica et Cosmochimica Acta 75, 6570-6583

Hillgren, V.J. (1991) Partitioning behavior of Ni, Co, Mo, and W between basaltic liquid and Ni-rich metal: Implications for the origin of the moon and lunar core formation. Geophysical Research Letters 18, 2077-2080

Hillgren, V.J. (1993) Partitioning behavior of moderately siderophile elements in Ni-rich systems: Implications for the Earth and Moon. PhD thesis. University of Arizona, 423 pp

Hillgren, V.J., Drake, M.J., Rubie, D.C. (1994) High-pressure and high-temperature experiments on core-mantle segregation in the accreting Earth. Science 264, 1442-1445

Hillgren, V.J., Drake, M.J., Rubie, D.C. (1996) High pressure and high temperature metal-silicate partitioning of siderophile elements: The importance of silicate liquid composition. Geochimica et Cosmochimica Acta 60, 2257-2263

Hillgren, V.J., Gessmann, C.K., Li, J. (2000) An experimental perspective on the light element in Earth's core. In: Canup, R. M. and Righter, K. eds. *Origin of the Earth and Moon*. The University of Arizona Press, Tucson AZ, 245-263

Holzheid, A., Borisov, A., Palme, H. (1994) The effect of oxygen fugacity and temperature on solubilities of nickel, cobalt, and molybdenum in silicate melts. Geochimica et Cosmochimica Acta 58, 1975-1981

Holzheid, A., Palme, H. (1996) The influence of FeO on the solubilities of cobalt and nickel in silicate melts. Geochimica et Cosmochimica Acta 60, 1181-1193

Holzheid, A., Sylvester, P.J., O'Neill, H., Rubie, D.C., Palme, H. (2000) Evidence for a late chondritic veneer in the Earth's mantle from high-pressure partitioning of palladium and platinum. Nature 406, 396-399

Holzheid, A., Palme, H. (2007) The formation of eucrites: Constraints from metal-silicate partition coefficients. Meteoritics and Planetary Science 42, 1817-1829

Ito E., Katsura, T., Suzuki, T. (1998) Metal/silicate partitioning of Mn, Co, and Ni at high-pressures and high temperatures and implications for core formation in a deep magma ocean. Geophysical monograph 101, American Geophysical Union, Washington, DC, 215-225

Jaeger, W.L., Drake, M.J. (2000) Metal-silicate partitioning of Co, Ga, and W: Dependence on silicate melt composition. Geochimica et Cosmochimica Acta 64, 3887-3895

Jana, D., Walker, D. (1997a) The influence of silicate melt composition on distribution of siderophile elements among metal and silicate liquids. Earth and Planetary Science Letters 150, 463-472

Jana, D., Walker, D. (1997b) The impact of carbon on element distribution during core formation. Geochimica et Cosmochimica Acta 61, 2759-2763

Jana, D., Walker, D. (1997c) The influence of sulfur on partitioning of siderophile elements. Geochimica et Cosmochimica Acta 61, 5255-5277

Jones, J.H., Drake, M.J. (1986) Geochemical constraints on core formation in the Earth. Nature 322, 221-228

Jones, J.H. (2003) Constraints on the structure of the martian interior determined from the chemical and isotopic systematics of SNC meteorites. Meteoritics and Planetary Science 38, 1807-1814

Karato, S., Murthy, V.R. (1997) Core formation and chemical equilibrium in the earth - I. Physical considerations. Physics of the Earth and Planetary Interiors 100, 61-79

Kegler, P., Holzheid, A., Frost, D.J., Rubie, D.C., Dohmen, R., Palme, H. (2008) New Ni and Co metal-silicate partitioning data and their relevance for an early terrestrial magma ocean. Earth and Planetary Science Letters 268, 28-40

Kleine, T., Munker, C., Mezger, K., Palme, H. (2002) Rapid accretion and early core formation on asteroids and the terrestrial planets from Hf-W chronometry. Nature 418, 952-955

Kleine, T., Mezger, K., Munker, C., Palme, H., Bischoff, A. (2004) ^{182}Hf-^{182}W isotope systematics of chondrites, eucrites, and martian meteorites: Chronology of core formation and early mantle differentiation in Vesta and Mars. Geochimica et Cosmochimica Acta 68, 2935-2946

Kong, P., Ebihara, M., Palme, H. (1999) Siderophile elements in Martian meteorites and implications for core formation in Mars. Geochimica et Cosmochimica Acta 63, 1865-1875

Lapen, T.J., Righter, M., Brandon, A.D., Debaille, V., Beard, B.L., Shafer, J.T., Peslier, A.H. (2010) A younger age for ALH84001 and its geochemical link to Shergottite sources in Mars. Science 328, 347-351

Leinenweber, K.D., Tyburczy, J.A., Sharp, T.G., Soignard,E., Diedrich, T., Petuskey, W.B., Wang, Y., Mosenfelder, J.L. (2012) Cell assemblies for reproducible multi-anvil experiments (the COMPRES assemblies). American Mineralogist 97, 353-369

Li, J., Agee, C.B. (1996) Geochemistry of mantle-core differentiation at high pressure. Nature 381, 686-689

Li, J., Agee, C.B. (2001) The effect of pressure, temperature, oxygen fugacity, and composition on partitioning of nickel and cobalt between liquid Fe-Ni-S alloy and liquid silicate: Implications for the Earth's core formation. Geochimica et Cosmochimica Acta 65, 1821-1832

Lodders, K., Palme, H. (1991) On the chalcophile character of molybdenum: Determination of sulfide/silicate partition coefficients of Mo and W. Earth and Planetary Science Letters 103, 311-324

Lodders, K., Fegley Jr, B. (1997) An oxygen isotope model for the composition of Mars. Icarus 126, 373-394

Mann, U., Frost, D.J., Rubie, D.C. (2009) Evidence for high-pressure core-mantle differentiation from the metal-silicate partitioning of lithophile and weakly-siderophile elements. Geochimica et Cosmochimica Acta 73, 7360-7386

McCord, T.B., Adams, J.B., Johnson, T.V. (1970) Asteroid Vesta: Spectral reflectivity and compositional implications. Science 168, 1445-1447

McCubbin, F.M., Hauri, E.H., Elardo, S.M., Vander Kaaden, K.E., Wang, J., Shearer, C.K. (2012) Hydrous melting of the martian mantle produced both depleted and enriched shergottites. Geology 40, 683-686

McDonough, W.F., Sun, S.-s. (1995) The composition of the Earth. Chemical Geology 120, 223-253

McDonough, W.F., (2003) Compositional model for the Earth's core. In: Carlson, R.W. ed. *Treatise on Geochemistry, Vol. 2, The Mantle and Core.* Elsevier Ltd, 547-568

McSween Jr, H.Y., Mittlefehldt, D.W., Beck, A.W., Mayne, R.G., McCoy, T.J. (2010) HED meteorites and their relationship to the geology of Vesta and the Dawn mission. Space Science Reviews 163, 141-174

Melosh, H.J. (1990) Giant impacts and the thermal state of the early Earth. In: Newsom, H.E. and Jones, J.H. eds. *Origin of the Earth.* Oxford University Press, 69-83

Mysen, B.O. (1983) The structure of silicate melts. Annual Review of Earth and Planetary Science 11, 75-97

Newsom, H.E., Drake, M.J. (1982) The metal content of the eucrite parent body: Constraints from the partitioning behavior of tungsten. Geochimica et Cosmochimica Acta 46, 2483-2489

Newsom, H. E. (1995) Composition of the solar system, planets, meteorites, and major terrestrial reservoirs. In: Ahrens, T.J. ed. *Global Earth Physics: A Handbook of Physical Constants*. AGU Reference Shelf, 159-189

O'Brien, D.P., Morbidelli, A., Levison, H.F. (2006) Terrestrial planet formation with strong dynamical fiction. Icarus 184, 39-58

Ohtani, E., Yurimoto, H., Seto, S. (1997) Element partitioning between metallic liquid, silicate liquid, and lower-mantle minerals: Implications for core formation of the Earth. Physics of the Earth and Planetary Interiors 100, 97-114

O'Neill, H.S.C. (1986) Mo-MoO_2 (MOM) oxygen buffer and the free energy of formation of MoO_2. American Mineralogist 71, 1007-1010

O'Neill, H.S.C. (1991) The origin of the Moon and the early history of the Earth – A chemical model. Part 1: The Moon. Geochimica et Cosmochimica Acta 55, 1135-1157

O'Neill, H.S.C., Pownceby, M.I. (1993) Thermodynamic data from redox reactions at high temperatures. I. An experimental and theoretical assessment of the electrochemical method using stabilized zirconia electrolytes, with revised values for the Fe-"FeO", Co-CoO, Ni-NiO and Cu-Cu_2O oxygen buffers, and new data for the W-WO_2 buffer. Contributions to Mineralogy and Petrology 114, 296-314

O'Neill, H.S.C., Dingwell, D.B., Borisov, A., Spettel, B., Palme, H. (1995) Experimental petrochemistry of some highly siderophile elements at high temperatures, and some implications for core formation and the mantle's early history. Chemical Geology 120, 255-273

O'Neill, H.S.C., Eggins, S.M. (2002) The effect of melt composition on trace element partitioning: An experimental investigation of the activity coefficient of FeO, NiO, CoO, MoO2, MoO3 in silicate melts. Chemical Geology 186, 151-181

O'Neill, H.S.C., Berry, A.J., Eggins, S.M. (2008) The solubility and oxidation state of tungsten in silicate melts: Implications for the comparative chemistry of W and Mo in planetary differentiation processes. Chemical Geology 255, 346-359

Palme, H., O'Neill, H.S.C. (2003) Cosmochemical estimates of mantle composition. In: Carlson, R.W. ed. *Treatise on Geochemistry, Vol. 2, The Mantle and Core.* Elsevier Ltd, 1-38

Peach, C.L., Mathez, E.A. (1993) Sulfide melt-silicate melt distribution coefficients for nickel and iron and implications for the distribution of other chalcophile elements. Geochimica et Cosmochimica Acta 57, 3013-3021

Rammensee, W., Wänke, H. (1977) On the partition coefficient of tungsten between metal and silicate and its bearing on the origin of the moon. Proc. Lunar Sci. Conf. 8, 399-409

Righter, K., Drake, M.J. (1995) The effect of pressure on siderophile-element (nickel, cobalt, molybdenum, tungsten, and phosphorus) metal-silicate partition coefficients. Meteoritics 30, 565-566

Righter, K., Drake, M.J. (1996) Core formation in Earth's Moon, Mars, and Vesta. Icarus 124, 513-529

Righter, K., Drake, M.J. (1997) A magma ocean on Vesta: Core formation and petrogensis of eucrites and diogenites. Meteoritics and Planetary Science 32, 929-944

Righter, K., Drake, M.J., Yaxley, G. (1997) Prediction of siderophile element metal-silicate partition coefficients to 20 GPa and 2800 °C: The effects of pressure, temperature, oxygen fugacity, and silicate and metallic melt compositions. Physics of the Earth and Planetary Interiors 100, 115-134

Righter, K., Hervig, R.L., and Kring, D.A. (1998) Accretion and core formation on Mars: Molybdenum contents of melt inclusion glasses in three SNC meteorites. Geochimica et Cosmochimica Acta 62, 2167-2177

Righter, K., Drake, M.J. (1999) Effect of water on metal-silicate partitioning of siderophile elements: A high pressure and temperature terrestrial magma ocean and core formation. Earth and Planetary Science Letters 171, 383-399

Righter, K., Humayun, M., Danielson, L. (2008) Partitioning of palladium at high pressures and temperatures during core formation. Nature 1, 321-323

Righter, K., Pando, K.M., Danielson, L., Lee, C.T. (2010) Partitioning of Mo, P and other siderophile elements (Cu, Ga, Sn, Ni, Co, Cr, Mn, V, and W) between metal and silicate melt as a function of temperature and silicate composition. Earth and Planetary Science Letters 291, 1-9

Righter, K. (2011) Prediction of metal-silicate partition coefficients for siderophile elements: An update and assessment of PT conditions for metal-silicate equilibrium during accretion of the Earth. Earth and Planetary Science Letters 304, 158-167

Righter, K., Sutton, S., Danielson, L., Pando, K., Schmidt, G., Yang, H., Berthet, S., Newville, M., Choi, Y., Downs, R. T., Malavergne, V. (2011) The effect of fO_2 on the partitioning and valence of V and Cr in garnet/melt pairs and the relation to terrestrial mantle V and Cr content. American Mineralogist 96, 1278-1290

Riner, M.A., Lucey, P.G., Desch, S.J., McCubbin, F.M. (2009) Nature of opaque components on Mercury: Insights into a Mercurian magma ocean. Geophys. Res. Lett. 36, L02201, doi: 10.1029/2008GL036128

Ringwood, A.E. (1966) Chemical evolution of the terrestrial planets. Geochimica et Cosmochimica Acta 30, 41-104

Rubie, D.C., Melosh, H.J., Reid, J.E., Liebske, C., Righter, K. (2003) Mechanisms of metal-silicate equilibration in the terrestrial magma ocean. Earth and Planetary Science Letters 205, 239-255

Rubie, D.C., Gessmann, C.K., Frost, D.J. (2004) Partitioning of oxygen during core formation on the Earth and Mars. Nature 429, 58-61

Rubie, D.C., Frost, D.J., Mann, U., Asahara, Y., Nimmo, F., Tsuno, K., Kegler, P., Holzheid, A., Palme, H. (2011) Heterogeneous accretion, composition and core-mantle differentiation of the Earth. Earth and Planetary Science Letters 301, 31-42

Sanloup, C., Jambon, A., Gillet, P. (1999) A simple chondritic model of Mars. Physics of the Earth and Planetary Interiors 112, 43-54

Sata, N., Hirose, K., Shen, G., Nakajima, Y., Ohishi, Y., Hirao, N. (2010) Compression of FeSi, Fe3C, Fe0.95O, and FeS under the core pressures and implication for light element in the Earth's core. Journal of Geophysical Research 115, doi: 10.1029/2009JB006975

Schnetzler, C.C., Philpotts, J.A. (1971) Alkali, alkaline earth, and rare-earth element concentrations in some Apollo 12 soils, rocks, and separated phases. Proc. Second Lunar Sci. Con. 2, 1101-1122

Schonbachler, M., Carlson, R.W., Horan, M.F., Mock, T.D., Hauri, E.H. (2010) Heterogeneous accretion and the moderately volatile element budget of Earth. Science 328, 884-887

Shahar, A., Ziegler, K., Young, E.D., Ricolleau, A., Schauble, E.A., Fei, Y. (2009) Experimentally determined Si isotope fractionation between silicate and Fe metal and implications for Earth's core formation. Earth and Planetary Science Letters 288, 228-234

Siebert, J., Corgne, A., Ryerson, F.J. (2011) Systematics of metal-silicate partitioning for many siderophile elements applied to Earth's core formation. Geochimica et Cosmochimica Acta 75, 1451-1489

Schmitt, W., Palme, H., Wänke, H. (1989) Experimental determination of metal/silicate partition coefficients for P, Co, Ni, Cu, Ga, Ge, Mo, and W and some implications for the early evolution of the Earth. Geochimica et Cosmochimica Acta 53, 173-185

Schnetzler, C.C., Philpotts, J.A. (1971) Alkali, alkaline earth, and rare-earth element concentrations in some Apollo 12 soils, rocks, and separated phases. Proc. Second Lunar Sci. Con. 2, 1101-1122

Siebert, J., Corgne, A., Ryerson, F.J. (2011) Systematics of metal-silicate partitioning for many siderophile elements applied to Earth's core formation. Geochimica et Cosmochimica Acta 75, 1451-1489

Siebert, J., Badro, J., Antonangeli, D., Ryerson, F.J. (2012) Metal-silicate partitioning of Ni and Co in a deep magma ocean. Earth and Planetary Science Letters 321-322, 189-197

Seifert, S., O'Neill, H.S.C., Brey, G. (1988) The partitioning of Fe, Ni and Co between olivine, metal, and basaltic liquid: An experimental and thermodynamic investigation, with application to the composition of the lunar core. Geochimica et Cosmochimica Acta 52, 603-616

Smith, J.V., Anderson, A.T., Newton, R.C., Olsen, E.J., Wyllie, P.J. (1970) A petrologic model for the Moon based on petrogenesis, experimental petrology, and physical properties. The Journal of Geology 78, 381-405

Smith, D.E., Zuber, M.T., Phillips, R.J., Solomon, S.C., Hauck II, S.A., Lemoine, F.G., Mazarico, E., Neumann, G.A., Peale, S.J., Margot, J.-L., Johnson, C.L., Torrence, M.H., Perry, M.E., Rowlands, D.D., Goossens, S., Head, J.W., Taylor, A.H. (2012) Gravity field and internal structure of Mercury from MESSENGER. Science 336, 214-214

Sohl, F., Schubert, G., and Spohn, T., 2005. Geophysical constraints on the composition and structure of the Martian interior. Journal of Geophysical Research 110, E12008, doi: 10.1029/2005JE002520

Solomon, S.C., Aharonson, O., Aurnou, J.M., Banerdt, W.B., Carr, M.H., Dombard, A.J., Frey, H.V., Golombek, M.P., Hauck II, S.A., Head III, J.W., Jakosky, B.M., Johnson, C.L., McGovern, P.J., Neumann, G.A., Phillips, R.J., Smith, D.E., and Zuber, M.T. (2005) New perspectives on ancient Mars. Science 307, 1214-1220

Stevenson, D.J. (1990) Fluid dynamics of core formation. In: Newsom, H.E. and Jones, J.H. Eds., *Origin of the Earth*. Oxford University Press, New York, 231-249

Tankins, E.S., Thomas, M.K., Erthal, J.F., Williams, F.S. (1965) The activity of oxygen in liquid iron-molybdenum and iron-tungsten alloys. Transactions of the American Society of Metals 58, 245-252

Thibault, Y., Walter, M.J. (1995) The influence of pressure and temperature on the metal-silicate partition coefficients of nickel and cobalt in a model C1 chondrite and implications for metal segregation in a deep magma ocean. Geochimica et Cosmochimica Acta 59, 991-1002

Tonks, W.B., Melosh, H.J. (1993) Magma ocean formation due to giant impacts. Journal of Geophysical Research 98, 5319-5333

Toplis, M.J. (2005) The thermodynamics of iron and magnesium partitioning between olivine and liquid: Criteria for assessing and predicting equilibrium in natural and experimental systems. Contributions to Mineralogy and Petrology 149, 22-39

Tuff, J., Wood, B.J., Wade, J. (2011) The effect of Si on metal-silicate partitioning of siderophile elements and implications for the conditions of core formation. Geochimica et Cosmochimica Acta 75, 673-690

Ulmer, P. (1989) The dependence of the Fe^{2+}-Mg cation-partitioning between olivine and basaltic liquid on pressure, temperature and composition. Contributions to Mineralogy and Petrology 101, 261-273

Wade, J., Wood, B.J. (2001) The Earth's 'missing' niobium may be in the core. Nature 409, 75-78

Wade, J., Wood, B.J. (2005) Core formation and the oxidation state of the Earth. Earth and Planetary Science Letters 236, 78-95

Wade, J., Wood, B.J., Tuff, J. (2012a) Metal-silicate partitioning of Mo and W at high pressures and temperatures: Evidence for late accretion of sulphur to the Earth. Geochimica et Cosmochimica Acta 85, 58-74

Wade, J., Wood, B.J., Norris, C.A. (2012b) The oxidation state of tungsten in silicate at high pressures and temperatures. Chemical Geology, in press

Walker, D., Norby, L., Jones, J.H. (1993) Superheating effects on metal-silicate partitioning of siderophile elements. Science 262, 1858-1861

Walker, R.J. (2009) Highly siderophile elements in the Earth, Moon and Mars: Update and implications for planetary accretion and differentiation. Chemie der Erde 69, 101-125

Walter, M.J., Thibault, Y. (1995) Partitioning of tungsten and molybdenum between metallic liquid and silicate melt. Science 270, 1186-1189

Wänke, H. (1981) Constitution of terrestrial planets. Philosophical Transactions of the Royal Society of London A 303, 287-302

Wänke, H., Dreibus, G. (1988) Chemical composition and accretion history of terrestrial planets. Philosophical Transactions of the Royal Society of London A 325, 545-557

Warren, P.H. (1985) The magma ocean concept and lunar evolution. Ann. Rev. Earth Planet. Sci. 13, 201-240

Warren, P.H., Ulff-Moller, F., Huber, H., Kallemeyn, G.W. (2006) Siderophile geochemistry of ureilites: A record of early stages of planetesimal core formation. Geochimica et Cosmochimica Acta 70, 2104-2126

Wasson, J.T. (1985) *Meteorites: Their record of early solar-system history*. W.H. Freeman and Company, New York, 267 pp

Weiss, B.P., Berdahl, J.S., Elkins-Tanton, L.T., Stanley, S., Lima, E.A., Carporzen, L. (2008) Magnetism on the Angrite parent body and the early differentiation of planetesimals. Science 322, 713-716

Wetherill, G.W. (1985) Occurrence of giant impacts during the growth of the terrestrial planets. Science 228, 877-879

Williams, H.M., Wood, B.J., Wade, J., Frost, D.J., Tuff, J. (2012) Isotopic evidence for internal oxidation of Earth's mantle during accretion. Earth and Planetary Science Letters 321-322, 54-63

Wood, J.A., Dickey Jr, J.S., Marvin, U.B., Powell, B.N. (1970) Lunar anorthosites and a geophysical model of the moon. Proc. Apollo 11 Lunar Sci. Conf. 1, 965-988

Wood, B.J., Walter, M.J., Wade, J. (2006) Accretion of the Earth and segregation of its core. Nature 441, 825-833

Wood, B.J., Wade, J., Kilburn, M.R. (2009) Core formation and the oxidation state of the Earth: Additional constraints from Nb, V, and Cr partitioning. Geochimica et Cosmochimica Acta 72, 1415-1426

Yin, Q., Jacobsen, S.B., Yamashita, K., Blichert-Toft, J., Telouk, P., Albarede, F. (2002) A short timescale for terrestrial planet formation from Hf-W chronometry of meteorites. Nature 418, 949-959

Yoder, C.F. (1995) Astrometric and geodetic properties of Earth and the Solar System. In: Ahrens, T.J. ed. *Global Earth Physics: A Handbook of Physical Constants*. AGU Reference Shelf, 1-31

Zhang, J., Herzberg, C. (1994) Melting experiments on anhydrous peridotite KLB-1 from 5.0 to 22.5 GPa. Journal of Geophysical Research 99, 17729-17745

Zuber, M.T., McSween Jr, H.Y., Binzel, R.P., Elkins-Tanton, L.T., Konopliv, A.S., Pieters, C.M., Smith, D.E. (2011) Origin, internal structure and evolution of 4 Vesta. Space Science Reviews 163, 77-93